

CR 72837

CALIBRATION OF COMBINED BENDING-TORSION FATIGUE
RELIABILITY RESEARCH MACHINES AND
RELIABILITY DATA REDUCTION

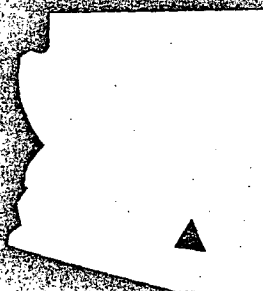
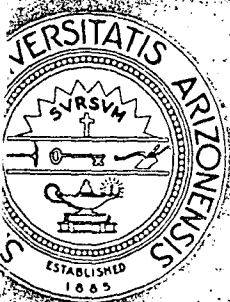
by

Dr. Dimitri Kececioglu and Jeffrey B. McConnell

(NASA-CR-72837) CALIBRATION OF COMBINED
BENDING-TORSION FATIGUE RELIABILITY DATA
REDUCTION D. Kececioglu, et al (Arizona
Univ., Tucson.) 31 Jul. 1969 166 p CSCL

N73-12497

Unclas
14B G3/15 48829



ENGINEERING EXPERIMENT STATION
COLLEGE OF ENGINEERING
THE UNIVERSITY OF ARIZONA
TUCSON, ARIZONA

NASA CONTRACTOR
REPORT

72837
NASA CR-~~728~~

NASA CR-XXX

CALIBRATION OF COMBINED BENDING-TORSION FATIGUE RELIABILITY
RESEARCH MACHINES AND RELIABILITY DATA REDUCTION

by Dr. Dimitri Kececioglu and Jeffrey B. McConnell

Prepared under Grant No. ^{NGL-}03-002-044 by The University of
Arizona

Tucson, Arizona

for

NATIONAL AERONAUTICS AND SPACE ADMINISTRATION - WASHINGTON,
D. C.

I

CALIBRATION OF COMBINED BENDING-TORSION
FATIGUE RELIABILITY RESEARCH MACHINES
AND
RELIABILITY DATA REDUCTION

by

Dr. Dimitri Kececioglu and Jeffrey B. McConnell

Prepared For

NATIONAL AERONAUTICS AND SPACE ADMINISTRATION

July 31, 1969

Contract NGA-03-002-044

Project Management
NASA-Lewis Research Center
Cleveland, Ohio

Vincent R. Lalli

College of Engineering
THE UNIVERSITY OF ARIZONA
Engineering Experiment Station
Tucson, Arizona

ABSTRACT

The combined bending-torsion fatigue reliability research machines, conceived, designed, and built at The University of Arizona are described. Three such machines are presently in operation at The University of Arizona. The calibration of these machines is presented in depth. Fatigue data generated with these machines for SAE 4340 steel grooved specimens subjected to reversed bending and steady torque loading are given. The data reduction procedure is presented. Finally, some comments are made about notch sensitivity and stress concentration as applied to combined fatigue.

TABLE OF CONTENTS

	<u>Page No.</u>
Abstract	ii
List of Illustrations	vi
List of Tables	ix
Symbols	xi
I Summary	1
II Introduction	3
III Description of Combined Bending-Torsion Fatigue Reliability Research Machines	9
IV Calibration of Research Machines	13
A. Calibration Requirements	13
B. Bending Calibration	15
1. Visicorder output from bending strain gages on toolholder versus true stress in toolholder	15
2. Visicorder output from bending strain gages in specimen groove versus true stress in specimen groove	20
2.1 Experimental determination of average stress concentration factor in specimen groove	23
3. Torque interaction into the bending bridge output	25
4. Relationship between toolholder bending stress and specimen groove bending stress	30

4.1	Toolholder strain gage output versus specimen strain gage output	31
4.2	Toolholder bending stress versus specimen bending stress	33
C.	Torque Calibration	37
1.	Torque load versus visicorder output	37
2.	Bending interaction into the torque bridge output	38
2.1	Effect of bending on torque bridge output - additional test	42
D.	Axial Effects	44
1.	Effect of axial load on bending bridge output	44
2.	Measurement of the axial stress	45
2.1	Measurement of the axial stress as a function of bending load	45
2.2	Measurement of the axial stress as a function of torque load	47
E.	Summary of Calibration Results	48
V	Research Data Reduction	51
A.	Conversion of Visicorder Outputs to Stress Levels	51
B.	Reduction of Endurance Strength Data For $r_s = \infty$ and $r_s = 0.90$	52
C.	Generation of S-N Diagrams Using Distribu- tional Stress Levels and Mean Cycles-To- Failure	54

D. Generation of Theoretical S-N Diagram	55
E. Comparison of Theoretical and Experimental S-N Curves	58
VI Stress Concentration and Notch Sensitivity Effects	59
A. Stress Concentration	59
B. Notch Sensitivity Survey	60
C. Proposed Notch Sensitivity Determination	62
VII Conclusions	63
VIII Recommendations	66
Acknowledgements	67
References	68
Appendix A. Data Reduction Results for $r_s = \infty$	133
Appendix B. Data Reduction Results for $r_s = 0.7$ and $r_s = 0.9$	139
Appendix C. Operating Checklist for Combined Bending-Torsion Fatigue Research Machines	144
Appendix D. Procedure for Operating Combined Bending-Torsion Fatigue Research Machines with Combined Bending and Torque Loads	147
Appendix E. Calibration of New Torque Gages for Machine #3, June 1, 1969	149
Appendix F. Maintenance Checklist for Combined Bending-Torsion Fatigue Research Machines	151

LIST OF ILLUSTRATIONS

<u>Figure No.</u>	<u>Page No.</u>
1 - Mabie-Gjesdahl fatigue testing machine	71
2 - Complex-fatigue reliability research machine - front view	72
3 - Complex-fatigue reliability research machine - top view	73
4 - Loading frame analysis and test specimen	74
5 - Bending load lever arm	75
6 - Strain gage and slip ring arrangement	76
7 - Bending moment instrumentation	77
8 - Torque instrumentation	78
9 - Torsional stresses for one gage	79
10 - Test set-up for the bending cantilever calibration	80
11 - Test set-up for torque interaction into bending bridge output	81
12 - Torque interaction into bending - Machine #1	82
13 - Torque interaction into bending - Machine #2	83
14 - Specimen groove output versus toolholder output - Machine # 1	84
15 - Specimen groove output versus toolholder output - Machine #2	85
16 - Specimen groove output versus toolholder output - Machine #3	86

Figure No.Page No.

17 - Free body diagram of toolholder	87
18 - Laboratory set-up of lever arm, pivot point, resisting moment measurement experiment	88
19 - Scale graduations of measurement experiment	89
20 - Torque output versus pan weight - Machine #1	90
21 - Torque output versus pan weight - Machine #2	91
22 - Torque output versus pan weight - Machine #3	92
23 - Bending interaction into torque - Machine #1	93
24 - Bending interaction into torque - Machine #2	94
25 - Bending interaction into torque - Machine #3	95
26 - Bending interaction into torque at high torque level - Machine #2	96
27 - Axial output versus bending load - Machine #1	97
28 - Axial output versus torque load - Machine #1	98
29 - The calibration flow chart	99
30 - Data reduction program	100
31 - Pan weight versus true bending stress for endurance strength for $r_s = \infty$	103
32 - Pan weight versus true bending stress for endurance strength for $r_s = 0.90$	104
33 - Cycles-to-failure distributions and en- durance strength distribution for $r_s = \infty$	105
34 - Cycles-to-failure distributions for $r_s + 0.70$ and endurance strength distri- bution for $r_s = 0.90$	106

Figure No.Page No.

35 - Fatigue strength versus mean cycles-to-failure and endurance strength for r_s of ∞ , 0.70, and 0.90, and the theoretical S-N diagram for $r_s = \infty$	107
36 - Three-dimensional distributional Goodman fatigue strength surface based on research results reported here for 10^7 cycles of life	108
37 - Notch sensitivity of normalized steel specimens	109
38 - Notch sensitivity of quenched and tempered alloy steel specimens	109
39 - Curves of notch sensitivity versus radius for steels, bending or axial loading	110
40 - The fatigue notch factor	110
41 - Notch sensitivity charts for steels and 245-T wrought aluminum alloys subjected to reversed bending or reversed axial loads	111
42 - Notch sensitivity curves for materials in reversed torsion	111
43 - Bending interaction into torque - Machine # 3, June 1969	112
44 - Torque output versus pan weight - Machine # 3, June 1969	113

LIST OF TABLES

<u>Table No.</u>	<u>Page No.</u>
1 - Instrumentation	114
2 - Toolholder output versus pan weight data for bending bridge calibration	115
3 - Toolholder output versus pan weight data in incremental form for bending bridge calibration in terms of change in toolholder output divisions for 10.27 lbs. of pan weight	116
4 - Calibration specimen groove strain gage output versus pan weight data	117
5 - Reduction of Machine #2 data given in Table 4	118
6 - Reduction of Machines #1 and #3 data given in Table 4	119
7 - Torque output versus bending output data from torque into bending interaction calibration	120
8 - Toolholder versus groove bridge output data for quasi-static calibration of groove stress	121
9 - Visicorder divisions converted to strain	122
10 - Torque output versus pan weight data for torque bridge calibration	123
11 - Torque reduction table	124
12 - Bending output versus torque output data for bending into torque interaction calibration	125
13 - Bending output versus torque output data at high torque level for bending into torque interaction calibration	126
14 - Axial output versus bending output for axial to bending interaction calibration	127

List of TablesPage No.

- | | |
|--|-----|
| 15 - Axial output versus torque output for axial load into torque interaction calibration | 128 |
| 16 - The calibration coefficients for each research machine | 129 |
| 17 - Stress levels and visicorder divisions for $r_s = 3$ and Machine #1 | 130 |
| 18 - Torque output versus pan weight data for new torque gages - Machine #3, June 1969 | 131 |
| 19 - Bending output versus torque output data for new torque gages - Machine #3, June 1969 | 132 |

SYMBOLS

<u>Symbol</u>	<u>English</u>
C	Radius of shaft, in
div	Divisions
E	Young's Modulus, psi
F	Force, lbs
G	Strain gage factor
I	Moment of inertia of cross-section, in ⁴
in	Inches
k_a	Surface finish factor
K_{ave}	Experimentally determined static stress concentration factor
k_b	Size factor
K_{BGR}	Groove bending calibration coefficient
$K_{B/T}$	Bending into torque interaction coefficient
K_{BTH}	Toolholder bending calibration coefficient
k_d	Temperature factor
k_e	Stress concentration design factor
K_f	Dynamic stress concentration factor
k_f	Miscellaneous effects factor

<u>Symbol</u>	<u>English</u>
K_{GR-TH}	Groove-toolholder calibration coefficient
K_T	Toolholder torque calibration coefficient
K_t	Static stress concentration factor
K_{ts}	Static stress concentration factor in shear
$K_{T/B}$	Torque interaction into bending calibration coefficient
L	Lever arm distance, in
lbs	Pounds
M	Moment, lb-in
N_a	Number of active arms in strain gage bridge
N_{cal}	Visicorder calibration divisions, div
N_{vis}	Visicorder output, div
q	Notch sensitivity factor
r_s	Stress ratio
R_{cal}	Calibration resistance, ohms
R_{gage}	Resistance of strain gage, ohms
\bar{S}_e	Mean of endurance strength, psi
S_e	Endurance strength, psi
S_{e10^3}	Fatigue strength for 10^3 cycles, psi
S_U	Ultimate strength, psi
W	Pan weight, lbs
w	Loading, lbs/in
W_{bear}	Weight of the bearing, lbs

SymbolsEnglish

w_{col}	Weight of the collet, lbs
w_{coup}	Weight of the coupling, lbs
w_{nut}	Weight of the collet assembly nut, lbs
w_{slip}	Weight of the slipring assembly, lbs
V	Coefficient of Variation, %

SymbolsGreek

ϵ	Normal strain, micro in/in
μ	Mean
σ	Normal stress, psi
σ_S	Standard deviation of normal distribution
σ_{S_e}	Standard deviation of endurance data, psi
τ	Shear stress, psi

SymbolsSubscripts

B	Bending
GR	Specimen Groove
out	Output
TH	Toolholder
T	Torque
vis	Visicorder

I SUMMARY

The calibration effort and data reduction techniques for the Combined Bending-Torsion Fatigue Reliability Research Machines is presented here. Because of the complexity of the problem of determining the true bending stress and the true shear stress present in the groove of the test specimen, eight distinct calibrations had to be performed on each machine. A description of each calibration test, the test setup, the procedure, the data, and the data reduction are given for each calibration test. Then the need for each test is presented in Section IV.E where a calibration flow chart was developed to aid in the data reduction procedure. Specific calibration parameters for each machine were determined and their needs demonstrated. The calibration equations in bending were shown to be

$$\sigma_{out_{TH}} = K_{GR-TH} K_{BGR} \sigma_{true_{GR}}$$

$$\sigma'_{out_{TH}} = \sigma_{out_{TH}} + K_{T/B} \tau_{out_{TH}}$$

$$N_{vis_B} = \frac{N_{cal} N_a G R_{cal}}{E R_{gage}} \sigma'_{out_{TH}}$$

and the calibration equations in torque were shown to be

$$\tau_{true_{GR}} = \frac{\sigma_{true_{GR}}}{r_s \sqrt{3}}$$

$$\tau_{out_TH} = \frac{1}{K_{ts}} \frac{1}{K_T} \frac{C_{TH}}{J_{TH}} \frac{J_{GR}}{C_{GR}} \tau_{true_GR}$$

Prior to this research effort, redesigning reliability into notches of the interference of the TH $\tau'_{out_TH} = \tau_{out_TH} + K_{B/T} \sigma_{out_TH}$ caused by keadology, and lower a Alscourier of Monte Carlo technique strength distribution $N_{vis_T} = \frac{N_{cal} N_a G R_{cal}}{E R_{gage}} \tau'_{out_TH}$ affecting each

Precedential (2) where a PERC ity was used to be the TH. In addition, the static stress concentration factor for the notched specimen was determined to be 1.28.

For data reduction, the calibration flow chart was generalized and computerized. The data reduction program as well as all the data generated to date are presented. Sample calculations for the data reduction technique are given. Cycles-to-failure data reduction is not included in this report and is the subject of another report.

The results of the data reduction are briefly presented in the form of S-N curves.

Lastly, the problem of notch sensitivity is discussed and a proposal made.

II INTRODUCTION

Prior to this research effort, the basic methodology for designing reliability into mechanical components by consideration of the interference of their stress-strength distributions was discussed by Kececioglu and Cormier (1)*. Included in this paper was a discussion of Monte Carlo techniques for determining stress and strength distributions, given the distributions of the factors affecting them.

Freudenthal (2) wrote a paper in which structural unreliability was considered to be the probability, or risk, of failure. The safety factor was shown to be a distribution function which is the quotient of the strength to the stress, where both strength and stress are considered as statistical variables. Freudenthal, Garrelts, and Shinozuka (3) prepared a comprehensive report, along the same lines, which discussed in more detail the mathematical techniques required, the appropriate statistical distributions involved, and problems which remained to be solved. Several example problems in structural reliability were worked out, an extensive bibliography was given. These efforts concentrated on simple fatigue and structural reliability.

The Battelle Memorial Institute and its Mechanical Reliability Research Center presented studies (4, 5) which described some of the fundamental problems in mechanical reliability and suggested methods for their solution.

Mittenbergs (4) discussed the fundamental aspects of reliability engineering as they pertain to mechanical devices. He stated that the failure modes of mechanical elements were basically:

*Numbers in parentheses refer to those under References.

1. Deformation.
2. Fracture.
3. Instability.

He also asserted that many factors combine to determine the reliability of a mechanical part under such failure modes. The interaction of strength and load distributions was discussed. The Sixth Progress Report of the Mechanical Reliability Research Center (5) summarized a two-year research effort. This extensive research effort contained a thorough discussion of mechanical reliability, and attempted to quantify the relationships of various factors on such phenomena as creep and fatigue. An extensive bibliography was included.

The IIT Research Institute conducted a program in "Methods for Prediction of Electro-Mechanical Systems Reliability" (6). The program was concerned with three major areas:

1. The study of prime mechanisms of failure in mechanical design. Specific items included fatigue, surface fatigue, wear, creep, and corrosion.
2. The application of failure mechanism and design information for the reliability evaluation of specific mechanical parts. Parts included were gears, bearings, springs, and shafts.
3. The determination of mechanical system reliability in terms of individual part reliability figures.

*Identical to
McKinley's*

A paper by G. Reethof, M. J. Bratt, and G. W. Weber of the Large Jet Engine Department, General Electric Company, entitled "A Model for Time Varying and Interfering Stress-Strength Probability Degradation" (7), provided a computer approach towards the solution of the time variant strength distribution case.

An extension of this study was made by Lipson et al (28), who conducted an extensive literature survey, gathered available fatigue

data, and developed an analysis of the stress-strength interference theory using the Weibull distribution extensively.

The above works provided some interesting and valuable contributions to the problem of designing specified reliabilities into mechanical components. However, a number of important aspects of this problem remained to be investigated. The problem of time-variant stress and strength distributions needed further treatment. The effects of various factors, which are themselves distributions, on the distributions of the failure-governing stress and strength had yet to be fully explored. The development of a formal engineering design methodology for designing mechanical components had yet to be developed. Finally, much of the work in mechanical reliability theory suffered from a lack of statistically adequate data, due to a lack of test results on a large number of identical mechanical components.

The purpose of the current investigation is to fill in the gaps in the above-mentioned areas, with the following specific objectives:

1. Develop a formal engineering methodology for designing into mechanical components, subjected to combined-stress fatigue which involves time-dependent strength distributions, specified reliabilities.
2. Explore the methods of functions of random variables as applied to structural reliability.
3. Explore the methods available for determining failure-governing stress and strength distributions and develop new ones.
4. Explore the methods available for calculating the reliability once the failure-governing stress and strength distributions are known and develop new ones.
5. Develop and fabricate fatigue testing machines for reliability research, so that the explored and

developed methodologies described above can be demonstrated.

6. Pursue a test program with a statistically significant number of test specimens to obtain data from which these methodologies can be demonstrated.

A literature survey was made in order to locate fatigue testing machines to generate the desired, combined bending-torsion fatigue data. *References on Fatigue* was surveyed from 1955 to 1963. The only paper of interest was the "Symposium on Large Fatigue Testing Machines and their Results" (9). No testing machines capable of handling combined steady torque and reversed bending moment were found in the paper. Other references (10, 11) were reviewed; information concerning combined-stress fatigue machines was not found.

The Proceedings of the Society for Experimental Stress Analysis (12) from 1945 to 1960 and *Experimental Mechanics* (13) from 1961 to December 1965 were reviewed in an attempt to locate a combined steady torque and reversed bending moment testing machine. Several fatigue testing machines were found, but only one was of direct interest to the NASA contract, a testing machine built by Mabie and Gjesdahl (14). This machine used the four-square principle for applying a steady torque while the rotating beam principle was used to produce the bending moment.

The four-square principle is not a new principle for developing steady torque. Industrial corporations, such as gear manufacturers, speed reducer manufacturers, and coupling manufacturers, all use this principle to evaluate their products (15).

In the Mabie-Gjesdahl Machine this principle was used to develop a maximum steady torque of 6,000 in-lb; however, the machine was only operated at a maximum of about 2,000 in-lb of torque (14, p. 86). At this loading the machine produced a high pitch whine (16), a result of the pitch line velocity of the spur

gears being 3,000 to 4,000 feet per minute (17).

The pre-set torque could not be maintained. The steady torque, four-square principle was coupled with a reversed bending moment, as shown in Figure 1. The desired bending moment was applied to the test piece so as to simulate a simply-supported beam. Through the use of a hydraulic cylinder and associated equipment the required bending moment load was developed (16). A reduction in bending moment occurred during testing as a result of hydraulic cylinder leakage. The bending moment was constant along the length of the test piece for a specific value of the bending load. The machine was designed for 5,000 in-lb and operated at a maximum of about 3,200 in-lb of bending moment. The reversed bending moment was gained through the rotation of the test piece in the four-square mechanism.

The Mabie-Gjesdahl test machine operated at 1,200 rpm. The machine was driven by a 3 hp, 1,200 rpm induction motor (18). Mabie (16) furnished two assembly drawings (19, 20) and additional design information as to the problem areas in his test machine. Mabie indicated that the disadvantages of this machine were that it was difficult to hold the torque and bending moment, and noise and vibration were present. However, the machine did not dissipate energy to apply torque to the specimen and operated on a proven principle.

The exact instrumentation on the Mabie-Gjesdahl test machine is not known. However, the torque values were measured and checked only in a static situation. The bending moment values were checked and related to the pressure gage on the hydraulic equipment. The load was applied statically and the pressure noted. Strain gages were used for the static torque measurements and also for the bending load. The bending load strain gages were mounted on the loading bar.

The test machine was calibrated dynamically with suitably mounted strain gages and slip-ring and brush assemblies. The exact equipment is not known. Correlation of these dynamic tests were made to the stresses obtained through calculations and an 8-12% error was noted (14). Correspondence with Mabie (12) indicated that the commercially purchaseable components exceeded \$5,000.00.

With these thoughts in mind, test machines similar to the Mabie-Gjesdahl principle were conceived, designed and built at The University of Arizona, starting the fall of 1965.

Three combined bending-torsion fatigue reliability research machines are presently in operation at The University of Arizona. A research program is being conducted for the National Aeronautics and Space Administration under the direction of Dr. Dimitri Kececioğlu at The University of Arizona, Tucson, Arizona, and Mr. Vincent R. Lalli at the NASA Lewis Research Center, Cleveland, Ohio. The description of these test procedures, test data and their reduction presented here are part of this research effort. The objective of this report is to obtain the calibration parameters presented in Figure 29. The experimental tests which must be run to determine these parameters are described. The data reduction technique is also given. The problem of stress concentration in the notch of the test specimens and the associated notch sensitivity are discussed, and recommendations for future work are made.

III DESCRIPTION OF COMBINED BENDING-TORSION FATIGUE RELIABILITY RESEARCH MACHINES

The combined bending-torsion fatigue reliability research machines are designed to simulate a shaft in service. The objective of the immediate research program is to examine the fatigue life of specimens made of SAE 4340 steel under combined loadings. The specimens are subjected to reversed bending and steady torque applied to a rotating specimen with a stress concentration, which produce combined bending-torsion stress, or combined-stress, fatigue.

General Description of Fatigue Machines

Each fatigue machine consists of a two-section, rotating shaft with a test specimen locked in the center, as shown in Figures 2 and 3. The horizontal shaft is coupled at each end to allow for relatively free deflection when the specimen is loaded. A seven and one-half horsepower, 1,800 rpm motor powers the shaft. The bending load is applied to the specimen by means of two yokes, one each on two bearings located symmetrically about the specimen on two commercial tool-holders. Below the shaft, the yokes are connected by a horizontal link, which concentrates the load at a single vertical link in the center. The vertical link is then connected to either a long or a short loading lever arm. These loading arms make possible the application of a great range of bending stresses in the specimen groove, by means of pan weight applied at the end of the loading arm. One pound of pan weight is approximately equal to two thousand psi in the groove. The torque is applied by means of a commercial Infinit -Indexer which is located on the back shaft of the machine.

General Description of the Instrumentation

Strain gages are located on one side of the main shaft, or tool-holder, immediately adjacent to the specimen. There are two four-gage bridges - one for bending and one for torque. Next to the gages is a slip-ring-brush assembly which electrically connects the rotating shaft with the stationary instrumentation. The output is amplified and permanently recorded photographically by means of a Minneapolis-Honeywell Visicorder.

The Test Specimen

The test specimen, shown in Figure 4, is six inches long and is composed of SAE 4340 steel. Its major diameter is 0.750 inches. A stress concentration factor is incorporated in the center by means of a groove, giving a minor diameter of 0.500 inches. The radius of the groove is 0.150 inches. A keyway is located at each end of the specimen for the positive application of the torque.

The Collet Assembly

The specimen is rigidly held in the drive shaft with a collet-type tool-holding fixture. This makes it possible to rapidly install and remove specimens. The Balas tool-holder, Part No. S16-8"-C12 with collet, Part No. C-12 was used for this purpose. The holder was altered slightly so that the test specimen key would fit properly. The key prevents relative motion between the specimen and the collet, thus enabling the positive transmission of torque.

Electric Motor

The fatigue machine is powered by a General Electric, induction, squirrel cage, 440-volt, three-phase, Type K, Tri-Clad, 700-line motor. This motor has a NEMA 213T frame. It fulfills the design requirements of 7.5 horsepower, 1,800 rpm, 440-volt, 3-phase motor. The control system consists of a magnetic starter with an off-on push button and the proper fuses.

Flexible Couplings

Sier-Bath, all steel, flexible couplings are used because of their ability to transmit torque and allow relative movement of shafts holding the test specimen for proper transmission of the bending moment. In addition, they are small in size and relatively low in cost. There are two Sier-Bath couplings located at either end of the two halves of the front shaft and a larger one on the back shaft. There are shrunk-fit on the shafts.

Gear Box

A Falk Corporation gear reducer box is used. It has a mechanical horsepower rating of 210 horsepower and a thermal rating of 272 horsepower, with cooling fans. Its speed is 1,800 rpm, and it has a AGMA gear ratio of 1.84.

Method of Torquing

The torque is applied to the specimen by means of a HDUI-200 Infinit-Indexer made by the Harmonic Drive Division of United Shoe Machinery Corp., Beverly, Massachusetts. The Infinit-Indexer has a flexible circular gear rotating within a slightly elliptical flexible, spline-like, outer gear. At the major axis the gear teeth do not mesh. When the shaft turns, the inner gear advances very slightly with respect to the outer gear inducing a steady torque. The torque level is adjusted by turning a large hexagonal shell on the outside housing of the Indexer with respect to the shaft.

Loading Frame

The loading frame is capable of producing a 3,540 in-lb bending moment in the specimen groove. There are two bearings located on each side of the front shaft. They are spherical, roller bearings with a tapered inside diameter capable of a maximum of 3° misalignment. The bearings require adapter sleeves and are SKF from service catalogue No. 450. The bearing housings are D/N UANASA-6700-E-006 type and are press fitted on to the bearings. Below

the front shaft is located a T-shaped frame which joins the bearing housings to the essentially horizontal, loading lever arm. The specifications of the lever are given in Figure 5.

Instrumentation

Strain gages are used on the tool-holder to monitor the bending and torque loads. They are not located in the specimen groove, but rather on the tool-holder directly behind the collets as shown in Figure 6. The reason for this is two-fold:

1. It is extremely difficult to mount strain gages in the limited space of the specimen groove.
2. Since the specimens are not reusable, the gages are not reusable also.

The positioning and electrical circuitry for the four-gage bending bridge is given in Figure 7. The strain gage bridge arrangement for torque is shown in Figure 8. Torque is measured by the method shown in Figure 9. These are double-gages, 90° apart and all in one piece. They are so mounted on the tool-holder surface that the two gages make 45° with the tool-holder axis of rotation. Table 1 contains the specifications of all the gages, as well as of the other electrical components. The slip-ring assembly is located adjacent to the strain gages, as shown in Figure 6. The slip-ring and brushes used are Breeze AJ-8005-A8 type. The slip-rings are counterbalanced with an aluminum collar of equal weight and nearly equal dimensions located on the other tool-holder, as shown in Figure 6. The amplifiers, galvanometers and recorder are matched units consisting of a Honeywell Model 119 carrier amplifier, M1650 galvanometers and a Model 906 C-1 recorder (Visicorder). This is the equipment used to amplify and record the output from the bending and torque gages.

2. CALIBRATION OF RESEARCH MACHINES

versus visicorder output

A. Calibration Requirements

It was desired that the bending stress and shear stress in the specimen groove be accurately known for each specimen. These two stresses cannot be monitored directly because it is not possible to locate strain gages directly in the specimen groove since each fatigue failure would destroy the gages. This would necessitate replacement of the gages after each test run. Therefore, the shear and bending stresses must be determined indirectly through the use of strain gages located on the toolholder shaft adjacent to the specimen.

The complete calibration procedure takes into account the following complications:

1. Since the strain gages are located on the toolholder rather than in the specimen groove, the groove stress must be calibrated against the strain gage output.
2. The specimen contains a groove, which introduces an additional unknown, the stress concentration factor. This value can either be taken from published data or determined through additional calibration.
3. The torque and bending gages may be damaged during installation and require calibration against a standard.
4. The torque and bending gages may be slightly misaligned during installation, and there may be interference or interaction between the torque and bending outputs.
5. There may be an axial force present in the specimen due to the geometry of the couplings and the loading frame. This axial force could be a function of the torque or the bending load, or both.

The above suggests that the following calibrations be performed:

1. Calibration of the bending gages in terms of bending stress versus visicorder output.

2. Calibration of the bending stress in the specimen groove versus visicorder output.
3. Torque interaction into the bending bridge.
4. Toolholder strain gage bending output versus specimen strain gage bending output.
5. Calibration of the torque gages in terms of shear stress versus visicorder output.
6. Bending interaction into the torque bridge.
7. Axial interaction into bending of the specimen groove gages.
8. Measurement of any axial force from torque and bending moment.

These calibrations are explained in detail on the following pages.

B. Bending Calibration

1. Visicorder output from bending strain gages on toolholder versus true stress in toolholder

Description of Test

This involved the calibration of the visicorder output in bending against the true bending stress. The true bending stress was obtained by introducing a known bending moment at the toolholder strain gages. In order that the bending moment at the gages be accurately known, it was desirable that the test set-up be as simple as possible in order that the error introduced was small when calculating the bending moment, and subsequently, the bending stress.

Test Set-up

The laboratory set-up is shown in Figure 10. The slipping side of the toolholder was removed from one of the fatigue machines. The toolholder was locked down, cantilever fashion, at the coupling end of the shaft. This was accomplished by gripping the toolholder shaft with a torque clamp-screw device between the loading bearing housing and the coupling. The screw end of the torque device was then locked in a vise on a laboratory table, thus securing the toolholder in a horizontal position. Next a small notch was machined near the end of a test specimen, and the specimen was installed in the collet of the toolholder. The purpose of the notch was to hold the wire which supports the loading pan in position. Therefore the specimen was positioned so that the notch was on top.

Electrical connection between the toolholder bridge and the amplifier was made with the use of thin uninsulated wire which was wedged between the silver plates and the di-electric on the appropriate arms of the slipping assembly. The opposite end of the wires were soldered to the correct leads of a bending bridge amplifier cable, after having been removed from the brush terminals of one of the fatigue machines.

The toolholder was removed from the clamp-screw device and placed in a vertical position, resting on the coupling. This insured that there was no bending on the strain gages while the electrical equipment was zeroed and balanced. The visicorder was zeroed and the bending bridge balanced according to the standard laboratory procedure. A five-hundred-thousand ohm calibration resistance was used for twenty-five visicorder calibration divisions. These calibration divisions were established left and right of zero bending in accordance with standard procedures.

Next the toolholder shaft was again clamped in the cantilever position, this time making sure that the bending gages were located directly on the top and bottom of the toolholder. This was accomplished in two ways:

1. A visual check to see that the gages were in the proper positions.
2. With the toolholder gripped loosely and free to rotate, the shaft was moved slightly to see where the visicorder bending output peaks and then clamped in that position.

It was necessary to have the gages aligned in this manner because the bending load was to be applied vertically, and this was the only position in which the bending gages will record full output. Finally, a stout wire was hung in the specimen notch and was attached to a loading pan.

Test Procedure

Weight was added to the loading pan in ten-pound increments until sixty pounds was reached. Then weight was removed in ten-pound increments until zero pan weight was again reached. The static strain gage output was monitored at each bending level. The visicorder output was carefully watched to see that the visicorder output returned to the same level each time zero pan weight was reached. This insured that there was no electrical drift occurring in the amplifier. Since the lever arm distance for application of the bending moment to the

toolholder gages was about seven inches and the maximum pan weight was sixty pounds, the bending moment only reached about 420 inch pounds. This was a good deal below the operating bending moment and therefore the amplifier strain gage system was extremely sensitive in this low range of operation. Because of the great sensitivity it was necessary to alter the test plan for some runs because of bending zero drift and other small problems. The sequence of the pan weights was not important as long as at least twelve data points were taken. After changing the pan weight, a wait of up to ten minutes was sometimes necessary before taking the visicorder run in order for the electrical system to reach equilibrium.

This test procedure was applied to the toolholder arms of all three fatigue machines.

It was important that the lever arm distance, the distance between the loading wire and the geometric center of the toolholder gages, be recorded before the test system was torn down.

The Data Reduction

The standard procedure for reducing data of the kind presented in Table 2 is to plot toolholder output versus pan weight and fit a straight line to the points; then convert the panweight axis to true bending stress at the toolholder and the output axis to apparent bending stress. However, this data was reduced using an analytical incremental method. This method determines the average increase in visicorder output per unit increase in pan weight. This is the slope of the above-mentioned curve. Since strain gage outputs are linear and are zero for zero load, it was not necessary to calculate the bending moment produced by the dead weight of the toolholder, thus eliminating a major source of error.

Looking at the data, it can be seen that the pan weights were not taken in ten-pound increments as previously stated. When the weights were calibrated against a standard, they were all found to be 10.27 pounds. These same weights were used throughout the entire calibration program.

First, the data were retabulated in incremental form as shown in Table 3. Note that the size of the strain increments is roughly constant, not a function of panweight; and therefore, the assumption that the data is linear is a good one.

The arithmetic average of the data was determined for each machine. These averages have the units visicorder divisions per 10.27 pounds. They had to be converted to true stress per visicorder output stress, a useful calibration parameter, which was the slope of the desired curve. The toolholder output can be converted to incremental output bending stress by

$$\Delta\sigma_o = \frac{E R_{\text{gage}}}{N_a G R_{\text{cal}}} \cdot \frac{\Delta N_{\text{vis}}}{N_{\text{cal}}} \quad (1)$$

where $\Delta\sigma_o$ = incremental output bending stress,

E = Young's Modulus for SAE 4340 steel = 30×10^6 psi,

R_{gage} = resistance of the bending gage = 190Ω ,

N_a = number of active arms in the strain gage bridge = 4,

G = gage factor = 3.23,

R_{cal} = the calibration resistance = $500 \text{ k}\Omega$,

ΔN_{vis} = the incremental visicorder output,

N_{cal} = visicorder calibration divisions.

The resulting output stresses for each machine were:

$$\Delta\sigma_{o_1} = 135.9 \text{ psi,}$$

$$\Delta\sigma_{o_2} = 129.9 \text{ psi,}$$

$$\Delta\sigma_{o_3} = 135.6 \text{ psi.}$$

where the subscripts indicate the machine numbers. These values were the apparent increase in bending strain when a 10.27 pound weight was loaded on the pan. It remained to calculate the actual bending

stress increase for 10.27 pounds of pan weight. The equation was:

$$\Delta\sigma_T = \frac{L\Delta WC}{I}$$

where

- $\Delta\sigma_T$ = incremental actual bending stress,
- L = lever arm distance,
- ΔW = incremental pan weight = 10.27 pounds,
- C = radius of the toolholder = 1.0 inch,
- I = moment of inertia of the toolholder cross-section =
0.74 in⁴.

The lever arm distances for each of the three machines were:

- L_1 = 8.745 in,
- L_2 = 8.199 in,
- L_3 = 8.237 in.

Performing the calculations, the true stresses for each machine per 10.27 pounds of pan weight were:

- $\Delta\sigma_{T_1}$ = 140.0 psi,
- $\Delta\sigma_{T_2}$ = 131.5 psi,
- $\Delta\sigma_{T_3}$ = 132.2 psi.

Forming the ratio, $K_{BTH} = \frac{\Delta\text{OUTPUT (apparent) STRESS}}{\Delta\text{TRUE STRESS}},$

$$K_{BTH_1} = 0.967,$$

A second amplifier cable was
of a fatigue machine and position

$K_{BTH_2} = 0.902$,
wire is BTH₂ and connected them

in the proper arrangement for

$K_{BTH} = 0.972$.
designed to accommodate a two-gage

bridge. The connections were

These parameters will not be used directly in the calibration
procedure presented in Section IV-E but have a variety of uses in
the daily operation of the fatigue machine. This parameter can be
used to determine true stress at the toolholder gages and is extremely
useful to have on hand.

2. Visicorder output from bending strain gages in specimen
divisions. This correlation of
groove versus true stress in specimen groove

Description of Test

In a previous section, it was pointed out that the fatigue test
specimen does not ordinarily contain strain gages in the groove.
But for calibration purposes, two test specimens with bending gages
in the grooves were prepared. Before these specimens can be used
in the calibration of the fatigue machines, their bridge outputs must
first be compared with the analytically determined true bending
stress in the specimen groove.

Since this calibration is identical in nature to the toolholder
strain gage calibration presented in the previous section, the same
test set-up was used. Indeed, it was possible to run the two tests
simultaneously.

Test Set-up

Instead of using an ordinary test specimen in the bending canti-
lever test set-up, the specimen with the gages in the groove was
used. It was locked in the collet with the bending strain gages
exactly on the top and bottom of the specimen. Therefore, the gages
on the toolholder and in the groove lined up. Once again, a notch
was machined at the extreme end of the test specimen in order to guide
the loading wire and maintain a constant lever arm.

A second amplifier cable was removed from the brush terminals of a fatigue machine and positioned near the cantilever system. Thin wire leads were connected from the strain gage terminals to the cable in the proper arrangement for a two-gage bridge. The amplifier is designed to accommodate a two-gage bridge as well as a four-gage bridge. All connections were soldered and insulated.

Test Procedure

The test procedure was identical to that in Section IV-B-1; however, instead of monitoring just the toolholder output, the groove output was also recorded. The calibration resistance used for the groove amplifier channel was 30 k Ω with the visicorder set at 25.0 divisions. Upon completion of the test, both lever arm distances were recorded.

Data Reduction

A glance at the data in Table 4 shows that the groove outputs for Machines #1 and #3 are not presented in form of visicorder divisions. The reason for this is that at the time of the tests, some difficulty was being experienced in balancing the specimen groove bending bridge with the Honeywell amplifier. Therefore, a static strain indicator was briefly substituted for the amplifier and visicorder. The strain indicator allows for the setting of the gage factor and bridge size and then gives strain directly in microinches per inch.

The data from Machine #2 was reduced by the incremental method which was presented in Section IV-B-1. The change in visicorder output for each 10.27 pound pan weight increment was determined. The changes in output were then averaged. The results are given in Table 5.

The incremental output stress in the groove was then calculated as follows:

$$\Delta\sigma_{o_2} = \frac{E R_{\text{gage}}}{N_a G R_{\text{cal}}} \frac{\Delta N_{\text{vis}}}{N_{\text{cal}}} \quad (1)$$

where

$$E = 30 \times 10^6 \text{ psi,}$$

$$R_{\text{gage}} = 120\Omega,$$

$$N_a = 2,$$

$$G = 2.08,$$

$$R_{\text{cal}} = 30 \text{ k}\Omega,$$

$$N_{\text{cal}} = 25.0 \text{ divisions,}$$

$$\Delta N_{\text{vis}} = 2.358 \text{ divisions,}$$

$$\Delta \sigma_{o_2} = 2718 \text{ psi.}$$

For Machines #1 and #3, the static strain gage indicator outputs were averaged for each panweight level. Then the incremental output strains were determined and averaged. The results are given in Table 6. The result is an overall average of the increase in strain in the groove for a 10.27 pound increase in pan weight. This average is then converted to incremental output stress.

$$\Delta \sigma_{o_1} = E \Delta \epsilon_{o_1} / 2 = (30 \times 10^6) (170.7 \times 10^{-6}) / 2 = 2560 \text{ psi}$$

$$\Delta \sigma_{o_3} = E \Delta \epsilon_{o_3} / 2 = (30 \times 10^6) (172.7 \times 10^{-6}) / 2 = 2589 \text{ psi}$$

The next step was to determine the true bending stress in the groove analytically using

$$\sigma_{\text{GR}} = \frac{MC}{I} \quad (2)$$

But the use of this equation is deferred until the next section, (IV-B-2.1), because of the complication which is introduced by the presence of stress concentration in the groove. This stress

concentration factor, not yet determined so far, must be included in Equation 2.

2.1 Experimental determination of the average stress concentration factor in specimen groove

There are two unknowns: K_t , the stress concentration factor for the specimen groove, and K_{BGR} , the visicorder output stress versus true stress curve slope. Since the procedure in Section IV-B-2.2 was the only experimental test, it was necessary to somehow extract both of these unknowns from this single test. A rigorous determination of K_t and K_{BGR} is not theoretically possible, but it was felt that even a less precise development is more desirable than resorting to tabular values of theoretical stress concentration factors.

The method used for determining K_t and K_{BGR} was the following: For each machine, the incremental output bending stress in the groove was set equal to the incremental true stress.

First, it was calculated $\Delta\sigma_o = \Delta\sigma_T$

or,

$$\Delta\sigma_o = K_t \frac{\Delta WLC}{I}$$

Solving for K_t

$$K_t = \frac{\Delta\sigma_o I}{WLC} \quad (3)$$

The solution of Equation 3 for each machine gives

$$K_{t_1} = 1.240$$

$$K_{t_2} = 1.160$$

$$K_{t_3} = 1.445$$

Definition of K_t

Since the same specimen was used for each of the three tests, the stress concentration factor must be the same. Its value was taken to be the arithmetic average of the three values. Therefore, the effective static stress concentration factor for all specimens is 1.28. This is a static stress concentration factor because the calibration procedure used was static in nature.

Next, it was necessary to allow for variation from machine to machine. This is reflected in the value of K_{BGR} for each machine.

First, $\Delta\sigma_T$ was calculated using the newly determined value of K_t , or

$$\Delta\sigma_T = K_{ave} \frac{\Delta WLC}{I}$$

Then K_{BGR} was calculated using the experimental results from Section IV-B-2,

$$K_{BGR} = \frac{\Delta \text{Output Stress}}{\Delta \text{True Stress}}$$

The results for each machine were

$$K_{BGR_1} = 0.967$$

$$K_{BGR_2} = 0.902$$

$$K_{BGR_3} = 0.972$$

K_{BGR} will be used in the data reduction technique of Section IV-E.

3. Torque Interaction into Bending Bridge Output

Description of Test

For the bending strain gages on the toolholder to perform satisfactorily, they must be in the proper position on the shaft and must have the correct orientation. No matter how much care is taken, due to human error during installation, the gages will always be slightly out of position. The effect of such misalignment is interaction of the torque load with the bending bridge output. The extent of this interaction and its direction must be determined. The procedure used was to maintain a constant bending load and vary the applied torque. A set-up was used, whereby the change in the bending bridge output was only due to torque interaction.

Test Set-Up

Because of its simplicity, a cantilever-type set-up was again used. A torque arm was needed to apply torque to the toolholder. This device was a standard test specimen with a steel bar welded perpendicular to the specimen at the groove. The bar was approximately thirty inches long and has a small hole near the far end through which a wire was strung to support a loading pan, as shown in Figure 11. The toolholder was cantilevered in exactly the same way as in previously described calibrations. Once again, the toolholder bending gages should be directly on the top and bottom of the shaft for full bridge output.

In this test, it was necessary to monitor bending and torque toolholder outputs; therefore, two amplifier cables were used and

were connected to the slip-ring by fine wires in the manner described in the earlier calibrations.

Next the specimen with the torque arm was placed in the toolholder collet. A key was placed in the keyway on the specimen so that the collet could support the torque without the specimen slipping. The specimen was then tightened in the collet with the loading pan, and the torque arm was placed in a position slightly above the horizontal. The reason for this was that the torque arm deformed elastically during loading. Using a level, the torque arm was positioned so that it was about one half a degree above the horizontal in the no-load configuration and one half a degree below the horizontal when the maximum load was applied. It should be noted that the error introduced by the change in lever arm distance due to elastic deformation of the torque arm is a function of the cosine of the change of the angle and is negligible.

Once the torque arm was positioned with respect to the toolholder, the entire assembly was removed from the screw device and placed with the toolholder in the vertical position. Then the torque and bending bridges were balanced; the visicorder outputs zeroed, and the calibration resistances (five hundred thousand ohms for bending and three hundred four thousand ohms for torque) and the calibration divisions (twenty-five divisions for bending and forty-five divisions for torque) were set on the visicorder. Then the assembly was returned to the test configuration. Next a bending load pan was suspended directly below the specimen groove. Also a torque load pan was hung from the end of the torque arm. A plane connecting the two pans must be perpendicular to the longitudinal axis of the toolholder and specimen. This was checked through plum lines and squares. Four ten-pound weights were added to the bending pan and the test set-up was ready for torque interaction calibration.

Test Procedure

Weight was removed in ten-pound increments from the bending pan and added to the torque pan. Both the bending and the torque channels

were monitored. When the weights were changed, there was a tendency for the torque arm to vibrate. This was dampened with the use of the hand. It was necessary at times to wait as long as ten minutes between data points, depending on how much drift there was in the amplifier and how long the amplifier took to reach equilibrium. When all the weight was in the torque pan, the weights were removed, ten pounds at a time, and placed in the bending pan. When all the weights were back in the bending pan, the two visicorder outputs for zero torque pan weight were compared. If they were identical, then it was concluded that no amplifier drift occurred during the data taking period and the data was good. If they did not compare favorably, then the data was scrapped, and the test was re-run. At least two good sets of up-and-down runs are needed for calibration purposes.

Data Reduction

The calibration data are presented in Table 7. After the test for Machine #3 was run, the visicorder output was closely inspected. It was found that there was no measurable change in the bending bridge output with torque load. Therefore, it was not necessary to carry the reduction any further; it was immediately concluded that there is no detectible torque interaction into bending for Machine #3.

The data from Machines #1 and #2 were reduced graphically. First, the torque bridge output in divisions was plotted versus the bending bridge output in divisions, as shown in Figures 12 and 13; then a straight line was fitted to the points. Next the slope of the curve was determined by selecting two points for the curve, and the rates of change were determined. For Machine #2, there are two sets of data and two slopes. The average slope was used. From Figure 12:

Machine #1

Point A -- (10.0, 11.912)

Point B -- (40.0, 10.425)

Conversion to strain $\Delta N_{vis\ torque} = 30 \text{ div}$

where the subscript denotes

For torque, the parameter is

$$\Delta N_{vis\ bending} = -1.487 \text{ div}$$

From Figure 13:

Machine #2

Point A -- (36.25, 18.70)

Point B -- (5.00, 17.72)

$$\Delta N_{vis\ torque} = 31.25 \text{ div}$$

$$\Delta N_{vis\ bending} = 0.98 \text{ div}$$

Next the visicorder outputs in divisions were converted to strain using Equation 1. The conversions to strain gave:

$$\Delta \epsilon_{B_1} = 1.75 \mu \text{ in/in}$$

$$\Delta \epsilon_{T_1} = -31.9 \mu \text{ in/in}$$

$$\Delta \epsilon_{B_2} = 1.15 \mu \text{ in/in}$$

$$\Delta \epsilon_{T_2} = 33.5 \mu \text{ in/in}$$

Conversion to stress instead of strain could have been used also where the subscript denotes torque or bending for Machines #1 or #2.

For torque, the parameters are:

$$R_{\text{gage}} = 120 \, \Omega$$

$$N_a = 4$$

$$G = 2.06$$

$$R_{\text{cal}} = 304 \, \text{k}\Omega$$

The slopes in terms of strain would be:

$$S_1 = -\frac{1.75}{31.9} = -0.0548 = K_{T/B_1}$$

$$S_2 = \frac{1.15}{33.5} = 0.0343 = K_{T/B_2}$$

Since stress is equal to the strain multiplied by Young's Modulus, the slope of the bending stress versus shear stress curve is identical to the strain curve slope. This slope is given the designation $K_{T/B}$ and will be used in the calibration procedure described later. Since there must be no interaction into bending for zero torque load, a plot of bending stress interaction versus shear stress could be constructed by drawing a line through the origin with slope $K_{T/B}$ and labeling the axes appropriately.

Solving for the bending stress

Note that the interaction for Machine #1 is negative, the interaction for Machine #2 is positive, and the interaction for Machine #3 is zero.

4. Relationship between toolholder bending stress and specimen groove bending stress

All previous tests involved the calibration of only the bending strain gage bridge outside of the fatigue machine. In this test, the bending bridge will be calibrated in the fatigue machine.

For an approximate analysis, it can be assumed that the bending moment along the toolholder shaft between the two loading bearings is constant. This would be true if the toolholder was weightless. Then the relationship between toolholder bending moment and specimen groove bending moment is

Determination of $M_{\text{toolholder}}$

This test involves $M_{\text{toolholder}} = M_{\text{groove}}$

The bending stresses are given by

$$\sigma_{\text{TH}} = \frac{M_{\text{TH}} C_{\text{TH}}}{I_{\text{TH}}}$$

$$\sigma_{\text{GR}} = K_f \frac{M_{\text{GR}} C_{\text{GR}}}{I_{\text{GR}}}$$

Combining these gives

$$\frac{\sigma_{\text{TH}} I_{\text{TH}}}{C_{\text{TH}}} = \frac{\sigma_{\text{GR}} I_{\text{GR}}}{K_f C_{\text{GR}}}$$

Solving for the bending stress in the specimen groove, the groove stress is obtained as

$$\sigma_{GR} = K_f \left(\frac{C_{GR}}{C_{TH}} \right) \left(\frac{I_{TH}}{I_{GR}} \right) \sigma_{TH} .$$

However, in a more sophisticated analysis, the dead weight of the toolholder must be considered. Two approaches are given. In Section IV-B-4.1, an experimental analysis is conducted. The results of these tests are applied to the calibration procedure presented later. The second approach is analytical and is presented in Section IV-B-4.2.

4.1 Toolholder strain gage output versus specimen strain gage output

Description of Test

This test involves the calibration of the bending bridge of the toolholder against the bending bridge of the specimen groove.

Test Set-Up

For this calibration to have any usefulness, the set-up must be the normal running mode of the fatigue machines. Therefore, a specimen with bending gages in the groove was installed in the toolholder collets according to the actual test procedure which is used in running specimens. For the full procedure, the laboratory checklist given in Appendix C should be consulted. The leads from the specimen were soldered directly to an amplifier, leaving some play in the leads so that the shaft can be rotated by hand a few times without causing the leads to wrap tightly around the specimen. The normal brush and slip-ring arrangement was used for monitoring the toolholder output.

The strain gage bridges were zeroed and balanced according to the checklist procedure. The toolholder shaft was rotated until the specimen groove gages were along the neutral axis, when balancing the

bridge. The toolholder gages will then be randomly oriented, which is perfectly all right since the loading frame is blocked up (see checklist procedure). The calibration resistances were 190 k Ω for the toolholder and 11 k Ω for the groove bridges, while the visicorder calibration divisions were both 25 divisions.

Test Procedure

A "quasi-static" test was run by rotating the fatigue machine shaft by hand rather than being turned full speed or left at rest, while readings were taken.

Weights were placed in the loading pan in two-and-one-half-pound increments until fifteen pounds of total weight was reached. Then the weights were removed from the loading pan at the same rate until the pan weight was zero. At each level, the toolholder shaft was rotated a few times by hand while the visicorder recorded the outputs from both bending bridges. It was made sure that both outputs showed an upper and lower peak so that the total bending width could be determined. At least twelve data points were taken.

The test was repeated for the other two fatigue machines.

Data Reduction

The calibration data are given in Table 8. The graphical reduction technique of the data was used. For each set of data, a plot of toolholder output in divisions versus groove output in divisions was made, as shown in Figures 14, 15, and 16. Straight lines were drawn to fit the data. Two points were selected on each line and the $\Delta N_{vis_toolholder}$ and ΔN_{vis_groove} were determined. Next the outputs were converted from divisions to strain by using Equation 1 with Young's Modulus removed. The results are given in Table 9. Lastly, the slopes of the toolholder bending strain versus groove bending strain plots were determined and given the designation K_{GR-TH} , with the following results:

$$K_{GR-TH_1} = 0.0203$$

$$K_{GR-TH_2} = 0.0198$$

$$K_{GR-TH_3} = 0.0215$$

Note again that the stress curve slope is identical to the strain curves slope. These parameters will be used in the calibration procedure presented in Section IV-E.

4.2 Toolholder bending stress versus specimen bending stress

In early calculations, it was assumed the bending moment along the toolholder was essentially constant between the strain gages and the specimen groove. While the assumption was acceptable during the design phases of the project, later calibration required more accurate knowledge of the change in bending moment between the strain gages and the specimen groove.

Ideally, it would be best to construct a mathematical model of the toolholder; in other words, completely describe the physical system in terms of point forces and loading functions. This involves the drawing of a free body diagram of the front shaft, so that a bending moment diagram can be calculated as a function of pan weight. In addition to being able to get the correct stress in the specimen groove for the increase in bending moment, it also becomes possible to theoretically determine the toolholder strain and compare it with the experiment results described in Section IV-B-1.

In the free body diagram of Figure 17, the weights of all the components and their positions along the shaft can be determined easily from the design data of each machine. The loadings at the

bearing housings can be expressed as a function of the pan weight if an analysis of the loading frame is undertaken.

To complete the mathematical model, the operation of the couplings at either end of the toolholder had to be fully understood. It was believed that a single-valued resisting moment, reaction force and pivot point could be associated with the coupling mechanism. An experiment was proposed and initiated to determine these three unknown parameters. A specimen was placed in the machine and the machine was set up as if it was about to be run. However, the chuck on one side was held only at one end. Then the opposite side of the machine was supported in a level position so that the linkage would exert an equal force on each section of the shaft when the machine was loaded. Next, a balance system was rigged above the machine, as shown in Figure 18. Care had to be taken to insure that the wire connected to the specimen was vertical at all times. Also, the balance bar had to be horizontal. A bubble-type level was attached to the top of the chuck with a rubber band. This was used to tell when the shaft was in a level position. Then a pointer was attached to the chuck. A scale was then connected to the opposite safety bridge and the pointer adjusted so that it would read out increments on the gage. The graduations on the scale stood for no physical quantities; they were only for reference.

Data Taking Procedure

First the machine was loaded in the lower weight pan. Five data points were taken starting at zero loading and increasing in five-pound increments to twenty pounds. Each load was carefully centered in the loading pan so that the load was balanced at all times. Then the balance pan was loaded until the force in the wire was great enough to lift the shaft to approximately a level position as indicated by the bubble level. Then the weight in the balance pan was carefully centered and the positions of the balance pins adjusted so that all forces acted at their measured distances from the fulcrum. At this time, using the level, a zero mark (level shaft position) was recorded on the

scale. Before and after each data point was taken, the zero mark was checked to see that it had not moved. Now, with the observer in a seated position so that he could line up his eye with the top of the backshaft and the pointer to maintain the same parallax throughout the experiment, the system was displaced from the equilibrium position and allowed to return. Small weights were added or subtracted on the balance pan to reach an equilibrium point when the shaft was horizontal. Since the pivot point in the coupling was stiff (large resisting moment), there was little sensitivity to weight added to the balance pan. Thus it was found that sensitivity could be increased by following the procedure just mentioned, that is, displace the shaft up and down from the equilibrium position and allow it to return freely. An example is now given to help clarify the procedure.

Figure 19 shows the scale graduations. The dotted line, B, is the position the pointer would indicate when the shaft is level. If the shaft was displaced upward and allowed to return to the equilibrium position, it would stop, say, at line A. Now if the shaft was displaced downward, it would come to an equilibrium position at point C, or two full graduations below A. However, lines A and C are equidistant above and below the level point, line B, and therefore the observer considered this set of circumstances to be the sought after equilibrium position and the weight in the balance pan at this time was considered to be the weight necessary to bring the shaft to a horizontal position for a given weight in the loading pan. The problem was further complicated by the fact that the pointer would not always return to line A when the shaft was displaced upward. It would be very close to line A, and the average of the displacements upward would give line A. The same is true for line C. This would indicate that a great deal of time and trials were necessary to procure each data point. This was, in fact, the case.

When the data from the preceding experiment was reduced, it was found that the lever arm distance calculated was physically impossible.

1. The operation of the coupling was erratic and no valid mathematical mode of its operation could be determined.

2... Since the coupling operation was indeterminate, a full mathematical model could not be determined and some of the objectives of this study would have to be compromised.

Since the results of this approach indicated that the exact resisting moment at the coupling, the lever arm, and the reaction forces could not be determined with the desired accuracy. This conclusion lead to the pursuit of the different calibration procedure presented in this report.

report. The team found that the
F-35 is superior in terms of
the flight performance in the
the low speed maneuvering and
the high speed maneuvering and
the high speed maneuvering and
the high speed maneuvering and
the high speed maneuvering and

1. The first group of people who are not in the labor force are those who are not in the labor force because they are not in the labor force.

1. The first step in the process is to identify the problem or issue that needs to be addressed. This involves gathering information and understanding the context of the situation.

C. Torque Calibration

1. Torque load versus visicorder output

Description of Test

As was the case in bending, it was necessary to calibrate the torque bridge on the tool-holder against a known torque loading. With this calibration, any visicorder output of the torque channel can immediately be converted to shear stress in the tool-holder. Since the applied torque is constant along the tool-holder shaft, shear stress in the tool-holder can be converted to shear stress in the specimen groove without further calibration.

Test Set-Up

The test set-up was identical to the system used in Section IV-B-3 to determine the torque interaction into bending. In fact, if the torque pan weights for each visicorder run are recorded at the time the torque interaction into bending calibration is run, then the same data can be used for both tests. This procedure was followed for all three machines.

Data Reduction

The calibration data are given in Table 10. The pan weight versus torque output plots are given in Figures 20, 21, and 22. A straight line was fitted to each set of data and two points are selected off each curve. The delta values were determined; the pan weight was converted to true torque using:

$$\Delta T = \Delta WL$$

$$\Delta \tau_{\text{true}} = \frac{\Delta TC}{J}$$

where

ΔW = increment of pan weight ,

L = torque lever arm distance ,

ΔT = increment of torque ,

C = radius of toolholder at the torque bridge ,

J = polar moment of inertia at the torque bridge .

The torque output was converted to apparent shear stress using reduction Equation 1. Lastly, the slopes were determined and given the designation K_T . The results appear in Table 11.

2. Bending Interaction into the Torque Bridge Output

Description of Test

If the torque strain gages in the toolholder torque bridge were slightly misaligned during installation, then there will be an interaction between the torque bridge output and the bending load. This interaction must be determined experimentally for each torque bridge. The method used in Section IV-B-3 to determine the effect of torque on the bending bridge output was used again. The torque load was varied, and the change in the torque bridge output recorded.

Test Set-Up

If the torque load applied to the torque bridge is allowed to be zero, then the set-up, Figure 10, used in Sections IV-B-1 and IV-B-2 can be used. Thus, three different calibration tests can be run with the same set-up, greatly reducing the time necessary to complete the calibration of the fatigue machines.

In this test the torque bridge and bending bridge outputs needed to be monitored. The cantilever system was connected electrically as described in Section IV-A.

Test Procedure

Weight ~~was~~ placed in the loading pan in ten-pound increments, as in Figure 10. A visicorder run was taken after each weight increase. One hundred ten pounds was the maximum pan weight used. From twelve to thirty data points were run depending on the reproducibility of the data. Each time zero pan weight was reached, the visicorder position was noted and compared with the previous one. If the difference was greater than 0.1 divisions, it was concluded that amplifier drift has occurred and the points between the zeroes were omitted.

Data Reduction

The calibration data are given in Table 12. For Machines #1 and #2, the data of bending bridge output was plotted against the torque bridge output, as shown in Figures 23 and 24. A straight line was fitted to the data and the slope of the line determined by taking incremental changes in torque and bending outputs and converting them to strain. Then the values were ratioed.

For Machine #1, two points on curve are:

Point A -- (8, 0.15)

Point B -- (0.35, -0.1)

$$\frac{\Delta N_{vis}}{\Delta N_{bending}} = 7.65$$

$$\frac{\Delta N_{vis}}{\Delta N_{torque}} = 0.25$$

Using Equation 1,

Since for more bending, the
 most elastic part of the
 casing was used.

$$\Delta\epsilon_B = \frac{(7.65)(190)}{(25.1)(4)(3.23)(6.5)(10^6)} = 8.97 \mu \text{ in/in}$$

The Machine #2 data was
 tabulated as follows:

$$\Delta\epsilon_T = \frac{(0.25)(120)}{(44.9)(4)(2.06)(0.304)(10^6)} = 0.267 \mu \text{ in/in}$$

ferent plotting system and get a

25. A line was plotted to give

minutes.

$$\text{Slope} = \frac{\Delta\epsilon_T}{\Delta\epsilon_B} = \frac{0.267}{8.97} = 0.0298$$

Sample

-3-11-55

For Machine #2, two points on curve are:

Point A -- (40.0, 1.8)

Point B -- (12.5, 0.45)

The first subject was through the

was completed by the test.

$$\Delta N_{vis. \text{ bending}} = 27.5$$

number of the electrical

The remaining four steps were

-3-11-55. Then the conversion

$$\Delta N_{vis. \text{ torque}} = 1.35$$

Using Equation 1,

$$\Delta\epsilon_B = \frac{(27.5)(190)}{(25.0)(4)(3.23)(500)(10^3)} = 33.58 \mu \text{ in/in}$$

Machine #2 data was

shown in the following

$$\Delta\epsilon_T = \frac{(.135)(120)}{(44.8)(4)(2.06)(350)(10^3)} = 1.255 \mu \text{ in/in}$$

$$\text{Slope} = \frac{1.2555}{33.58} = 0.0374$$

Since for zero bending, the bending interaction into torque must also be zero; the slopes are all that are needed to completely define the interaction. The slope was given the designation $K_{B/T}$.

The Machine #3 data were reduced slightly differently. The tabulation of the data in Table 12 shows that the datum of the data was shifted with each subset. Therefore, each subset was given a different plotting symbol, and the data was plotted as shown in Figure 25. A line was fitted to each subset, and the slopes were determined.

Test Set	Symbol	Slope
For this test, a slope of	o	-0.02835
Reversed torque, for torque	□	-0.0608
target, for subset, for	x	-0.0409
effect of torque on the bending	Δ	-0.0591
	*	-0.0543

The dot subset was thrown out because it is far out of line. This was justified by the fact that this data was taken first, and equilibrium of the electrical equipment may not have been established.

The remaining four slopes were averaged. The average slope is -0.0538. Then the conversion to strain was made.

$$\text{Slope} = \left(\frac{R_{\text{gage}}}{N_{\text{cal}} N_{\text{a}}^{GR} \text{cal}} \right) \left(\frac{N_{\text{cal}} N_{\text{a}}^{GR} \text{cal}}{R_{\text{gage}}} \right) \left(\frac{N_{\text{vis torque}}}{\frac{5N}{2} \text{vis bending}} \right) = -0.01698$$

The coefficient of the bending visicorder divisions is a correction factor made necessary by a change in the attenuation on the bending channel of the amplifier.

2.1 Effect of bending on torque bridge output - additional test

Description of Test

From the definition of interaction, it is evident that the bending interaction into torque should not be a function of the mean torque load. That is, the misalignment of the torque gages does not vary with torque load; therefore, the interaction would not vary. A spot check was necessary to show that this reasoning is correct. The result can also be extended to the torque interaction into the bending bridge output. This test was only applied to Machine #2.

Test Set-Up

For this test, a high mean torque was applied to the cantilevered toolholder. The torque arm was required to apply this torque. The test set-up was identical to that used to determine the effect of torque on the bending bridge output and is that of Figure 11.

Test Procedure

Twenty pounds was placed in the torque loading pan. This weight was left untouched for the remainder of the test. The remainder of the test proceeded in the manner described for the previous bending into torque interaction calibration.

Data Reduction

The data are given in Table 13 and plotted in Figure 26. The reduction of the data was the same as that given for the previous bending into torque interaction calibration:

From two points on fitted line:

Point A -- (25.0, 26.1)

Point B -- (10.0, 25.25)

$$\Delta N_{\text{vis torque}} = 0.85$$

$$\Delta N_{\text{vis bending}} = 15.0$$

$$\epsilon_B = \frac{N_{\text{vis gage}}^R}{N_{\text{cal a}}^N G_{\text{cal}}^R} = \frac{(15.0)(190)}{(25.0)(4)(3.23)(500)(103)} = 17.65 \mu \text{ in/in}$$

$$\epsilon_T = \frac{N_{\text{vis gage}}^R}{N_{\text{cal a}}^N G_{\text{cal}}^R} = \frac{(0.85)(120)}{(44.8)(4)(2.06)(350)(103)} = 0.788 \mu \text{ in/in}$$

$$\text{Slope} = \frac{0.788}{17.65} = 0.0447$$

This compares favorably with the slope presented for the zero mean torque interaction and therefore, for Machine #2, the average of the two, 0.0410, is taken to be $K_{B/T}$.

D. Axial Effects

1. Effect of axial load on bending bridge output

Description of Test

It was not known whether the loading configuration of the fatigue machines imparts an axial stress in the test specimen. If there is such a force, then it must either be eliminated or accounted for in the determination of the stress ratio. The axial stress could be zero, a constant, a function of bending load, a function of torque load, or a function of both bending and torque loads. This axial stress must be accounted for in order to complete the calibration of the fatigue machines.

The tool-holder bending bridge was set up so that it measured the bending strain and canceled out any axial force applied. If two of the arms on the bridge are reversed, the bridge will now measure the axial load, cancel out any bending load. A preliminary step in the measurement of the axial stress was to determine if any axial load interaction into the bending bridge output was present. If there is no interaction, then any change in the axial stress bridge, when a bending load is applied, will be a true measure of the axial stress in the specimen groove. If there is interaction, then the corrected output will be a measure of the axial force.

The test to be performed was not bending interaction into the axial bridge, but the axial interaction into the bending bridge. Since any interaction is due to misalignment of the bending gages, if one form of interaction is present, then the other must also be present.

Test Set-Up

The tool-holder was removed from the fatigue machine and placed in a vertical position, resting the coupling end on a hard, level surface. A specimen with gages in the groove was installed in the collet. The bending bridge of the specimen was connected to the amplifier. Then the amplifier channel was balanced. A

weight pan was next balanced on the end of the specimen and a visicorder run taken. Then weight was stacked in ten-pound increments on the pan until sixty pounds was reached. The bending bridge output was recorded after each addition of weight.

Data Reduction

The visicorder output showed that in all cases there was no measurable axial interaction into the bending bridge. From a previous discussion, it can also be concluded that there was no bending interaction into the axial bridge of the gaged specimen.

2. Measurement of the Axial Stress

2.1 Measurement of the axial stress as a function of bending load

Description of Test

Since it was established that there was no bending interaction into the axial stress for the gaged specimen, the axial stress could be measured.

In this first test, the axial stress was investigated as a function of the bending load. The test was conducted only on Machine #1 and the results were reduced before any decision was made about extending the analysis to the other two machines.

Test Set-Up

The specimen which was used in the axial interaction test was installed in Machine #1 according to the installation checklist. The brush assembly which monitors the tool-holder torque output was lifted from the slip-rings so that they were inoperative. The long leads from the specimen were connected to the torque terminals on the brush support so that the bridge formed would measure axial stress and cancel out bending. The tool-holder bending bridge and the specimen axial bridge were zeroed and balanced according to the checklist.

Test Procedure

With the long arm in use, weight was added to the loading pan in five-pound increments. Between each increment a visicorder run was taken while the tool-holder was turned quickly by hand. Weight was added until twenty pounds was reached, and then the test was repeated.

Data Reduction

The data are given in Table 14. A plot of the data is given in Figure 27. It shows a non-zero axial stress which is a linear function of the bending load.

The magnitude of the axial stress was determined next. For a twenty-pound range in pan weight there was a 1.7 division range in axial groove gage bridge output. Converting this to strain,

$$\epsilon_o = \frac{N_{vis}}{N_{cal}} \frac{R_{gage}}{N_a G R_{cal}} = \frac{(1.7)(120)}{(50.0)(2)(2.09)(290,000)} = 3.38 \mu \text{ in/in}$$

or in terms of stress

$$\sigma_o = E\epsilon_o = 30 \times 10^6 \times 3.38 \times 10^{-6} = 101.4 \text{ psi}$$

This is a negligible amount of axial stress. Since the pan weight range was twenty pounds on the long arm, an axial stress of about 100 psi would be the maximum that would ever be encountered in any test run. Therefore, the axial stress due to bending load can be omitted. The analysis was not extended to the other two machines because the axial stress was found to be so small that a value ten times as great would still be negligible.

2.2 Measurement of the axial stress as a function of torque load

Description of Test

Next, the axial force was measured as a function of the torque load with the bending load held constant. This test was performed only for Machine #1.

Test Set-Up

The torque brushes were placed in contact with the slip-rings and the bending gages lifted. The axial bridge of the specimen was wired to the bending terminals on the brush mount. The specimen was installed according to checklist procedures. The torque bridge and the specimen axial bridge were zeroed and balanced. Five pounds were placed in the loading pan at the end of the long arm.

Test Procedure

Torque load was varied randomly through the Infinit-Indexer and a visicorder run taken at each level. Fourteen levels were run.

Data Reduction

The data is given in Table 15. The specimen groove gage output plotted against the torque output appears in Figure 28 and is a linearly varying axial stress. The range of the stress is 3.7 divisions. The strain for this output is,

$$\epsilon_o = \frac{N_{vis}}{N_{cal}} \frac{R_{gage}}{N_a G R_{cal}} = \frac{(3.9)(120)}{(49.8)(2)(2.08)(290,000)} = 7.78 \mu \text{ in/in}$$

which is 233.4 psi in terms of stress.

This value, though larger than the one for bending load, is still negligible. The small value of the axial stress over a large range of torque indicated that the test did not have to be repeated for the other two machines.

E. Summary of Calibration Results

The calibration of the complex fatigue reliability research machines was thus completed. Bending, torque and axial interaction tests, calibration of the bending, torque and specimen groove bridges against a standard, and tool-holder bending output versus specimen groove bending output tests were thus performed for each machine. The relationship between the variables in each case proved to be linear and a slope could be associated with each calibration. Since for all cases, the functional relationship begins at the origin, the slope of each curve completely defines the function. These slopes have been given calibration coefficient designations and appear in Table 16. The two footnotes of the table are explained in Appendix E.

Now, it is necessary to combine the calibration results into an orderly method of determining the true shear and bending stresses in the specimen groove given a visicorder output, or vice versa. Actually, the calibration procedure requires that the calibration method be run in both directions. First, in any test run, the desired stress ratio and bending stress level are selected. From these, the shear stress level can be calculated and, through the use of the calibration coefficients, the number of divisions of bending and torque on the visicorder can be determined given the machine to be used, the calibration resistance, and the calibration divisions. Next, the test is run and a visicorder record taken. The record is then reduced. The four experimental parameters, bending divisions, torque divisions, bending calibration divisions, and torque calibration divisions, are measured. Using the calibration procedure in reverse direction, the actual bending stress, shear stress, and stress ratio are determined. When an entire stress level is run, some statistical comments can be made concerning the stress levels and stress ratios achieved. This is discussed in Section V-A.

Table IV contains the stress

The calibration procedure will now be described in detail with the aid of the Calibration Flow Chart of Figure 29. Steps 1 and 2 on the flow chart require a selection of a stress ratio and a bending stress level. The true shear stress in the specimen groove to give this ratio is found in Step 3 from the relationship

$$\tau_{\text{true GR}} = \frac{\sigma_{\text{true GR}}}{r_s \sqrt{3}}$$

where $\sigma_{\text{true GR}}$ is the true bending stress in the groove and r_s is the desired stress ratio. Next, in Step 4, the true bending stress in the groove is converted to output stress in the groove using K_{BGR} and then $K_{\text{GR-TH}}$, the relationship between output bending stress in the groove, is employed. On the torque side, Step 5 gives the equation for converting shear stress in the groove to shear stress in the tool-holder. This is a purely geometric relationship employing no calibration parameters. However, on the bending side an empirical relationship was necessary because the bending moment along the tool-holder shaft is not constant. For torque, it is a safe assumption that the torque applied along the tool-holder shaft is constant. The static stress concentration factor is shear, K_{ts} , is included in this term. A published value of K_{ts} , 1.22 (26), is used here. Also, in Step 5, the true shear stress in the tool-holder is converted to output stress. Steps 6 and 7 are the corrections for interaction. The shear stress value is used to correct bending stress and vice versa. The calibration coefficients are $K_{\text{T/B}}$ and $K_{\text{B/T}}$. Steps 8 and 9 convert the corrected output stresses to visicorder divisions, completing the procedure.

Table 17 contains the stress levels and visicorder divisions for $r_s = 3$ and Machine #1 using the procedure just described.

V RESEARCH DATA REDUCTION

A. Conversion of Visicorder Outputs to Stress Levels

Once the visicorder divisions for bending and torque are determined according to the methods of Section IV-E, the test runs are made. A visicorder record is made and kept for each specimen. When a stress level is complete, the shear and bending divisions, and the shear and bending calibration divisions, are measured on each visicorder record. These four values, along with the test number, specimen number, the calibration resistances, the pan weight and the machine number, are punched on IBM cards for computer analysis. A computer program in Fortran IV has been prepared which gives the actual shear stress, bending stress and stress ratio for each run, as shown in Figure 30. It also determines the mean and standard deviation of the shear and bending stresses and the stress ratio for each bending stress level assuming a normal distribution for this data.

The program contains a number of "IF" statements which select the proper machine number and mode for a data card. The mode is determined by the date on which the specimen was run.

MODE 1: For 26 July 1966 to 10 August 1967

MODE 2: For 11 August 1967 to 1 June 1969

MODE 3: For 1 June 1969 to next gage failure

A new mode is initiated whenever a strain gage on any machine fails, necessitating recalibration. Thus, the computer program differentiates between past and present machine configurations. The program is set up so that a new configuration can be integrated into the data reduction by adding three "IF" statements and listing the new calibration parameters. In addition, the program can accommodate the stress ratio infinity as well as all finite ratios.

B. Reduction of Endurance Strength Data for $r_s = \infty$ and $r_s = 0.90$

For stress ratios of infinity and 0.90, the increment used in the staircase method (27, pp. 14-17) was one pound pan weight on the short arm. Therefore, the results of the staircase method, the mean and standard deviation of the bending stress for endurance, is in terms of pan weight. It is now necessary to convert pan weight to true stress.

Just like the finite times-to-failure runs, visicorder records were made for the endurance limit runs. The visicorder records were measured, the data placed on computer cards, and a computer run made, just as described in Section V-A. Only the points which were used in the staircase method (successes or failures) were used. The output contains the bending stress levels, torque stress levels ($r_s = 0.90$ only) and the stress ratios ($r_s = 0.90$ only). Also the mean and standard deviation of the data set as a whole is outputted; however, these are meaningless for endurance runs, hence are discarded. However, the stress ratio is needed.

For a given pan weight, all the bending stresses for that pan weight were averaged. This was done for each pan weight. The result was the mean true bending stress for each pan weight.

Next, the true bending stress in the groove was plotted against pan weight for both $r_s = \infty$ in Figure 31 and $r_s = 0.90$ in Figure 32. Straight lines were then fitted to the points. Since the mean, \bar{S}_e , and standard deviation, σ_{S_e} , of the endurance strength were determined in terms of pan weight by the staircase method (27, pp. 14-17), Figures 31 and 32 made it possible to relate pan weight to true stress. The results are as follows:

For $r_s = \infty$

$$\bar{S}_e = 25.5 \text{ lbs} = 61,500 \text{ psi}$$

$$\sigma_{S_e} = 1.34 \text{ lbs} = 3,500 \text{ psi}$$

0. For $r_s = 0.90$

The mean $\bar{S}_e = 26.0 \text{ lbs} = 61,000 \text{ psi}$

standard deviation $\sigma_{S_e} = 2.25 \text{ lbs} = 3,000 \text{ psi}$

para: The mean and standard deviation of the stress ratio for $r_s =$

0.90 from the data reduction computer program, given in Appendix B, though printed out, are not intended for any use. The program is devised for finite life data; hence it automatically calculates these and prints them out.

The S-N curve for $r_s = 0.90$ is shown in Figure 3.

C. Generation of S-N Diagrams Using Distributional Stress Levels and Mean Cycles-to-Failure

The reduced data of Appendices A and B provide the mean and standard deviation of each stress level. With these distributional parameters and the corresponding mean cycles-to-failure data (27, pp. 52-54) it was possible to construct S-N curves for $r_s = \infty$ and $r_s = 0.70$, with the 3σ limits of the distribution of the actually applied bending stresses also given, assuming the stresses applied are normally distributed.

The S-N curve for $r_s = \infty$ appears in Figure 33 and for $r_s = 0.70$ in Figure 34.

D. Generation of Theoretical S-N Diagram

It would be interesting to compare the S-N diagram results generated in this research with a theoretical S-N diagram constructed according to the procedure recommended by Shigley (23, p. 162).

The fatigue strength of specimen, S_e , at 10^3 cycles $\approx 0.9S_u$

$$S_u = 178 \text{ ksi, for unnotched specimens}$$

$$S_{e10^3} \approx 0.9 \times 178$$

$$S_{e10^3} \approx 160 \text{ ksi}$$

The endurance strength is given by

$$S_e = k_a k_b k_d k_e k_f S_u' \quad (4)$$

For the specimens used in this research

$$k_a = \text{surface finish factor} = 0.89 \text{ for ground finish (23, p. 167)}$$

$$k_b = \text{size factor} = 0.85 \text{ for } D = 2.0 \text{ in. bending (23, p. 168)}$$

$$k_d = \text{temperature factor} = 1, \text{ no temperature effect}$$

$$k_e = \text{stress concentration design factor} = \frac{1}{K_f} \quad (23, \text{ p. } 170)$$

$$K_f = 1 + q (K_t - 1) \quad (23, \text{ p. } 170)$$

$$q = 0.92 \quad (23, \text{ p. } 171)$$

is given in Figure 75.

$$K_t = 1.45 \quad (26, \text{ p. } 49)$$

$$K_f = 1 + 0.92 (1.45 - 1)$$

$$K_f = 1.41$$

$$k_e = \frac{1}{1.41} = 0.709$$

$$k_f = \text{miscellaneous effects factor} = 1$$

$$S_e' = \text{theoretical endurance strength} = 0.5 S_U \quad (23, \text{ p. } 162)$$

$$S_U = 178 \text{ ksi}$$

Therefore

$$S_e' = 0.5 \times 178 = 89 \text{ ksi}$$

Using Equation 4

$$S_e = (0.89)(0.85)(1.0)(0.709)(1.0)(89) = 47.7 \text{ ksi}$$

With S_e and $S_{e_{10^3}}$ thus determined, an S-N diagram was plotted and is given in Figure 35.

E. Comparison of Theoretical and Experimental S-N Curves

In Figure 35, the theoretical and experimental S-N curves for $r_s = \infty$ and the experimental S-N for $r_s = 0.70$ are given. It can be seen that the theoretical curve is about 11% lower than the experimentally determined curve in the finite life region and the endurance strength is about 22.5% less. This indicates that the conventional approach for constructing a theoretical S-N curve is fairly pessimistic, at least for the operating conditions of this research. There is no theoretical basis for $S_{e10^3} = 0.90 S_U$ relationship. It is an accepted designer's thumb rule. A more accurate multiplier to determine the S_{e10^3} for the steel researched here would be 1.00 instead of 0.90, using the unnotched ultimate strength. A more accurate multiplier to determine S_e' would be 0.65.

From Figure 35, it can be seen that the fatigue strength decreases as torque is added to the specimen. Also, the $r_s = \infty$ and $r_s = 0.70$ lines diverge as cycles life increases. All of these are as expected.

The small standard deviations of the bending stress distributions and the stress ratio distributions at the various levels shown in Figures 33 and 34 indicate that a given stress level and stress ratio can be maintained by the fatigue reliability research machines fairly precisely. The coefficient of variation, the ratio of the standard deviation to the mean expressed as a percentage, does not exceed 2.7% for the bending stress level of $r_s = \infty$. This is shown in Figure 33. For $r_s = 0.70$ in Figure 34, the coefficient of variation for the bending stress level is at most 5.6%, and the coefficient of variation for the stress ratio is at most 8%.

A Goodman diagram of endurance strengths for $r_s = \infty$, $r_s = 0.90$, and $r_s = 0$ is given in Figure 36 which combines the fatigue and static strength results into the most useful design information for combined-stress design situations. This diagram is made possible by the data generated by this research.

VI. STRESS CONCENTRATION AND NOTCH SENSITIVITY EFFECTS

A. Stress Concentration

The best published value of the static stress concentration factor for the notched specimens used in this research is 1.45 (26). In Section IV-B-2.1, an attempt was made to isolate the effective static stress concentration factor from K_{BGR} . The resulting value was 1.28. Since the experimental value was arrived at by an averaging technique rather than by a rigid procedure of measurement, there is room for error in this result. Likewise, the published values leave much to be desired since they do not take into account the test conditions. It was felt that the experimental value was a definite improvement over the theoretical value and was used in the calibration procedure to determine the bending stress in the groove. The accuracy of the result could be improved upon by outfitting more specimens with strain gages and repeating the calibration. The same reduction technique would be used but more data points would be had to average, thus increasing the accuracy of determining the effective static stress concentration factor.

For the torque strain gage bridge a published value of the static stress concentration was used. There is an error involved in this also, as the exact stress concentration factor in shear is not known at this time. It is believed that any corrections would not be in excess of 5 percent. Nevertheless, further investigations should be initiated to obtain a better value for the static stress concentration factor in torsion.

B. Notch Sensitivity Survey

In fatigue tests the reduction in fatigue strength is found to be less than that predicted by the static stress concentration factor, K_t (24, p. 249). The ratio of the nominal fatigue strength of an unnotched specimen to that of a notched specimen is defined as the fatigue stress-concentration factor, K_f . K_f has also been called the strength reduction factor, the fatigue notch factor, and the effective stress concentration factor. Therefore, K_f can be experimentally determined by forming the ratio (23, p. 170)

$$K_f = \frac{\text{endurance limit of notch-free specimens}}{\text{endurance limit of notched specimens}} \quad (5)$$

The reduction in fatigue strength is explained by the fact that the theoretical peak stress $K_t S_n$ is lowered to $K_f S_n$ by plastic flow, where S_n is the nominal stress in the corresponding unnotched specimen (22, p. 128).

It is also useful to define the notch sensitivity factor as (23, p. 170)

$$q = \frac{K_f - 1}{K_t - 1}$$

If $q = 0$, then there is no sensitivity for the notch; while if q is unity, $K_f = K_t$, and there would be no observed reduction in the fatigue strength of notched specimens. This would be the case for perfectly elastic materials (25, p. 244).

The notch sensitivity is a very useful but also elusive parameter. As the notch radius increases, q tends toward unity as shown in Figures 37, 38, 39, 41, and 42. q also tends to unity for fine-grained, relatively homogeneous materials (23, p. 172) as shown in Figure 40. Notch sensitivity is also a function of the size of the part. K_f may be higher for large parts than for small parts (24, p. 251). Steel generally has a higher q than lower grades of iron

(23, p. 172). This can be explained by the relative grain sizes. At low cycle life, fatigue strength in notched specimens can be a little higher than notch-free specimens (25, p. 246). Finally, q may also be a function of the stress amplitude (25, p. 246). Peterson, (26) a widely used reference on notch sensitivity, does not take this into account.

C. Proposed Notch Sensitivity Determination

Unlike the value of the static stress concentration factor, the notch sensitivity of the test specimen is critical. The calibration method which was used to determine the stress concentration does not incorporate notch sensitivity because it was a static test.

In the calibration procedure, the notch sensitivity effect was not included. The reasons for this are:

1. An experimental notch sensitivity determination has not as yet been carried out, and
2. The published data of Section VI-B indicate that the notch sensitivity effect will be very small, perhaps 2 or 3 per cent. Such minor adjustments to the stress levels can be made at a later date if deemed appropriate.

Due to the irregularities and apparent contradictions in the notch sensitivity, the most accurate method of determining the appropriate value of q for the SAE 4340 notched steel specimens of this research is to do it experimentally. Then shape, size, and material errors would be eliminated. K_f , and consequently, q , can be determined experimentally by Equation 5.

It is proposed that unnotched specimens similar to those used in the $r_s = 0$ studies for this research be prepared. The number needed would be approximately 38. This is the amount needed with the staircase method of endurance strength distribution determination. Only the unnotched specimen need be run since notch endurance strength for $r_s = \infty$ has already been generated. The proposed test would give an accurate value for the notch sensitivity of these specimens.

VII CONCLUSIONS

1. The fatigue machines are extremely difficult to calibrate dynamically. Attempts were made over a period of one year to obtain valid dynamic calibrations but were abandoned because of large inconsistencies in the results. Finally, the static calibration procedure reported here was embarked upon and was successfully completed. Since all calibrations except one are gage calibrations, there is no error introduced by not calibrating dynamically. The determination of exact specimen groove stress from the toolholder gage bridge output does, however, require dynamic calibration so that the true fatigue stress concentration factor in bending can be determined. The determination of this factor requires extensive research and the minor improvements achieved may or may not be of the desired quality in view of the difficulties involved.

2. The calibration procedure is set up so that if a gage failure occurs, the fatigue machine may be recalibrated and put back into operation in three days.

3. Machine #1 has the following calibration equations:

$$N_{vis_B} = \frac{N_{cal} N_{a}^{NGR} N_{cal}}{E R_{gage}} \left[(0.967)(0.0203) \sigma_{true_{GR}} + (0.0548) \tau_{out_{TH}} \right]$$

$$N_{vis_T} = \frac{N_{cal} N_{a}^{NGR} N_{cal}}{E R_{gage}} \left[\frac{(0.0157)}{(0.882)} \tau_{true_{GR}} + (0.0298) \sigma_{out_{TH}} \right]$$

4. Machine #2 has the following calibration equations:

$$N_{vis_B} = \frac{N_{cal} N_{aGR} N_{cal}}{E R_{gage}} \left[(0.902)(0.0198)\sigma_{true_{GR}} + (0.0343)\tau_{out_{TH}} \right]$$

$$N_{vis_T} = \frac{N_{cal} N_{aGR} N_{cal}}{E R_{gage}} \left[\frac{(0.0157)}{(0.840)}\tau_{true_{GR}} + (0.0410)\sigma_{out_{TH}} \right]$$

5. Machine #3 has the following calibration equations:

$$N_{vis_B} = \frac{N_{cal} N_{aGR} N_{cal}}{E R_{gage}} \left[(0.972)(0.0215)\sigma_{true_{GR}} \right]$$

$$N_{vis_T} = \frac{N_{cal} N_{aGR} N_{cal}}{E R_{gage}} \left[\frac{(0.0157)}{(0.842)}\tau_{true_{GR}} + (-0.0238)\sigma_{out_{TH}} \right]$$

Note that there is no torque interaction into the bending channel for Machine #3 and that the bending interaction into the torque channel is negative.

6. The axial stress in the specimen was found to be negligible.

7. The effective static stress concentration factor of the specimen groove in bending was determined to be 1.28.

8. The data reduction shows that the machines were very successful in maintaining and reproducing the torque and bending loads. With other past machines difficulty has been experienced in maintaining constant bending and torque loads.

9. From Figures 33 and 34 and Appendices A and B, it may be seen that the fatigue reliability research machines maintained the desired bending stress levels with a coefficient of variation of less than 2.7% for $r_s = \infty$ and less than 5.6% for $r_s = 0.70$.

1. Calibration, test runs greatly expedited if the entire presently employed drift time on each run, consequently, the recording system, with a very slight modification.

[The page contains faint, illegible markings.]

VIII RECOMMENDATIONS

1. Calibrations, test runs, and data reduction would be greatly expedited if the amplification system was improved upon. Presently, amplifier drift must be carefully taken into account on each run, consequently, a relatively drift-free amplifying and recording system, with a very short warm up time, should be obtained.
2. A pan weight versus true stress in the groove calibration should be conducted. Although, like the determination of K_{BTH} , this relationship would not be an integral part of the calibration procedure, it has a wide variety of uses during daily operation of the fatigue machines; e.g., in determining the pan weight directly from the required bending and shear stresses.
3. The notch sensitivity determination proposal for bending should be undertaken, thus insuring that this dynamic phenomenon has been accounted for in the calibration procedure.
4. Now that experience has been gained in running the machines, the staircase method for determining the endurance strengths can be improved. Increments of bending stress rather than increments of pan weight should be used because they are more reproducible.
5. Research with these machines should be continued and expanded to include other stress ratios, notch geometries, and materials.

ACKNOWLEDGEMENTS

The contributions of the following people to this effort are gratefully acknowledged:

1. Mr. Vincent R. Lalli, NASA Project Manager.
2. H. Wilson Broome, John L. Smith, and Scott Clemans, all from The University of Arizona.

REFERENCES

1. "Designing a Specified Reliability Directly Into a Component," Dimitri Kececioglu and David Cormier, Proceedings of the Third Annual SAE-ASME-AIAA Aerospace Reliability and Maintainability Conference, Washington, D. C., June 29-July 1, 1964, pp. 546-565.
2. "Safety, Reliability and Structural Design," A. M. Freudenthal, American Society of Civil Engineers Transactions, Vol. 127, 1962, Part II, pp. 304-323.
3. "The Analysis of Structural Safety," A. M. Freudenthal, J. M. Garrelts, and M. Shinozuka, Institute for the Study of Fatigue and Reliability, Columbia University, New York, N. Y., June 1965, 129 pp.
4. "Fundamental Aspects of Mechanical Reliability from Mechanical Reliability Concepts," A. A. Mittenbergs, ASME Design Engineering Conference, New York, N. Y., May 17-20, 1965, pp. 17-33.
5. "Sixth Progress Report to MRRC Members," A. H. Clover, A. R. Rosenfield, A. A. Putnam, R. E. Mesloh, L. M. Cassidy, R. Simon, and A. A. Mittenbergs, Battelle Memorial Institute, Columbus Ohio, March 31, 1965.
6. "Methods for Prediction of Electro-Mechanical System Reliability," T. L. Bush, A. P. Meyers, and D. F. Semonaitis, IIT Research Institute Technology Center, Chicago, Ill., May 1965, 173 pp.
7. "A Model for Time Varying and Interfering Stress-Strength Probability Density Distributions with Considerations for Failure Incidence and Property Degradation," M. J. Bratt, G. Reethof, and G. W. Weber, Proceedings of the Third Annual SAE-ASME-AIAA Conference on Aerospace Reliability and Maintainability, Washington, D. C., June 29-July 1, 1964, pp. 566-575.
8. "References on Fatigue," ASTM STP 9G-9N, American Society for Testing Materials, Philadelphia, Pa., 1955-1963.
9. "Proceedings of the Symposium on Large Fatigue Testing Machines and Their Results," ASTM STP No. 216, American Society for Testing Materials, Philadelphia, Pa., 1957, p. 151.

10. "Seventy-Seven Year Index," American Society of Mechanical Engineers, N. Y., 1957.
11. "Applied Science and Technology Index," The H. W. Wilson Co., N. Y., 1958 to Dec., 1965.
12. "Proceedings of the Society for Experimental Stress Analysis," Society for Experimental Stress Analysis, Cambridge, Mass., 1943-1960.
13. "Experimental Mechanics," Journal of the Society for Experimental Stress Analysis, Easton, Pa., 1961 - Dec., 1965.
14. "A Fatigue Testing Machine for Reversed Bending and Steady Torque," H. H. Mabie and M. S. Gjesdahl, Proceedings of the Society for Experimental Stress Analysis, Vol. 14, No. 1, Cambridge, Mass., 1956, pp. 83-88.
15. Photographs and correspondence submitted to Dr. Dimitri B. Kececipglu, NASA NGR-03-002-044, University of Arizona, Tucson, Arizona, Oct., 1965, by the Falk Corporation, Milwaukee, Wisconsin.
16. Correspondence with H. H. Mabie, Professor of Mechanical Engineering, Virginia Polytechnic Institute, Blacksburg, Virginia, Sept., 1965.
17. Correspondence with Arthur H. Burr, Professor in charge, Department of Machine Design, Sibley School of Mechanical Engineering, Cornell University, Ithaca, N. Y., Oct. 1, 1965.
18. Correspondence with Arthur H. Burr, Professor in charge, Department of Machine Design, Sibley School of Mechanical Engineering, Cornell University, Ithaca, N. Y., Sept., 1965.
19. "Four-Square Test Machine," D/N 100, 8-10-51, by H. H. Mabie, Department of Mechanical Engineering, Pennsylvania State College.
20. "Four-Square Test Machine Modified," D/N 100, 9-13-57, Sibley School of Mechanical Engineering, Cornell University, Ithaca, New York.
21. Correspondence with H. H. Mabie, Professor of Mechanical Engineering, Virginia Polytechnic Institute, Blacksburg, Virginia, Jan., 1966.

22. "Metal Fatigue: Theory and Design," A. F. Madaayag, John Wiley and Sons, Inc., New York, 1969, 425 pp.
23. "Mechanical Engineering Design," J. E. Shigley, McGraw-Hill Book Company, Inc., New York, 1963, 631 pp.
24. "Stress, Strain, and Strength," R. C. Juvinall, McGraw-Hill Book Company, Inc., New York, 1967, 580 pp.
25. "Strength, Fracture, and Fatigue of Materials," T. Yokobori, P. Noordhoff, Ltd., Groningen, The Netherlands, 1964, 372 pp.
26. "Stress Concentration Design Factors," R. E. Peterson, John Wiley and Sons, Inc., New York, 1953, 155 pp.
27. "Design and Development of and Results from Combined Bending-Torsion Fatigue Reliability Research Machines," D. B. Kececioglu, M. J. Saroni, H. W. Broome, and J. McConnell, NASA, Washington, D. C., July 15, 1969, 57.
28. "Reliability Prediction - Mechanical Stress/Strength Interference," C. Lipson, N. J. Sheth, and R. L. Disney, Rome Air Development Center, Griffiss Air Force Base, New York, 1967, 450 pp.
29. "Interaction Among The Various Phenomena Involved in the Design of Dynamic and Rotary Machinery and Their Effects on Reliability," D. B. Kececioglu and E. B. Haugen, Office of Naval Research, Washington, D. C. 1968, 379 pp.

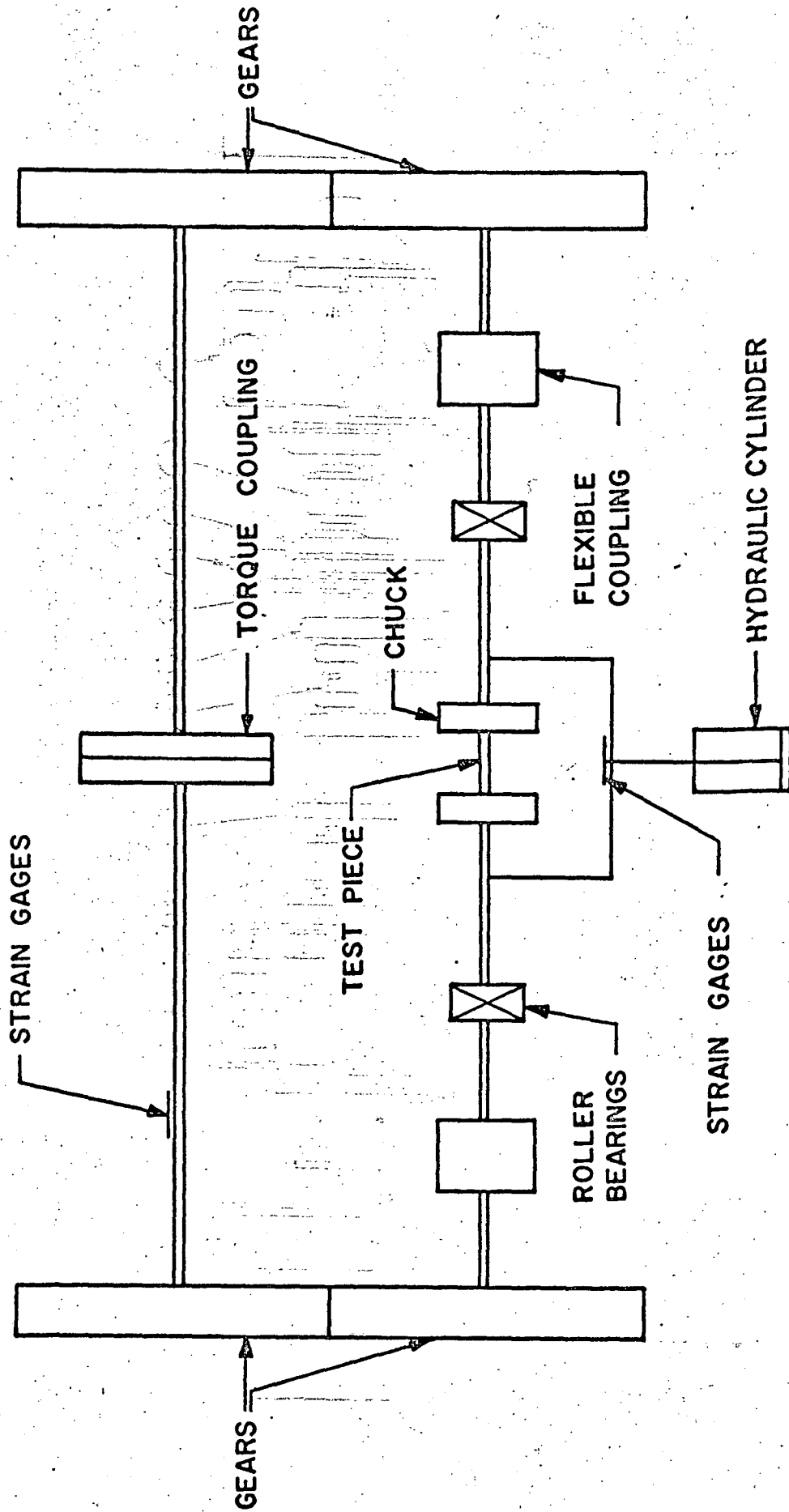
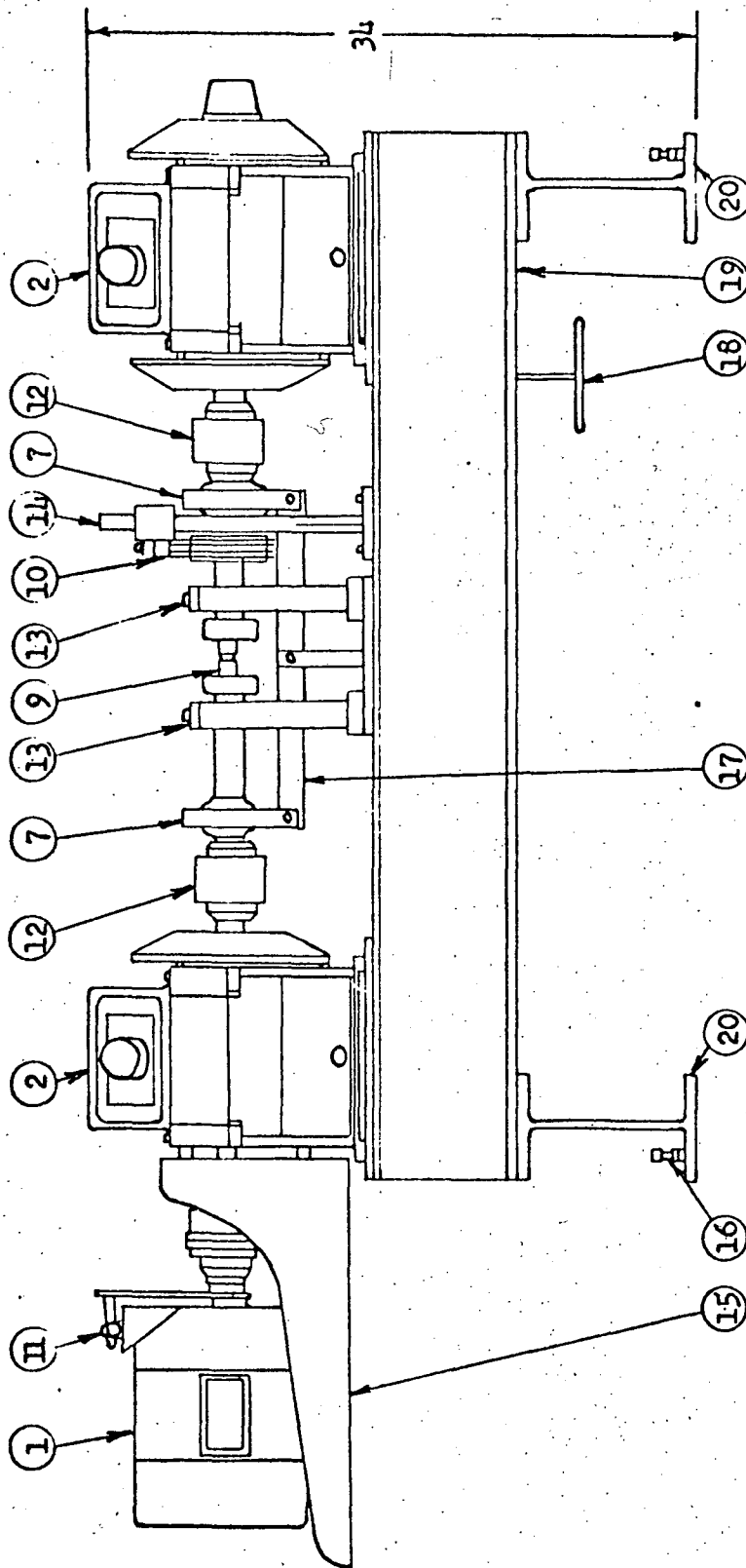


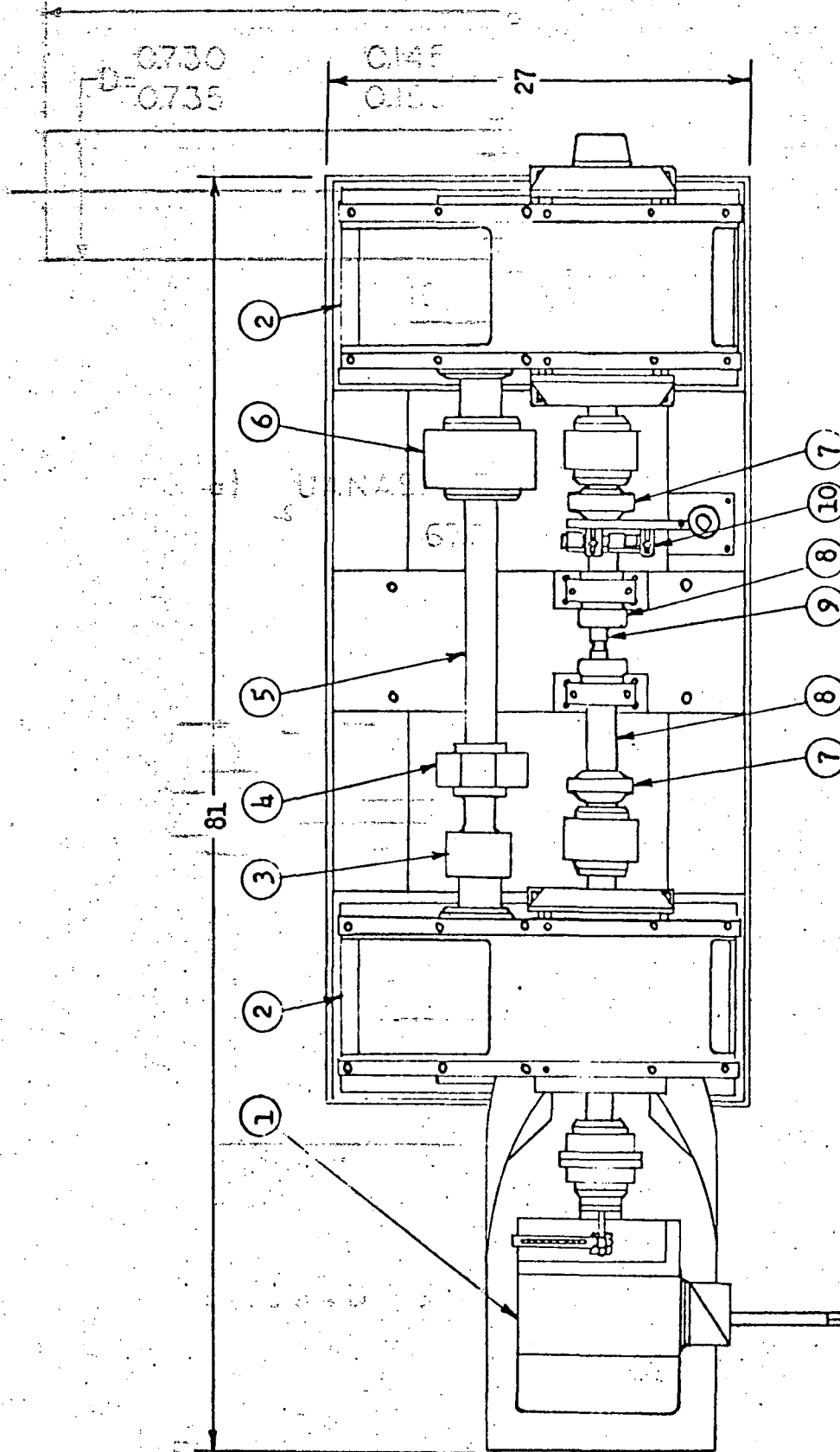
FIGURE 1. MABIE - GJESDAHL FATIGUE TESTING MACHINE



- 1. Motor
- 2. Gearboxes
- 7. Loading Frame Bearing
- 9. Test Specimen
- 10. Slip Rings and Brushes
- 11. Counter
- 12. Coupling
- 13. Safety Bridge

- 14. Brush Holder
- 15. Motor Bracket
- 16. Mount Bolts
- 17. Loading Frame
- 18. Weights
- 19. Machine Mount
- 20. Floor Mounts

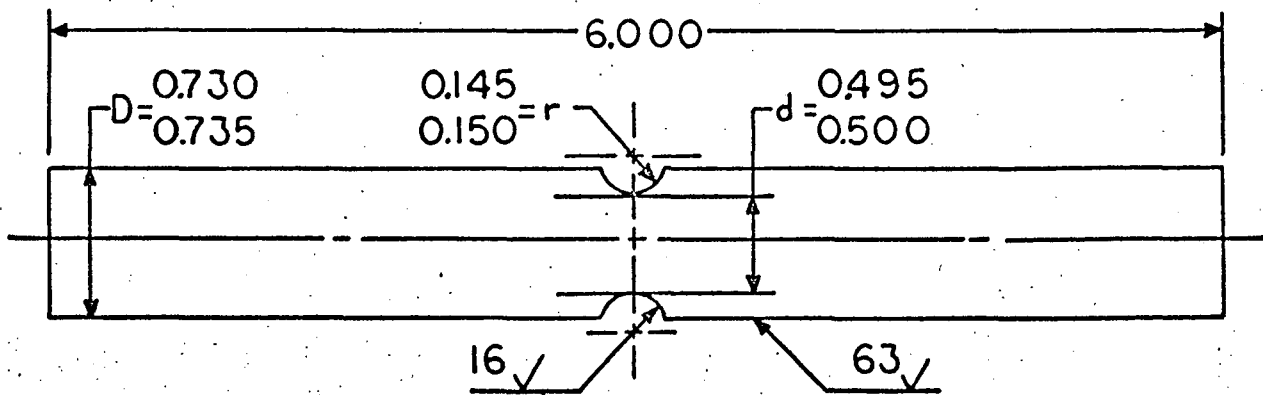
FIGURE 2. COMBINED BENDING-TORSION FATIGUE RELIABILITY RESEARCH MACHINE - FRONT VIEW



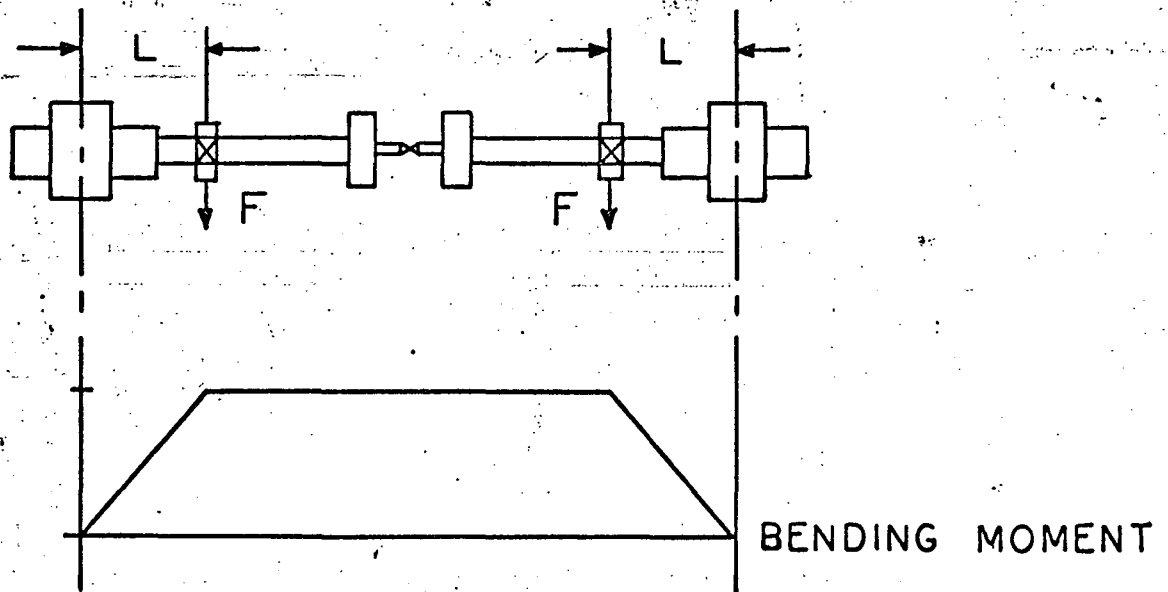
- 1. Motor
- 2. Gearboxes
- 3. Coupling
- 4. Infinite Indexer
- 5. Backshaft

- 6. Coupling
- 7. Loading Frame Bearing
- 8. Straight Shank Toolholder
- 9. Test Specimen
- 10. Slip Rings and Brushes

FIGURE 3. COMBINED BENDING-TORSION FATIGUE RELIABILITY RESEARCH MACHINE - TOP VIEW



a) UANASA TEST SPECIMEN
6700-B-002



b) LOADING FRAME ANALYSIS

FIGURE 4. LOADING FRAME ANALYSIS
AND TEST SPECIMEN

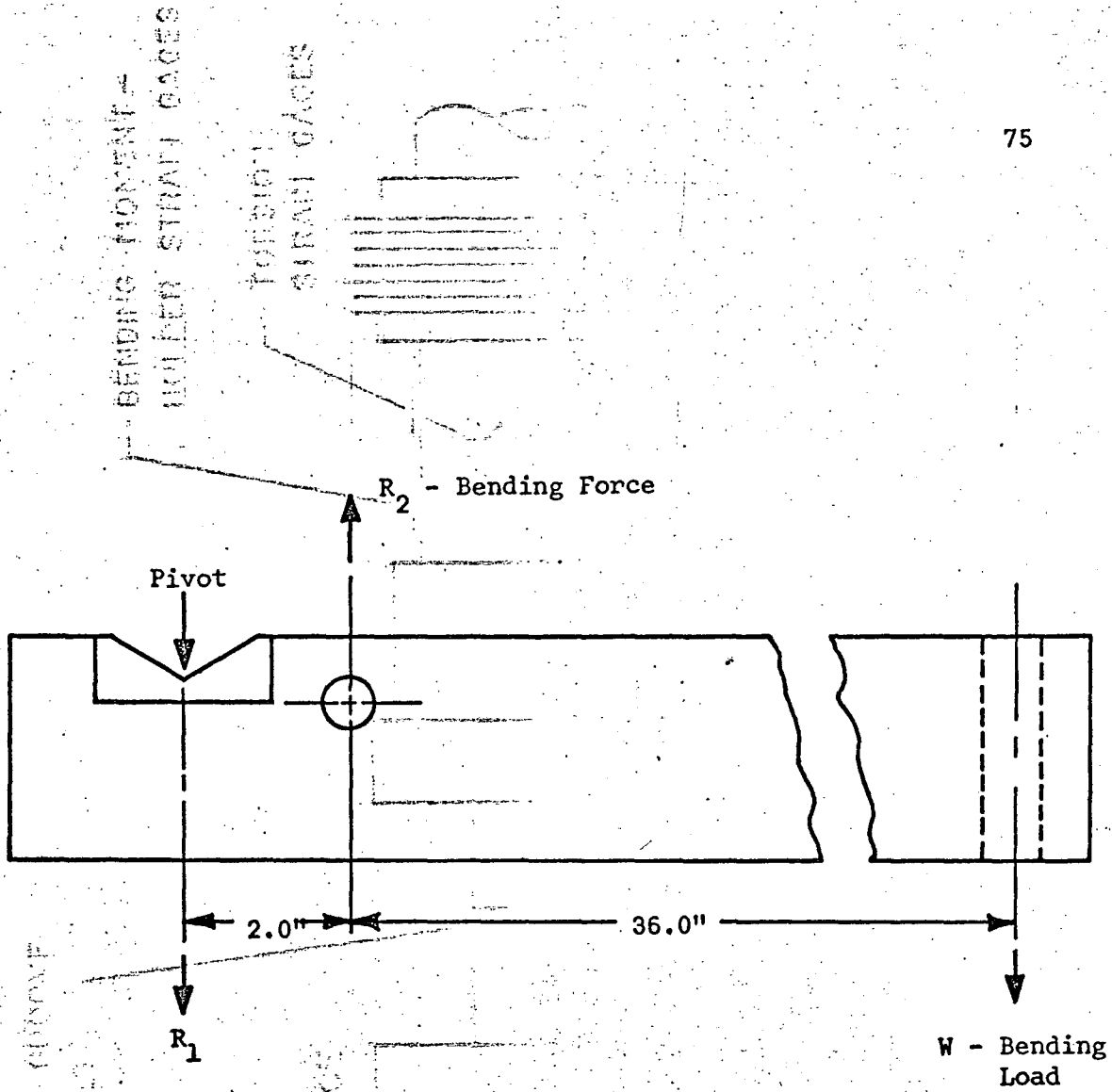
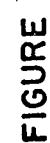
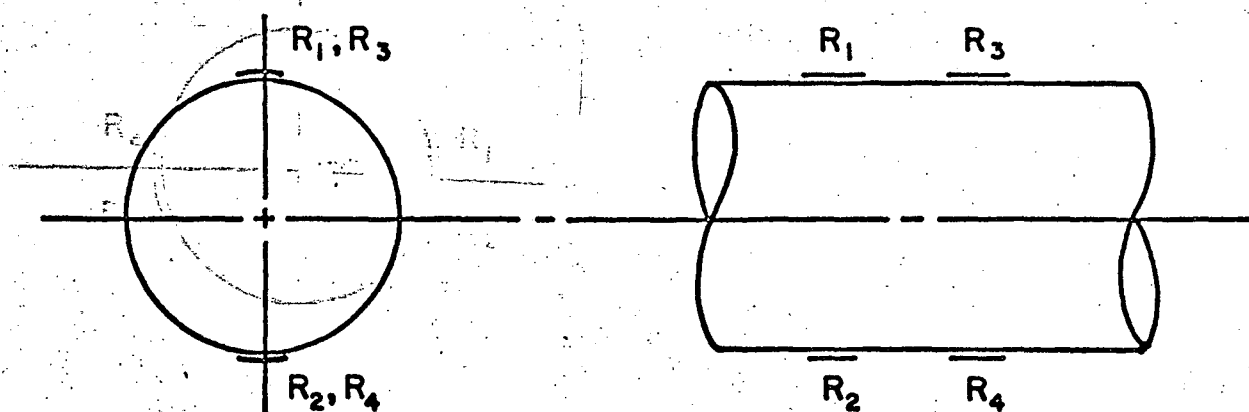
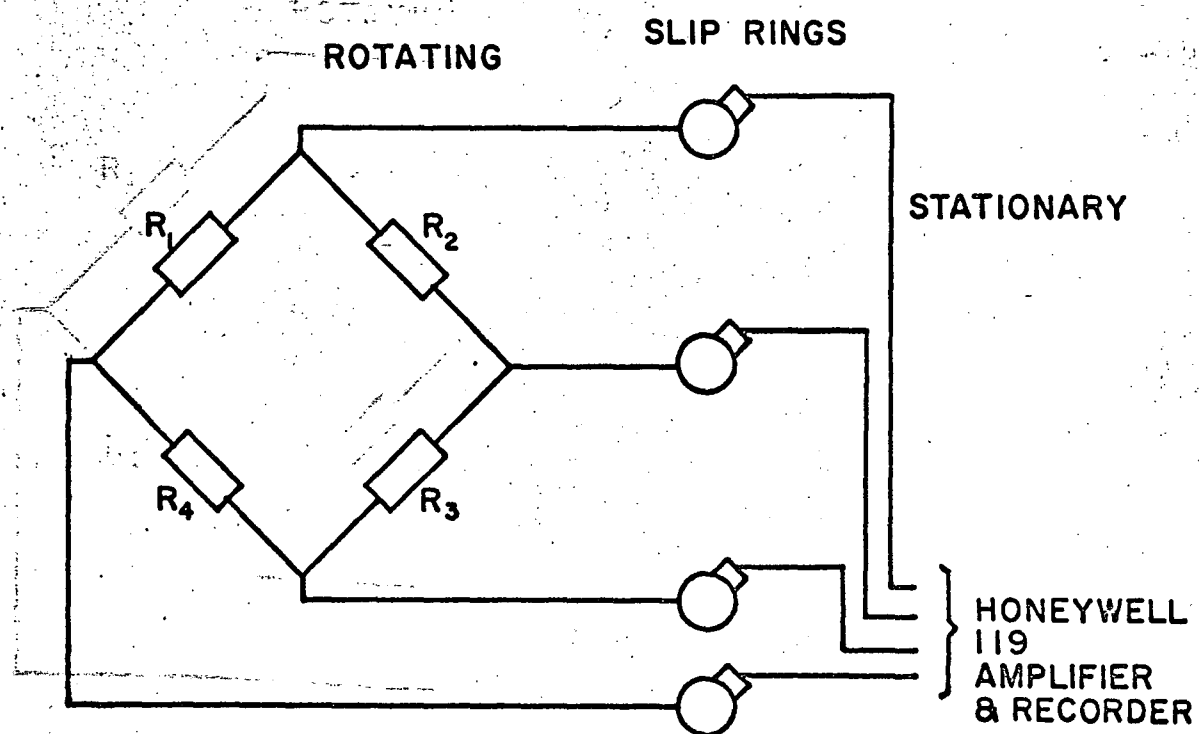


FIGURE 5. BENDING LOAD LEVER ARM.



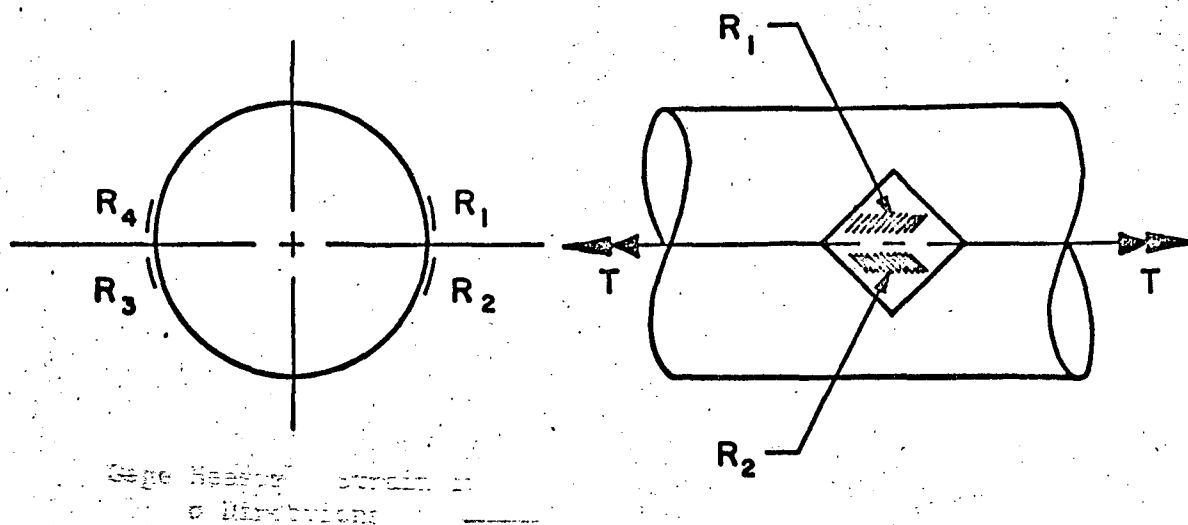


(a) BENDING MOMENT STRAIN GAGES

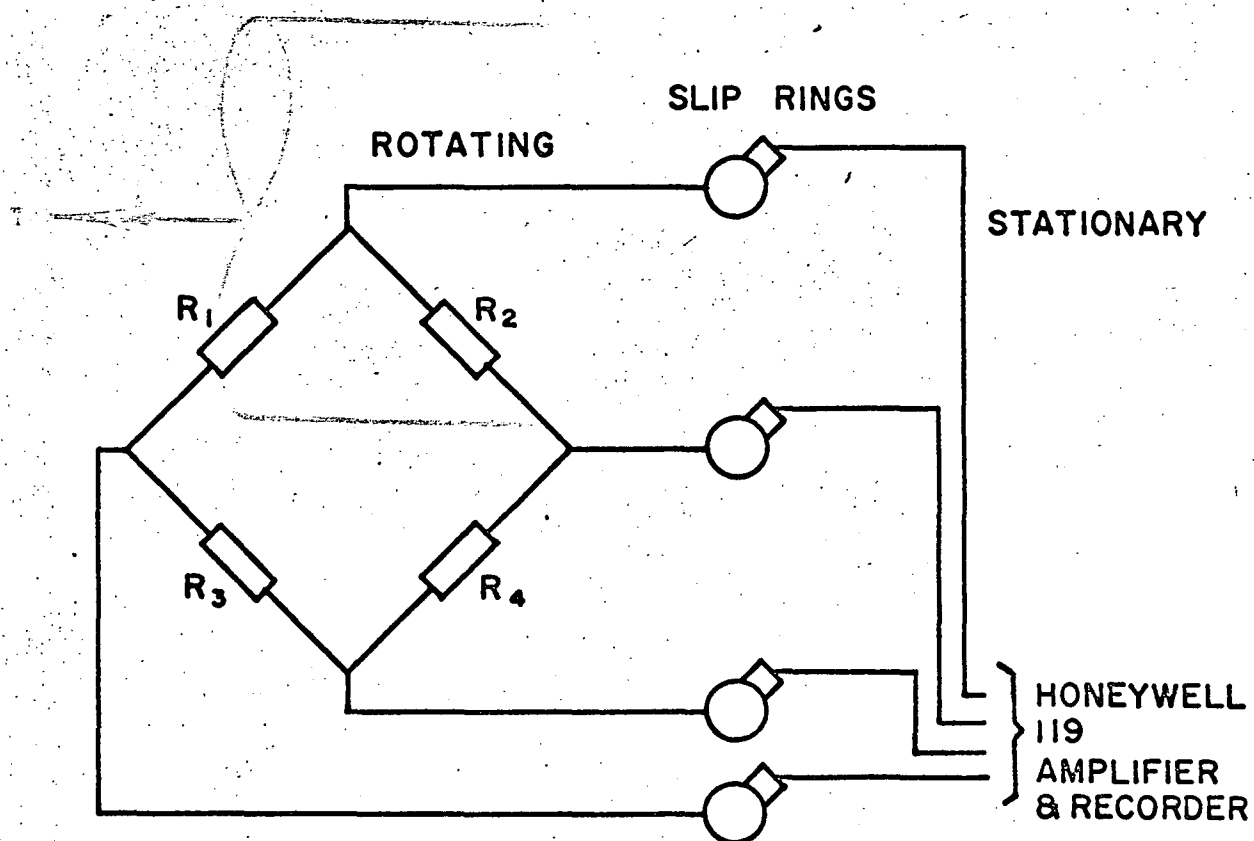


(b) STRAIN GAGE BRIDGE ARRANGEMENT

FIGURE 7. BENDING MOMENT INSTRUMENTATION



(a) TORSION STRAIN GAGE



(b) STRAIN GAGE BRIDGE ARRANGEMENT

FIGURE 8. TORQUE INSTRUMENTATION

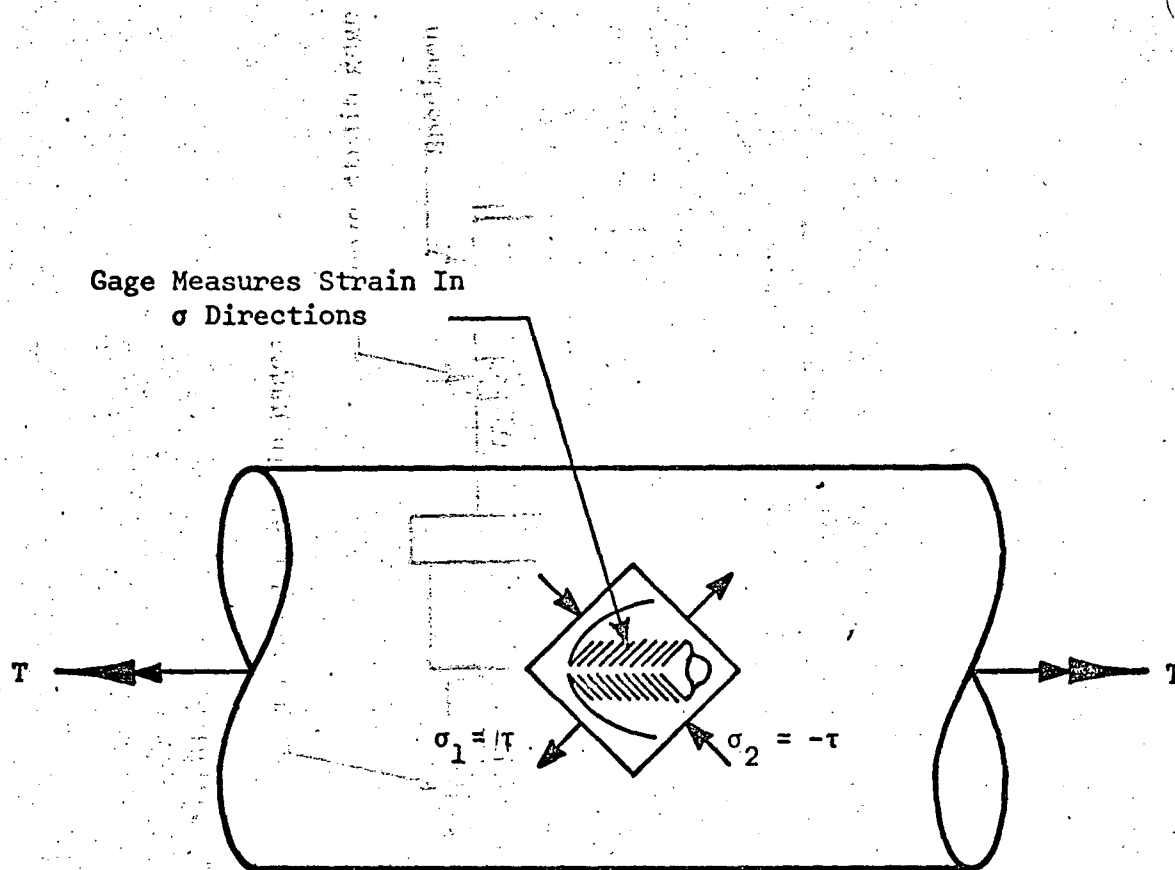


FIGURE 9. TORSIONAL STRESSES FOR ONE GAGE.

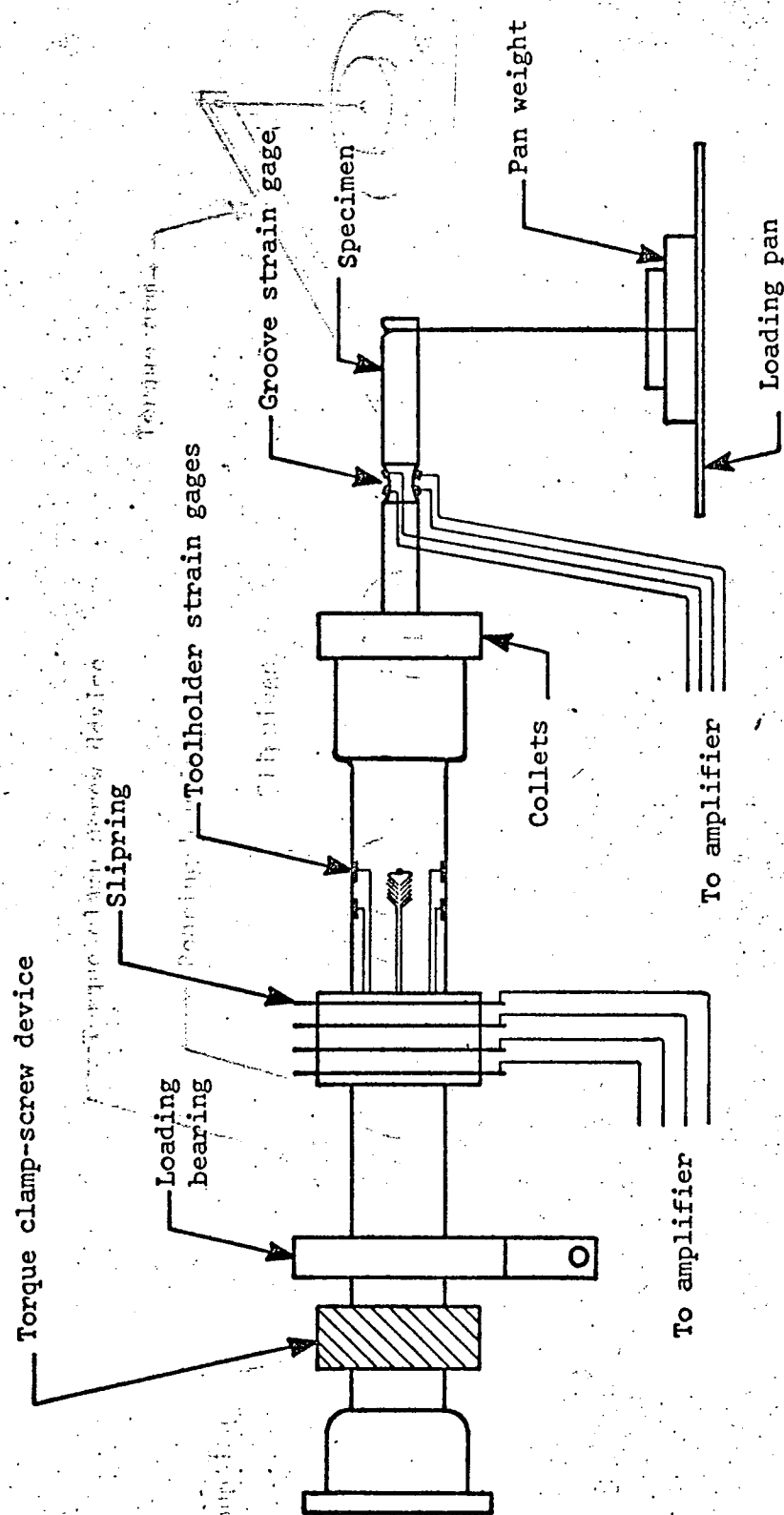


FIGURE 10. TEST SET-UP FOR THE BENDING CANTILEVER CALIBRATION.

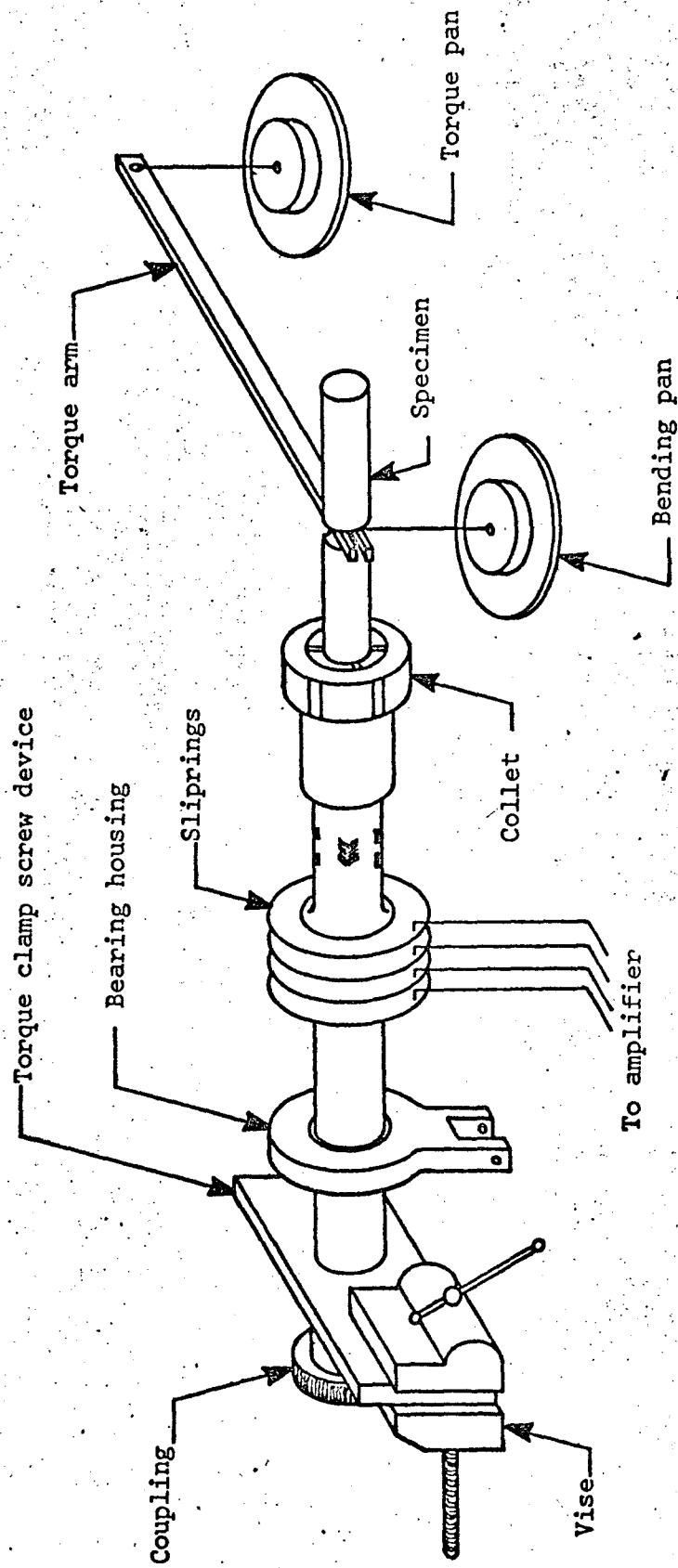


FIGURE 11. TEST SET-UP FOR TORQUE INTERACTION INTO BENDING BRIDGE OUTPUT.

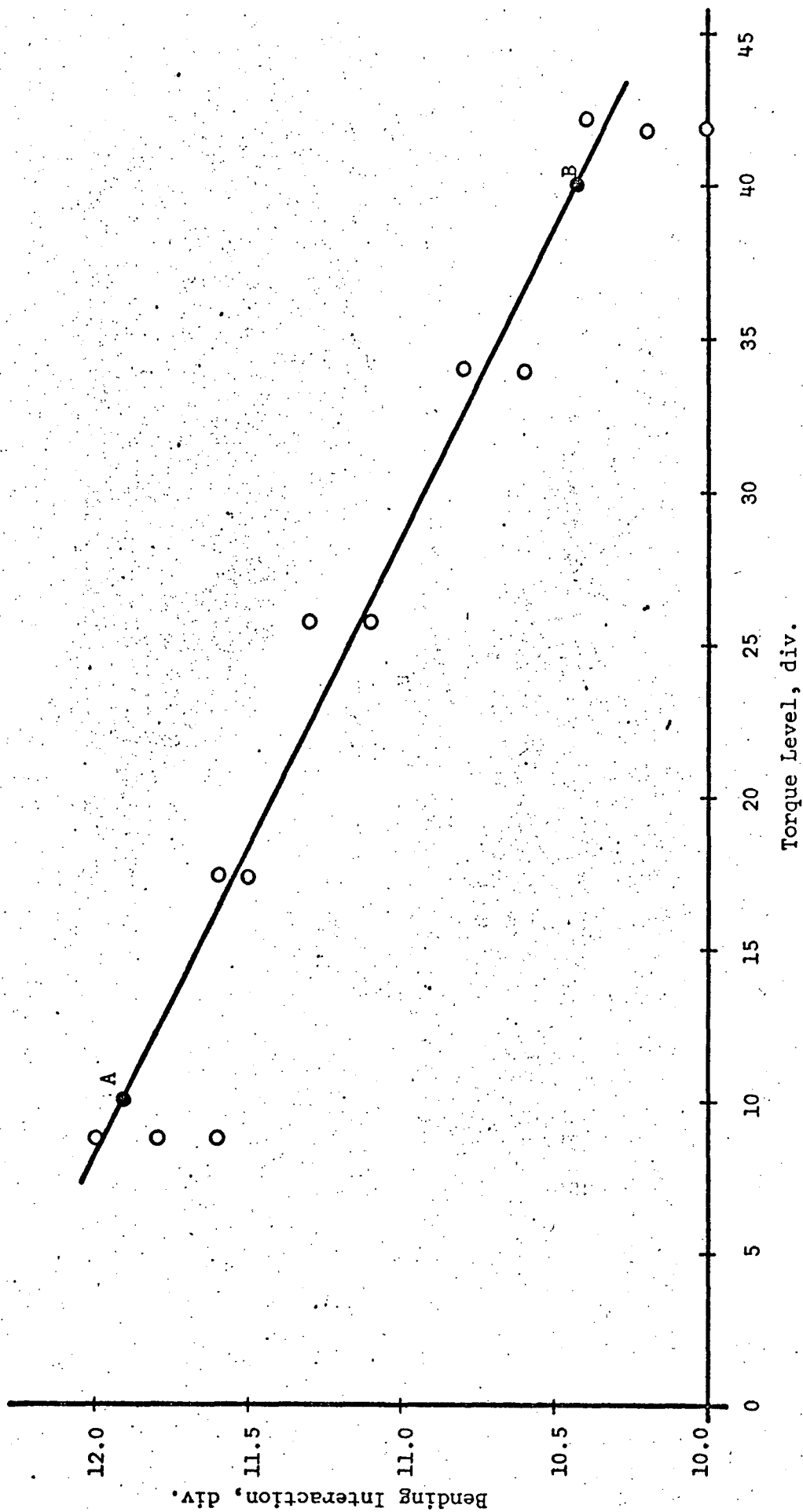


FIGURE 12. TORQUE INTERACTION INTO BENDING FOR MACHINE #1.

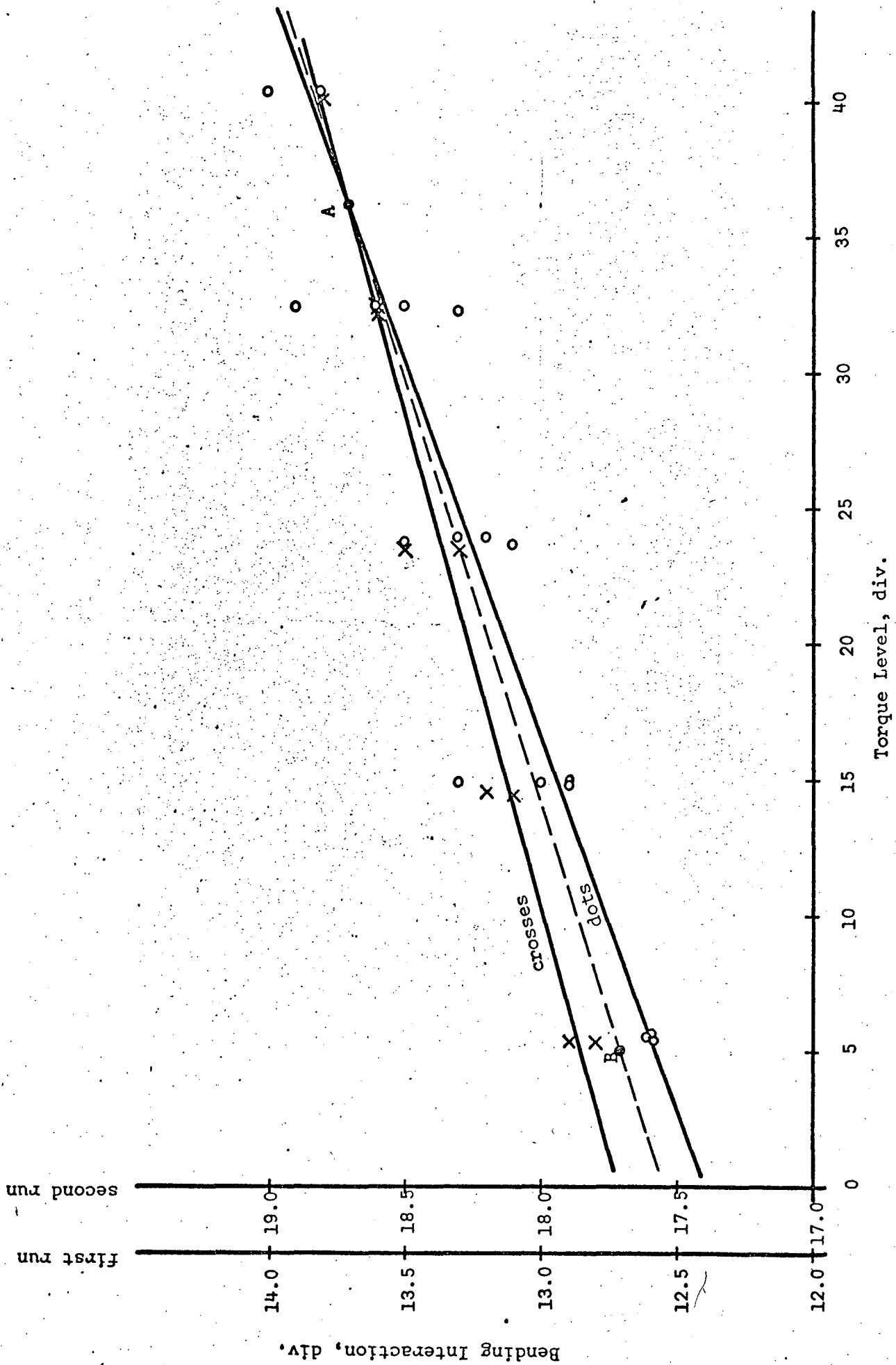


FIGURE 13. TORQUE INTERACTION INTO BENDING MACHINE #2.

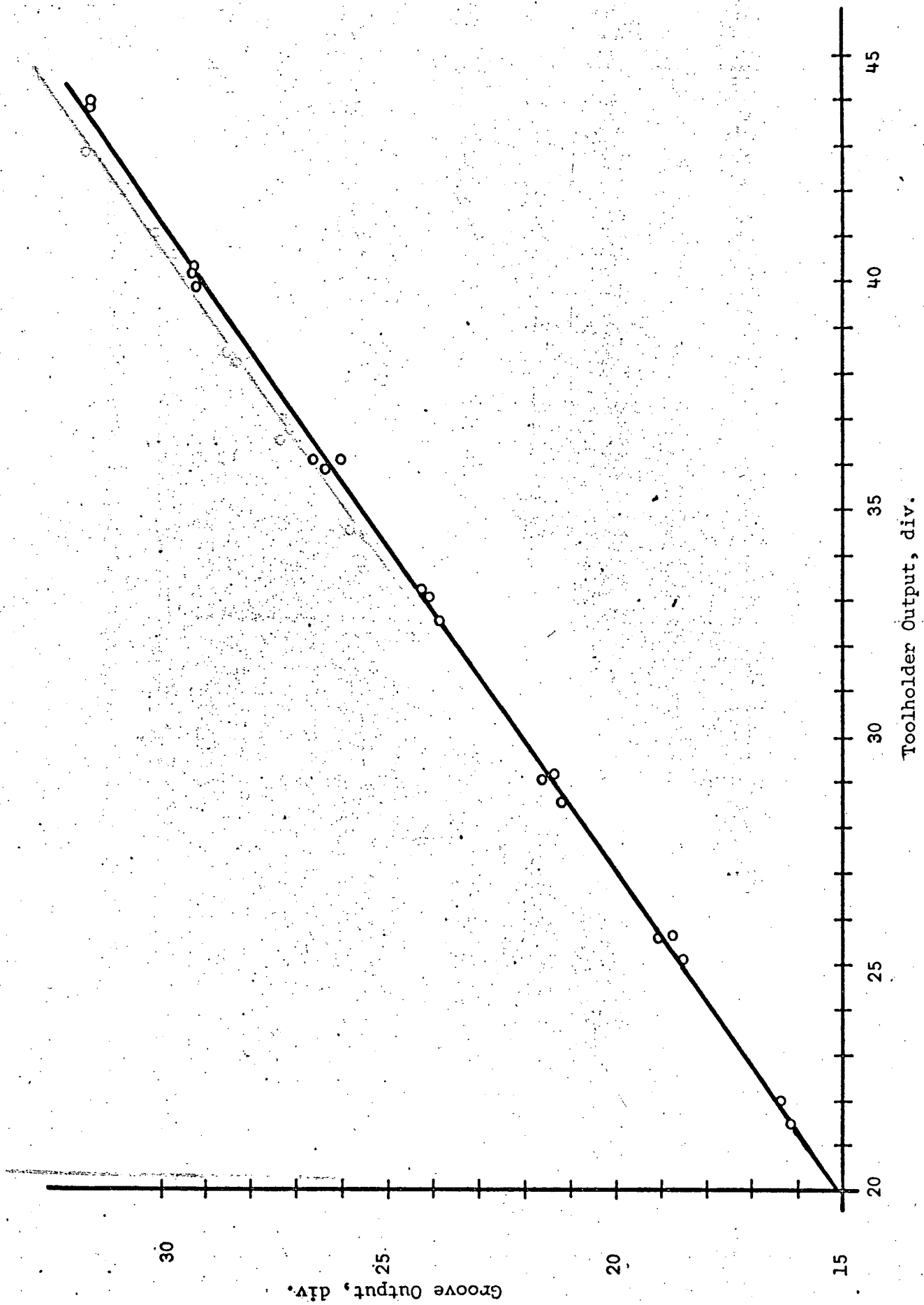


FIGURE 14. SPECIMEN GROOVE OUTPUT VERSUS TOOLHOLDER OUTPUT - MACHINE #1.

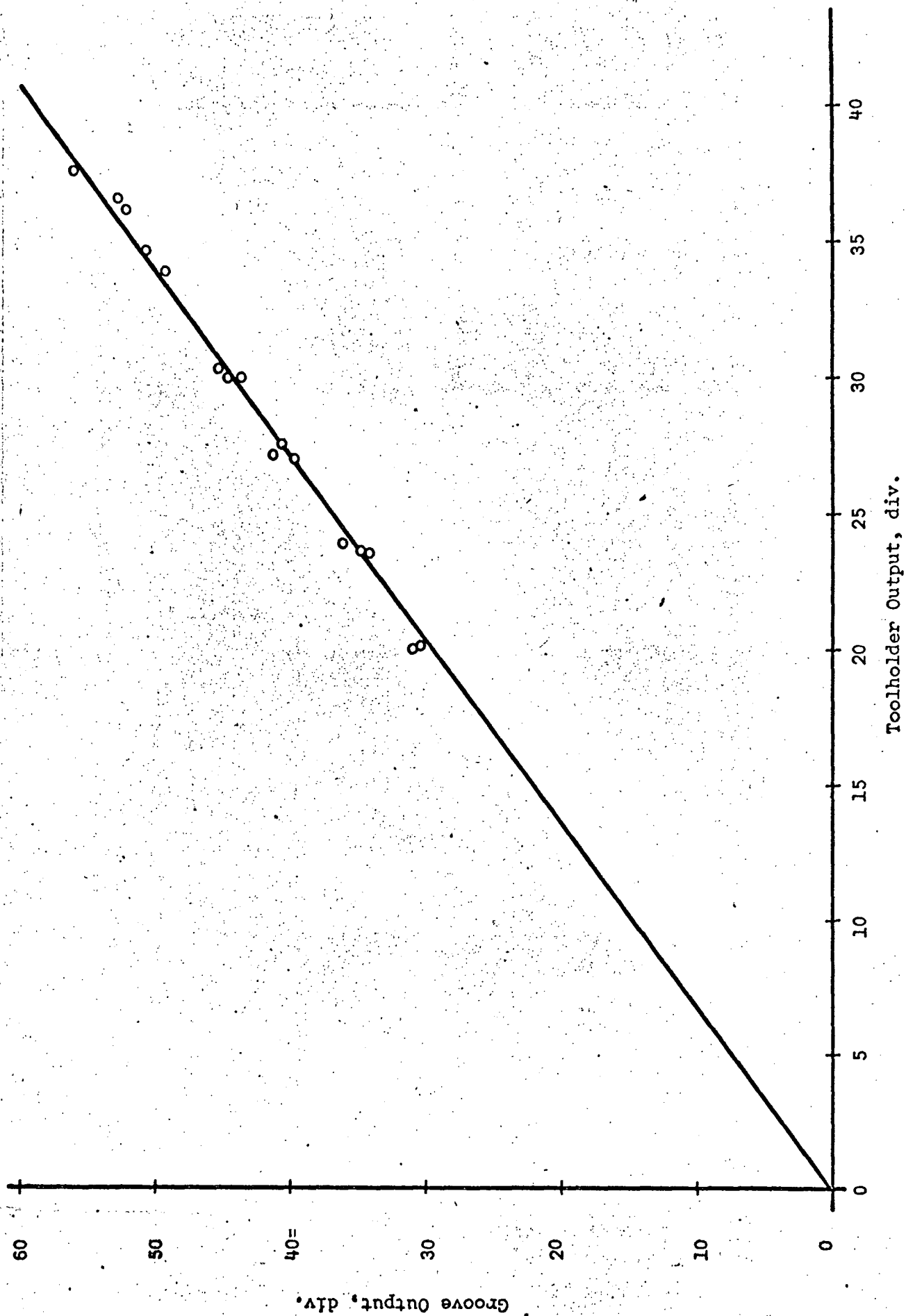


FIGURE 15. SPECIMEN GROOVE OUTPUT VERSUS TOOLHOLDER OUTPUT - MACHINE #2.

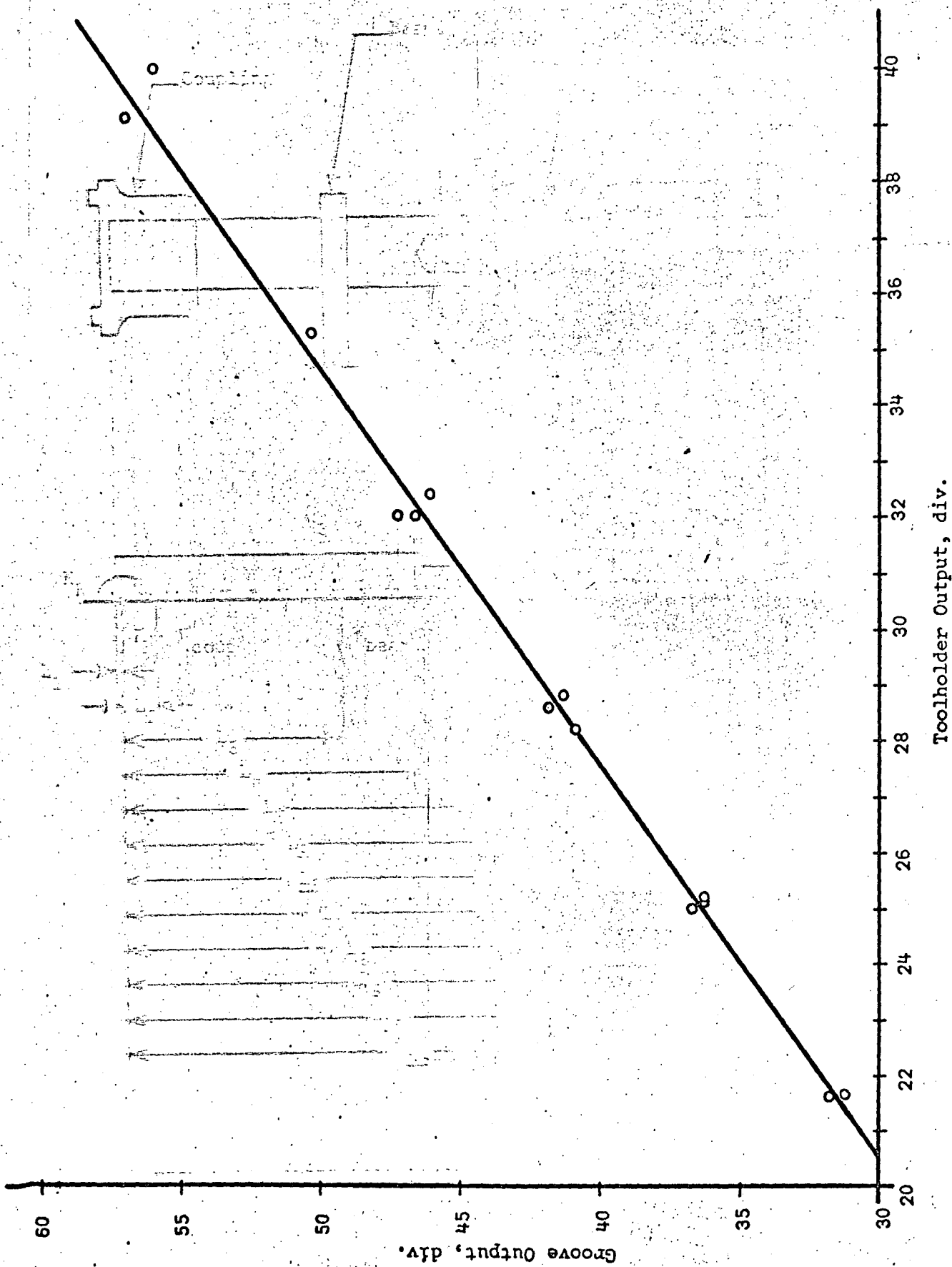


FIGURE 16. SPECIMEN GROOVE OUTPUT VERSUS TOOLHOLDER OUTPUT - MACHINE #3.

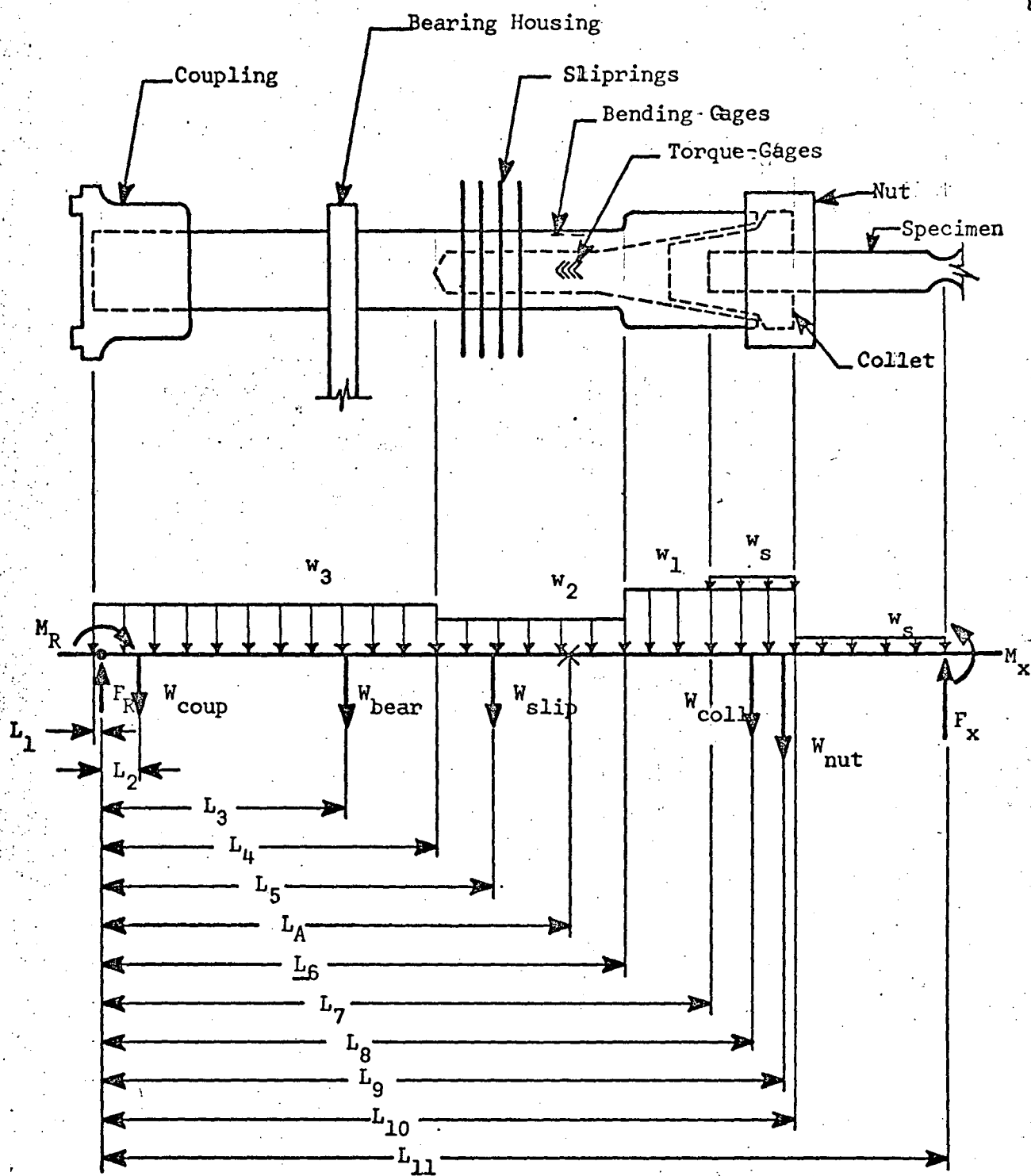


FIGURE 17. FREE BODY DIAGRAM OF TOOLHOLDER.

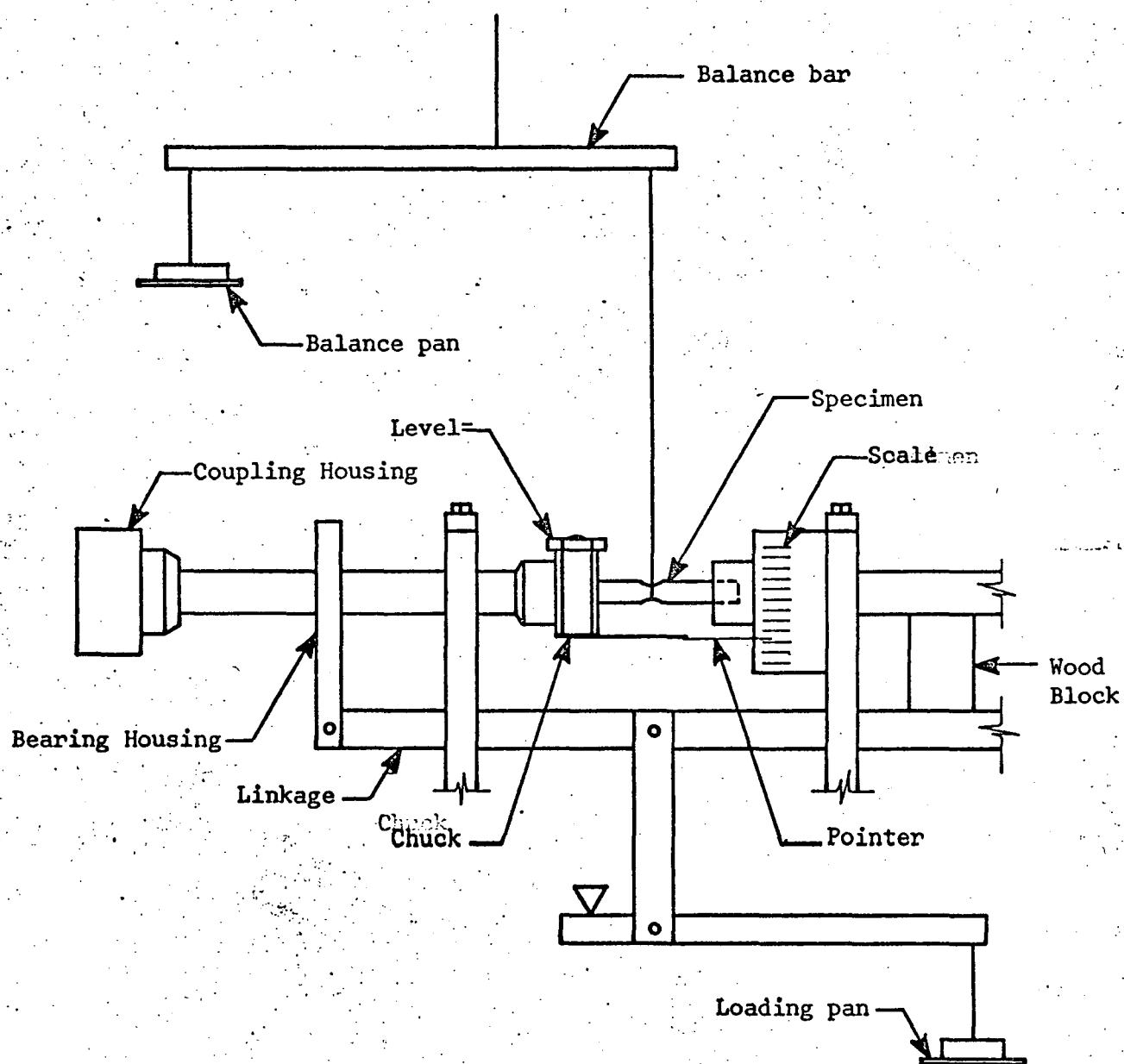


FIGURE 18. LABORATORY SET-UP OF LEVER ARM, PIVOT POINT, RESISTING MOMENT MEASUREMENT EXPERIMENT.

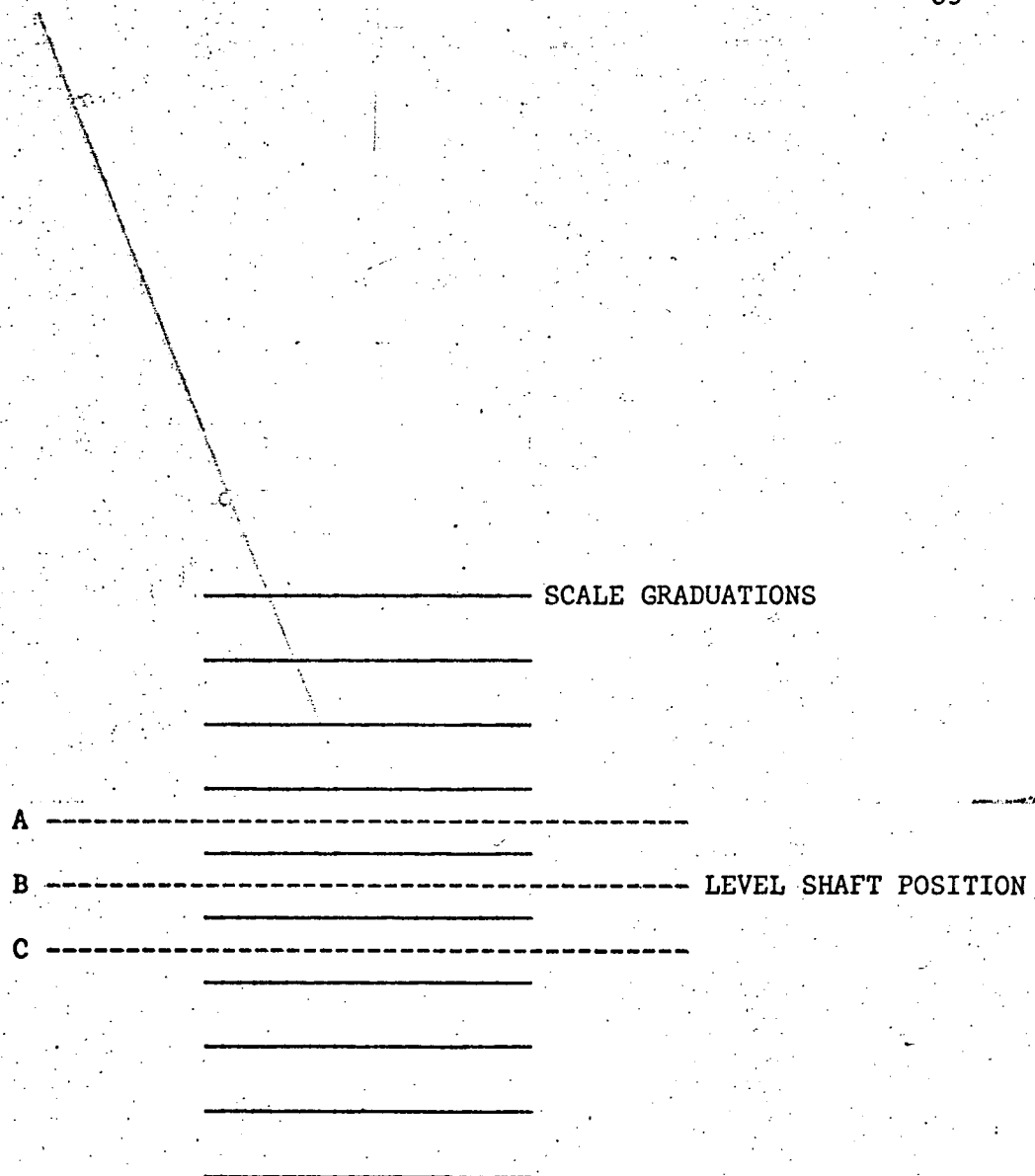
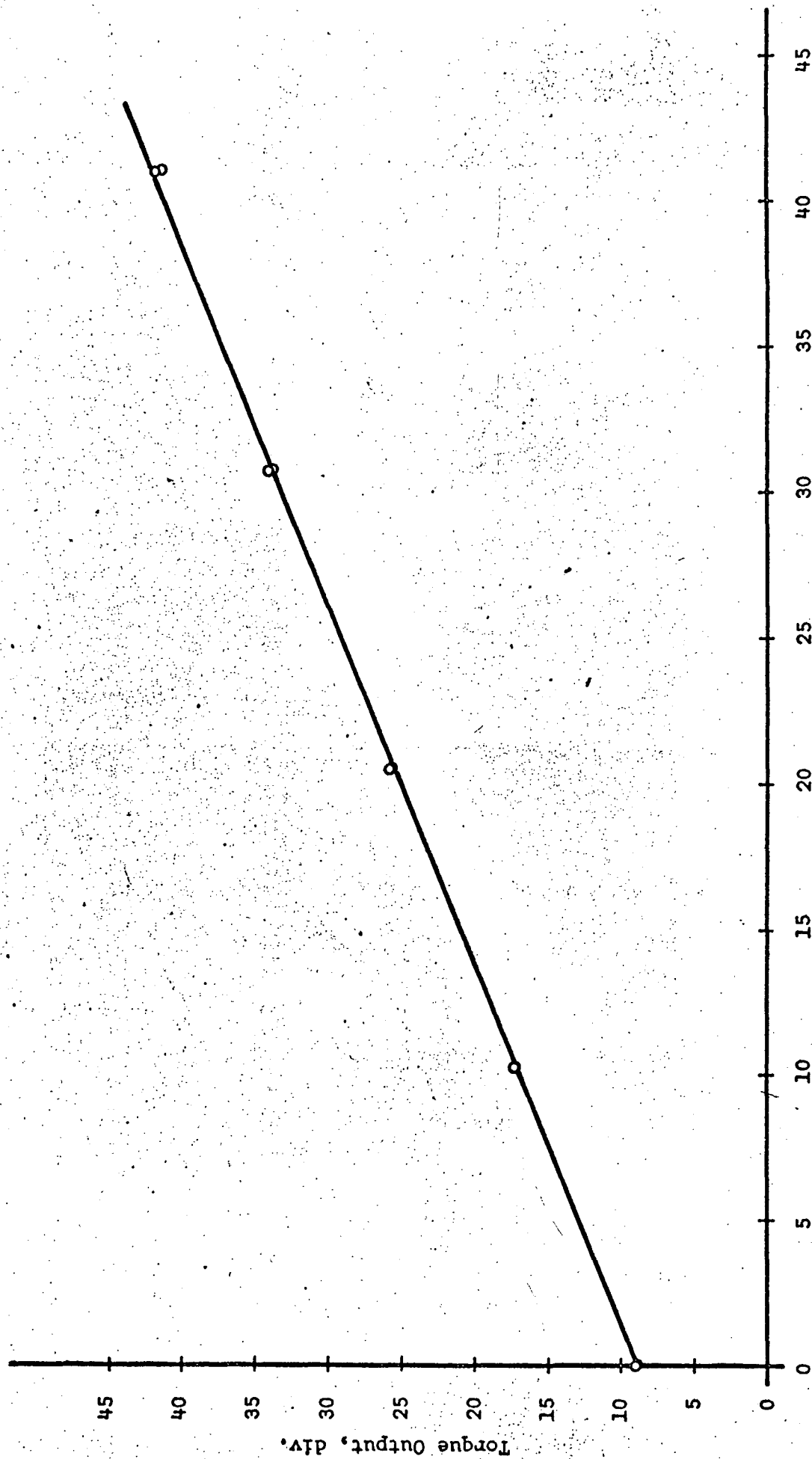


FIGURE 19. SCALE GRADUATIONS OF MEASUREMENT EXPERIMENT



Pan Weight, lbs.

FIGURE 20. TORQUE OUTPUT VERSUS PAN WEIGHT - MACHINE # 1.

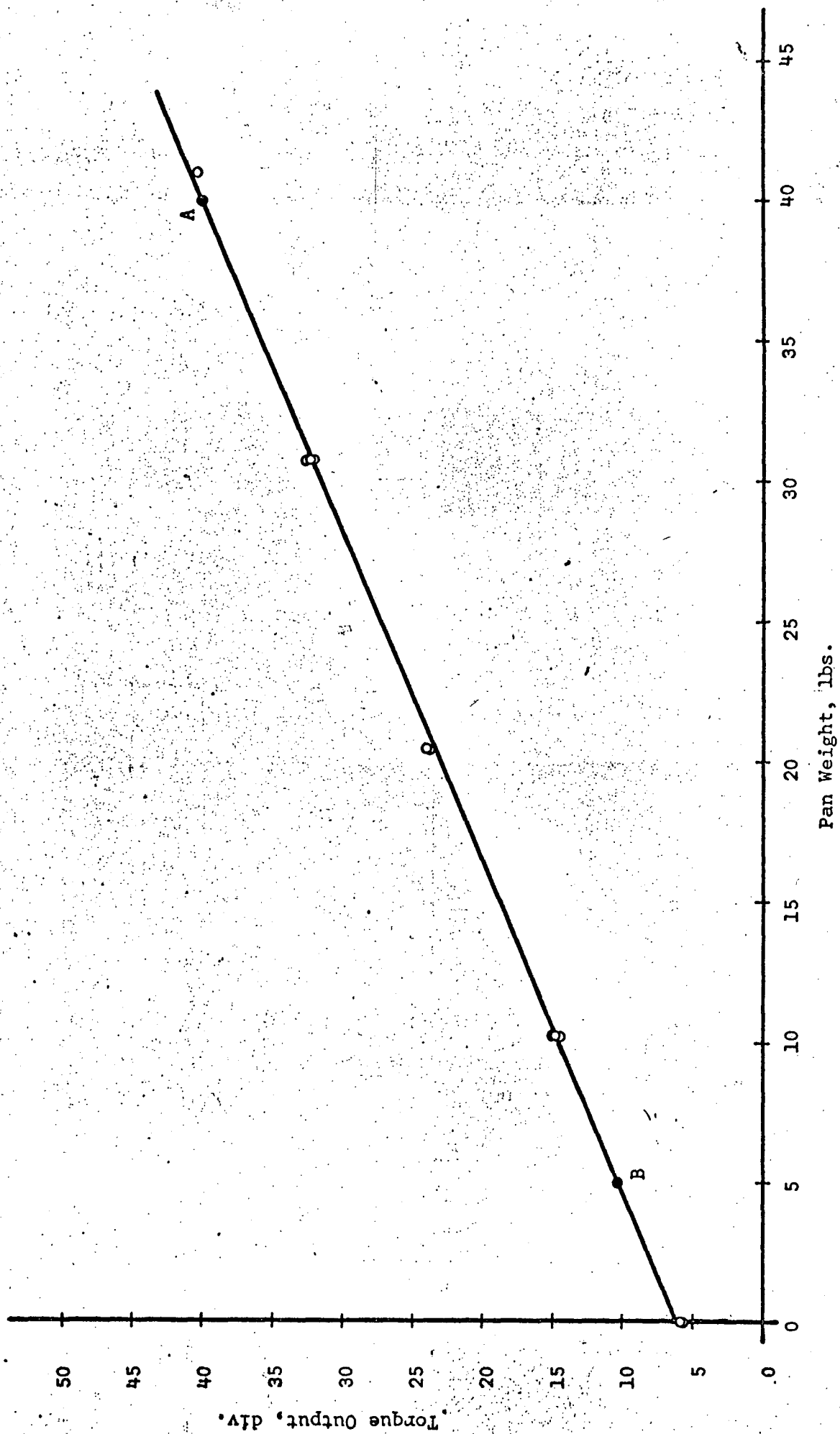


FIGURE 21. TORQUE OUTPUT VERSUS PAN WEIGHT - MACHINE #2

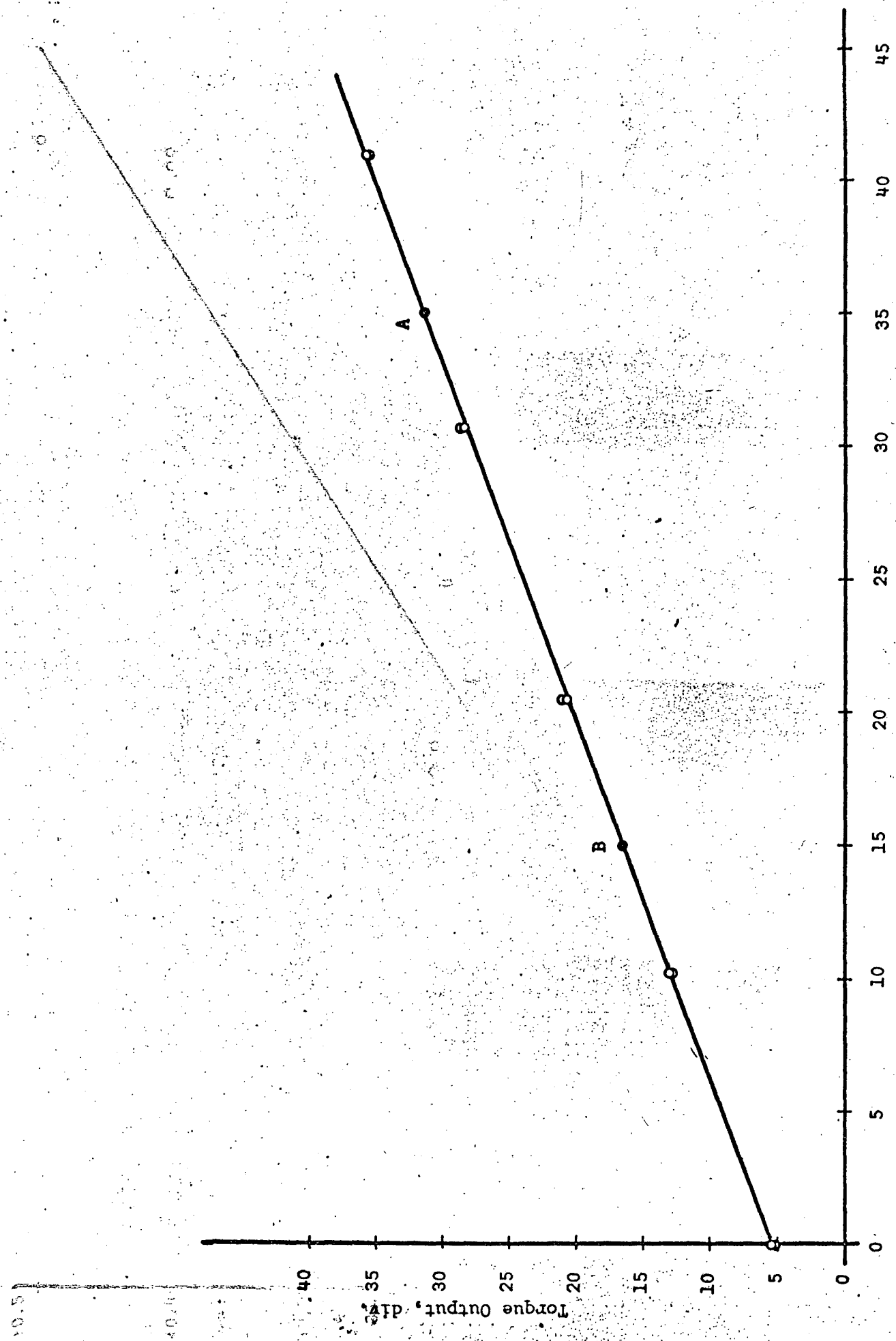


FIGURE 22. TORQUE OUTPUT VERSUS PAN WEIGHT - MACHINE #3.

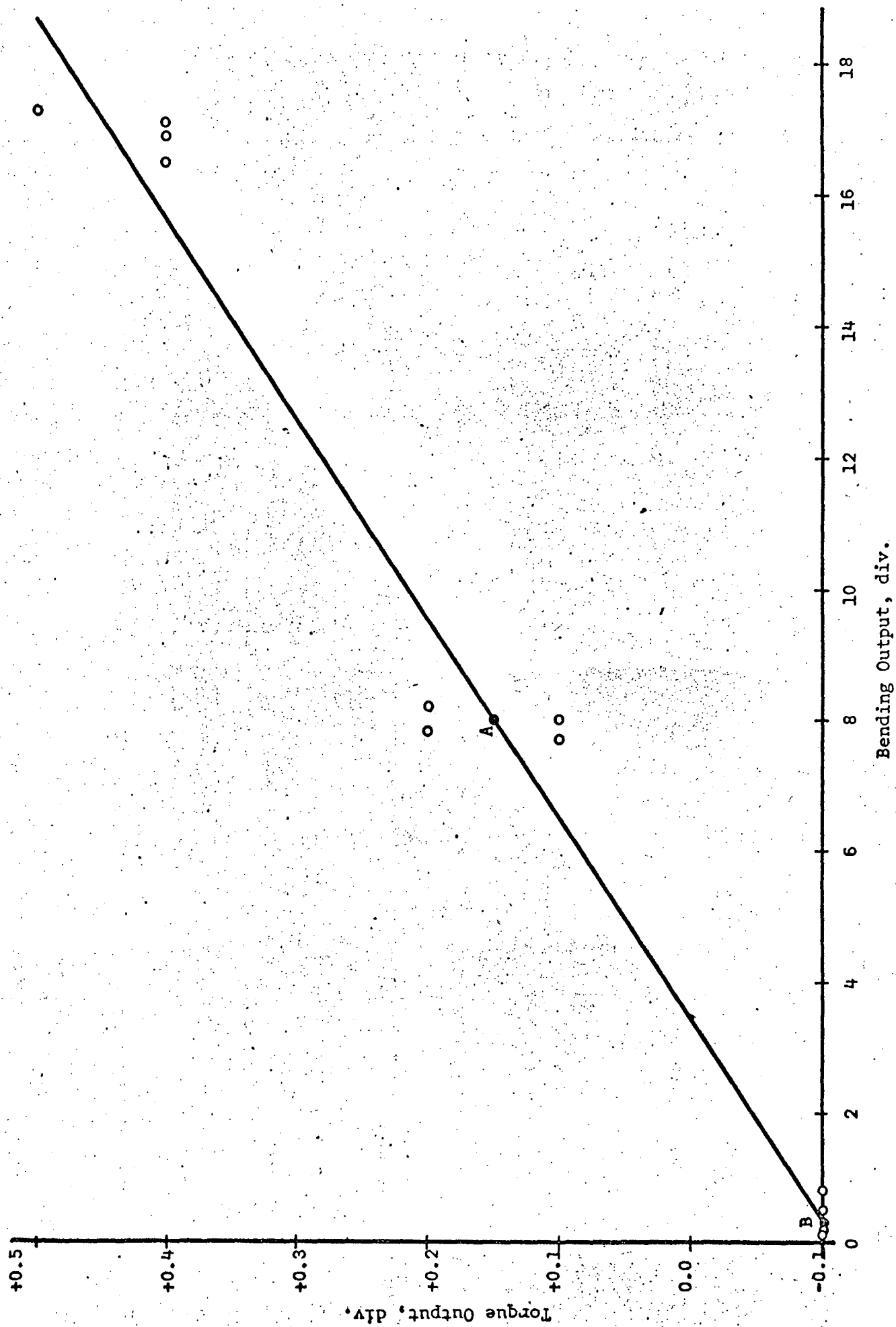


FIGURE 23. BENDING INTERACTION INTO TORQUE - MACHINE #1.

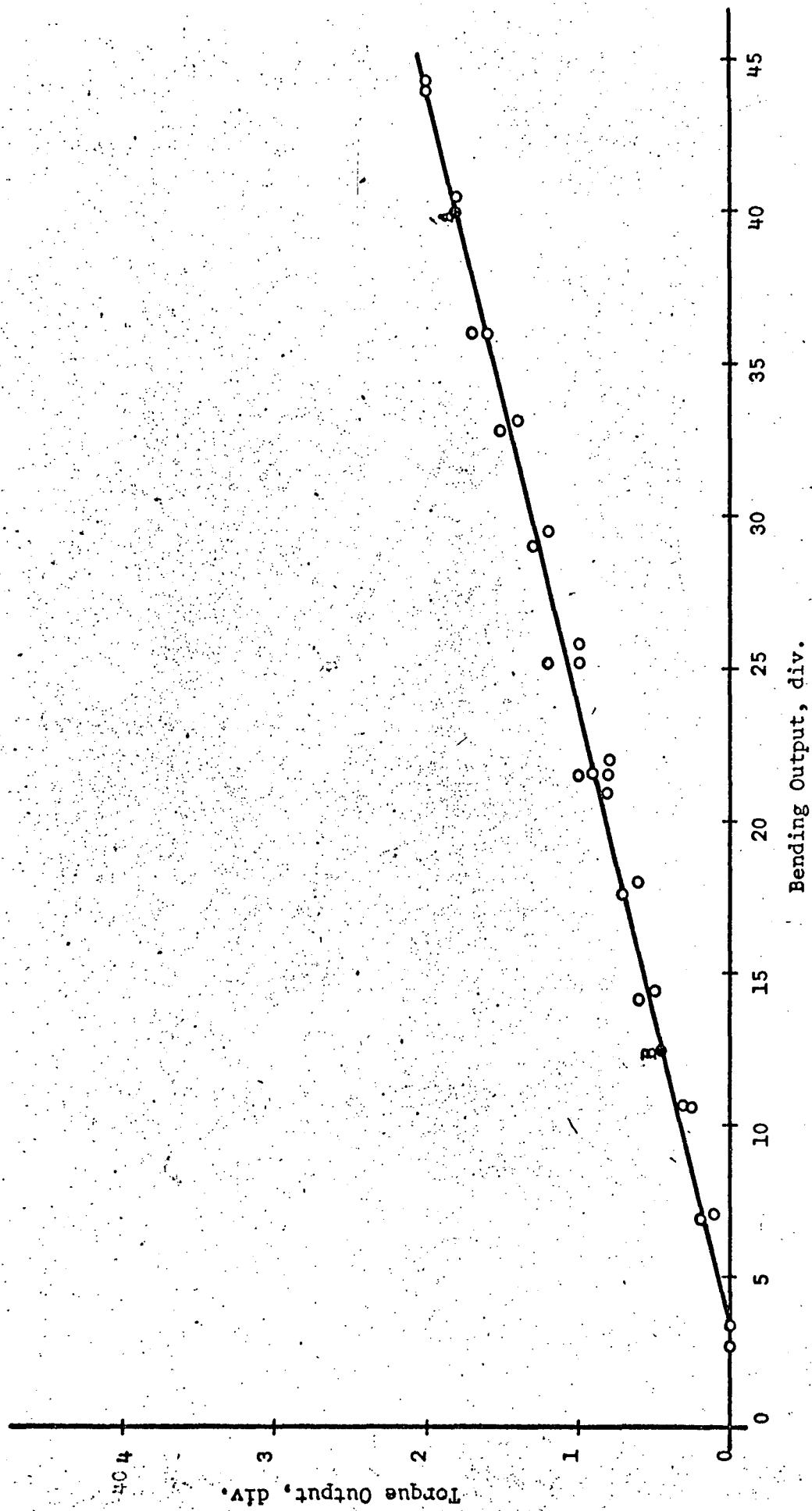
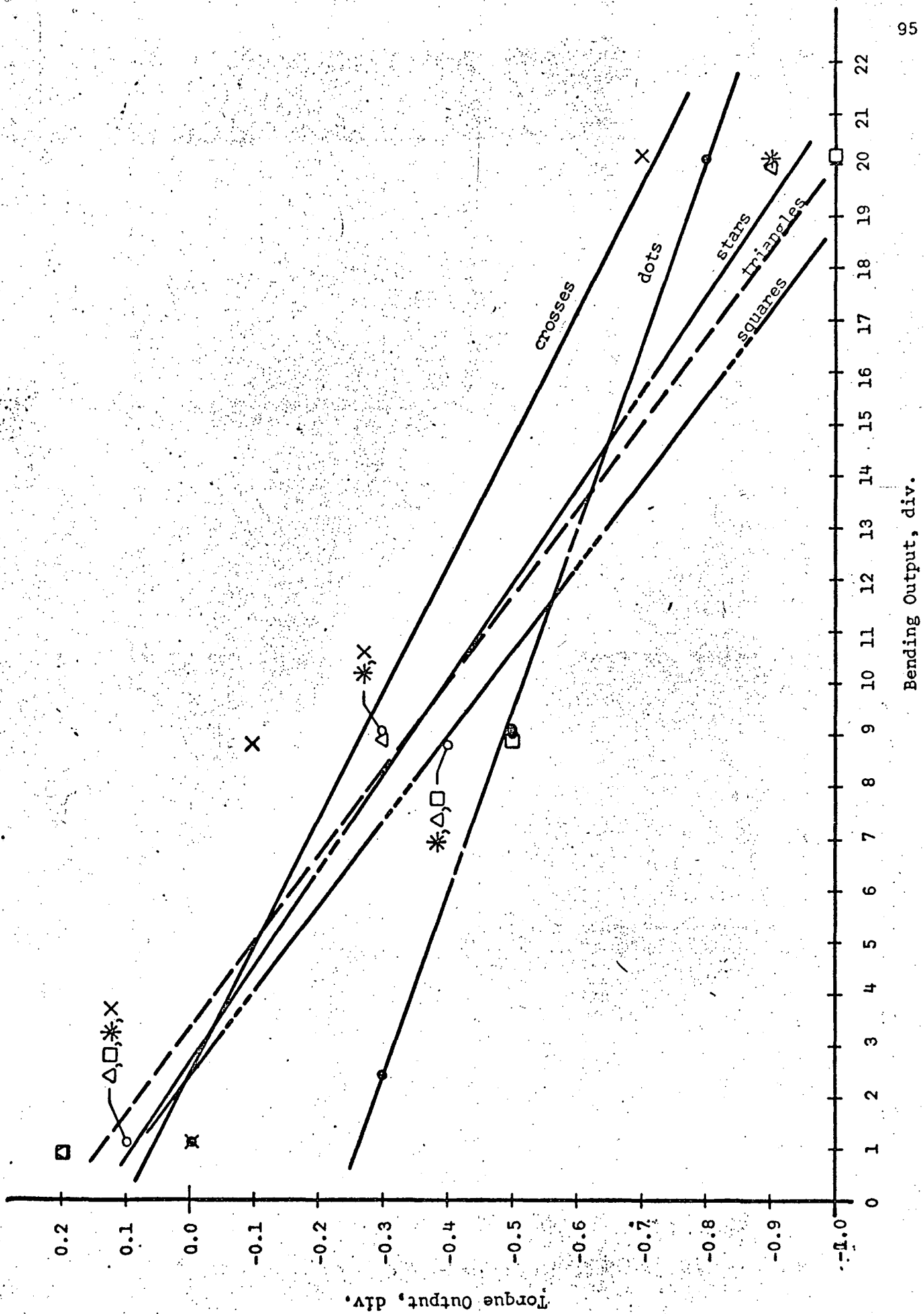


FIGURE 24. BENDING INTERACTION INTO TORQUE - MACHINE #2.



Bending Output, div.

FIGURE 25. BENDING INTERACTION INTO TORQUE - MACHINE #3.

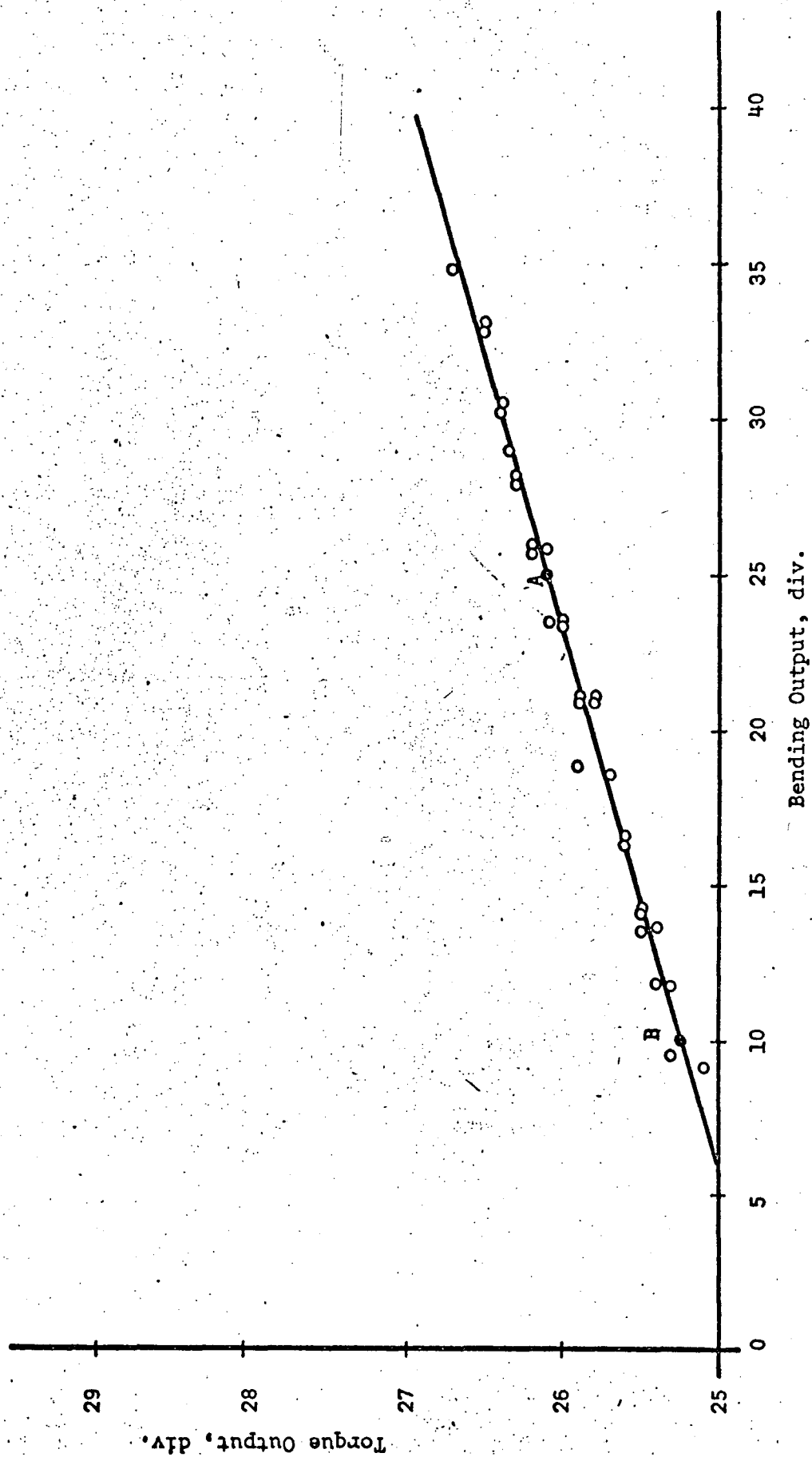
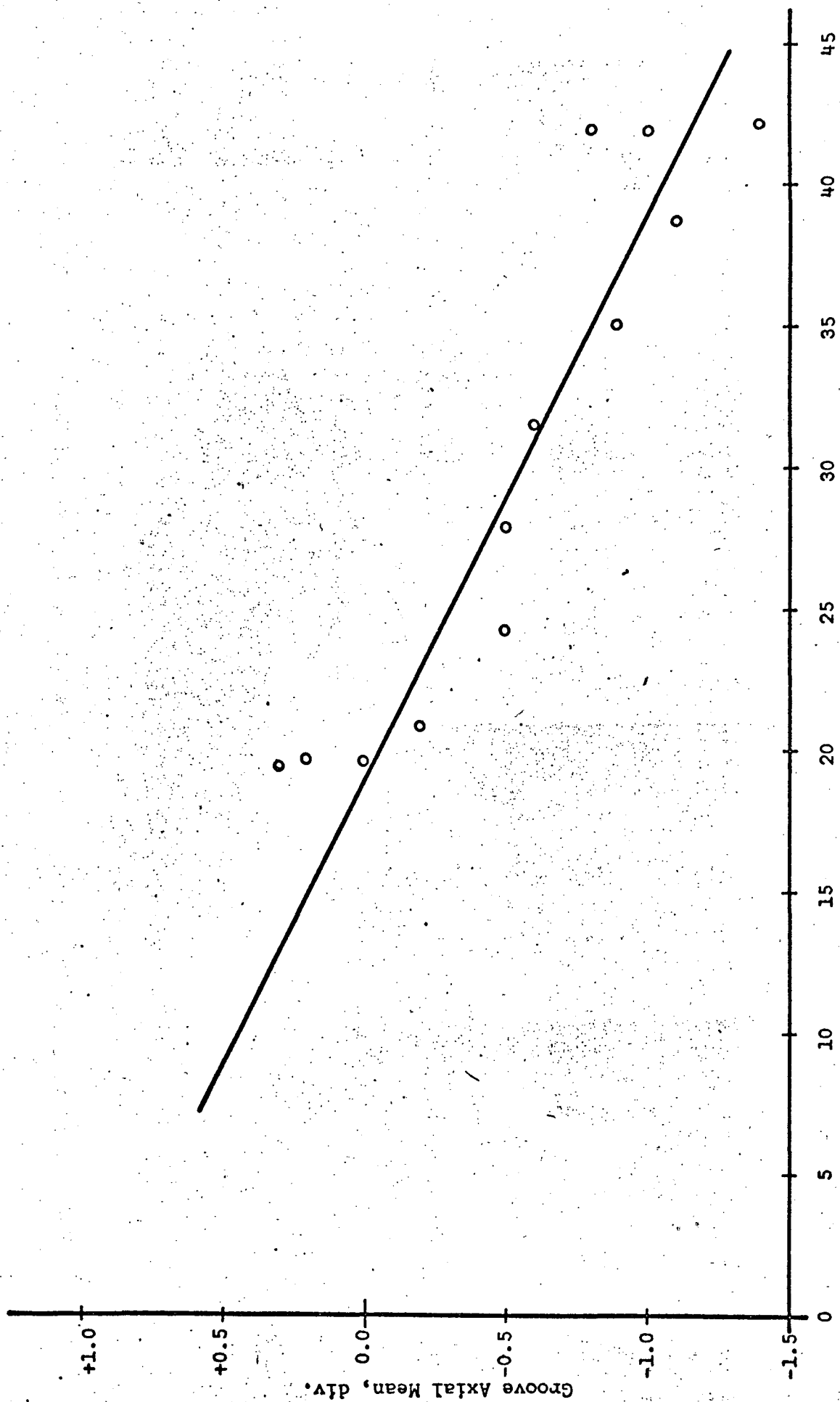


FIGURE 26. BENDING INTERACTION INTO TORQUE AT HIGH TORQUE LEVEL - MACHINE #2.

C

B



Bending Level, div.

FIGURE 27. AXIAL OUTPUT VERSUS BENDING LOAD - MACHINE #1.

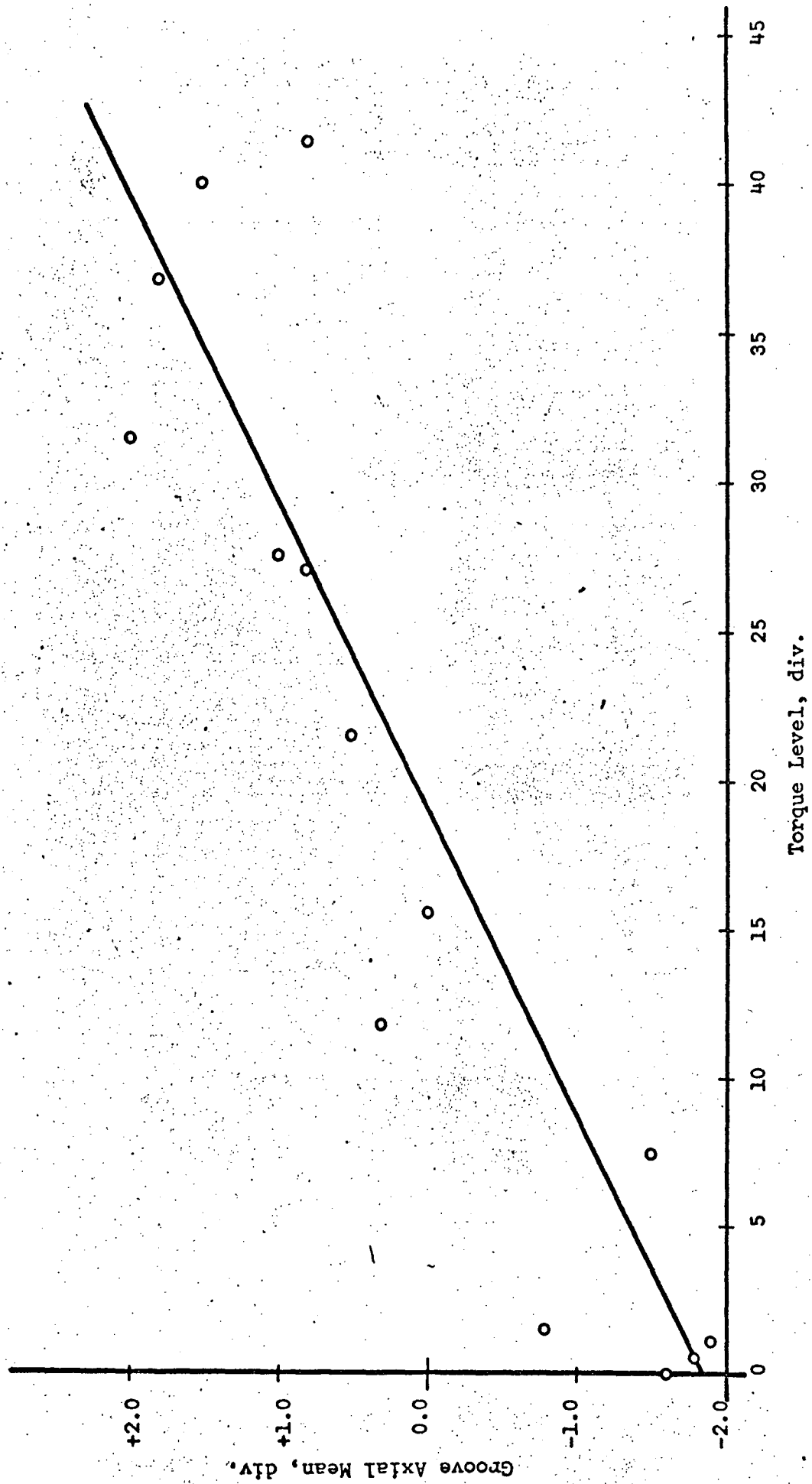


FIGURE 28. AXIAL OUTPUT VERSUS TORQUE LOAD - MACHINE #1.

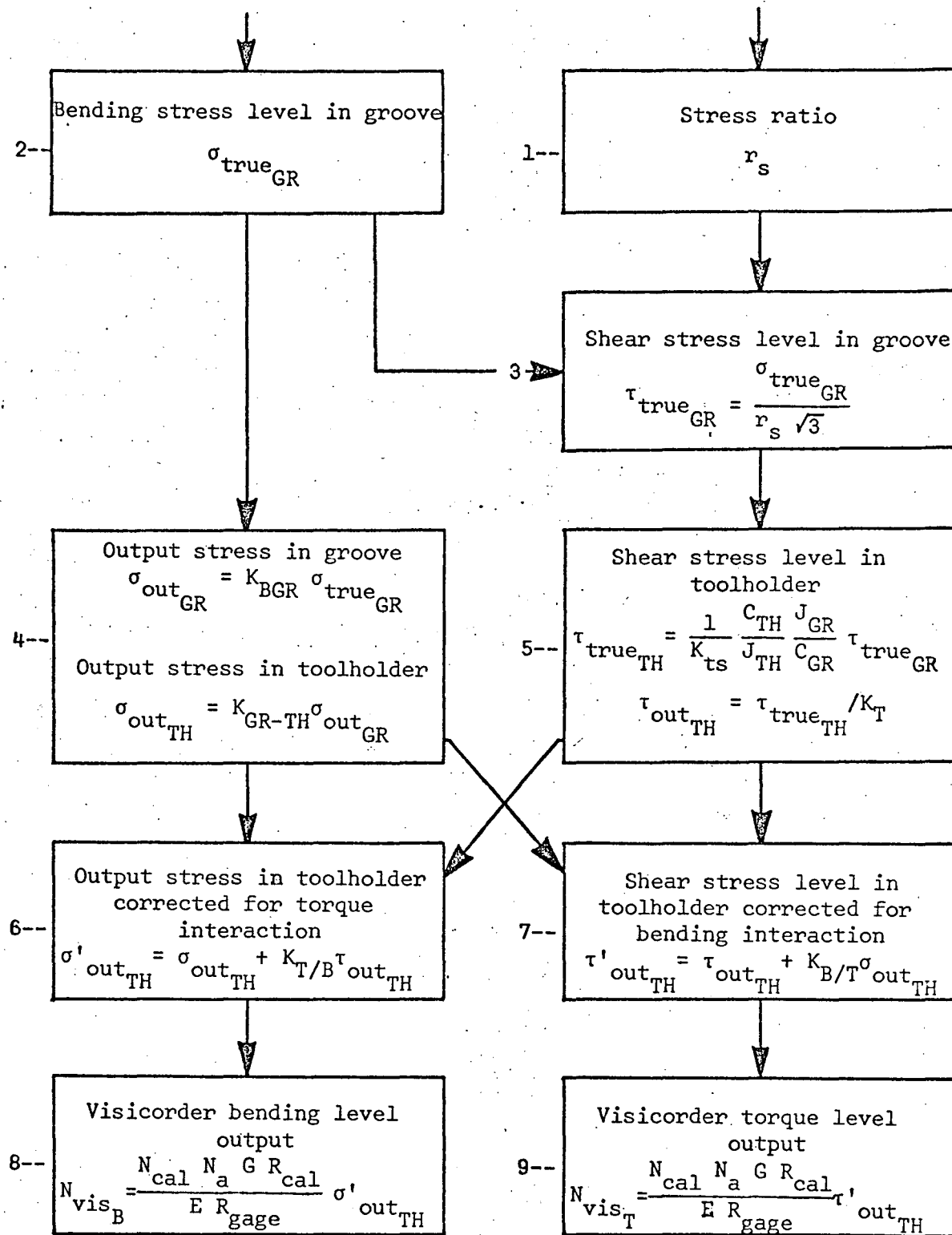


FIGURE 29. THE CALIBRATION FLOW CHART.

```

-----
DIMENSION STOR(50), TAUGR(50), R(50)
NCOUNT = 0
C READ IN THE NUMBER OF STRESS LEVELS IN RUN
  READ 161, NOSTLV
161 FORMAT (I5)
170 PRINT 90
  90 FORMAT(1H1//)
  NCOUNT = NCOUNT + 1
  PRINT 60
C FORMAT FOR OUTPUT HEADINGS
  60 FORMAT (3X,4HTEST,3X,8HSPECIMEN,3X,7H MACHINE,5X,3HPAN,7X,4HRCAL,7X
1,4HNCAL,7X,4HNS,6X,4HRCAL,6X,4HNCAL,6X,4HNVIS,5X,7HBENDING,4X,
25H3HEAR,4X,6HST,35/4X,3HNO.,6X,3HNO.,7X,3HNO.,5X,6HWEIGHT,4X,
37HREADING,4X,7HBENDING,4X,7HBENDING,4X,6HTORQUE,4X,6HTORQUE,4X,
46HTORQUE,5X,6HSTRESS,4X,6HSTRESS,4X,5HRATIO//)
C READ IN THE NUMBER OF CARDS IN THE STRESS LEVEL AND THE MODE
C OF OPERATION OF THE MACHINE
  READ 100, NCARDS, MODE
100 FORMAT(2I5)
  DO 120 I = 1, NCARDS
C READ IN THE TEST NO., SPECIMEN NO., MACHINE NO., PANWEIGHT, AND THE
C CALIBRATION RESISTANCE, VISICORDER CALIBRATION DISTANCE AND VISICORDER
C OUTPUT DIVISIONS FOR BENDING AND TORQUE
  80 READ 10, NOTEST, NOSPEC, MACHNO, NPANWT, RCALB, ENCALB, ENVISB, RCALT,
  1ENCALT, ENVIST
  10 FORMAT (4I5, 6F10.2)
  CARDS = NCARDS
C DEFINE THE ELASTIC MODULUS, NO. OF ACTIVE ARMS OF THE BRIDGES, THE
C RESISTANCES OF THE BENDING AND TORQUE GAUGES, AND THE BENDING AND
C TORQUE GAUGE FACTORS
  E=30000000.
  ENA=4.
  HGAGEB=190.
  RGAGEB=120.
  GB=3.23
  GT=2.06
C SELECTION OF MACHINE AND MODE
  IF (MACHNO.EQ.1.AND.MODE.EQ.1) GO TO 21
  IF (MACHNO.EQ.2.AND.MODE.EQ.1) GO TO 31
  IF (MACHNO.EQ.1.AND.MODE.EQ.3) GO TO 20
  IF (MACHNO.EQ.2.AND.MODE.EQ.3) GO TO 30
  IF (MACHNO.EQ.3.AND.MODE.EQ.3) GO TO 32
  IF (MACHNO.EQ.1.AND.MODE.EQ.2) GO TO 20
  IF (MACHNO.EQ.2.AND.MODE.EQ.2) GO TO 30
  IF (MACHNO.EQ.3.AND.MODE.EQ.2) GO TO 40
C CALIBRATION PARAMETERS FOR GIVEN MODE AND MACHINE
  31 CBGR=.902
  CGRTH=.0198
  GO TO 50
  21 CBGR=.972
  CGRTH=.0203
  GO TO 50
  32 CBGR=.972
  CGRTH=.0215
  CT=.842
  CTB=0.0
  CBT=-.0238

```

FIGURE 30. DATA REDUCTION PROGRAM

```

      GO TO 50
20  CBGR=.967
    CORTH=.0203
    CT=.882
    CTB=.0548
    CBT=.0298
    GO TO 50
30  CBGR=.902
    CORTH=.0198
    CT=.840
    CTB=.0343
    CBT=.0410
    GO TO 50
40  CBGR=.972
    CORTH=.0215
    CT=.944
    CTB=.0
    CBT=.01698
50  IF (ENVIST.EQ.0.0) GO TO 160
    GO TO 51
C   CALCULATION OF BENDING STRESS LEVEL FOR INFINITY RATIO
160 SOUTH=(ENVISB*E*RGAGEB)/(ENCALB*ENA*GB*RCALB)
    STRGR(I) = SOUTH / (CGRTH * CBGR)
    TAUGR(I) = 0.0
    PRINT 71,NOTEST,NOSPEC,MACHNO,NPANWT,RCALB,ENCALB,ENVISB,RCALT,
    I,ENCALT,ENVIST,STRGR(I),TAUGR(I)
71  FORMAT(4X,I3,6X,I3,8X,I1,8X,I2,F14.1,F10.2,F11.2,F12.1,F9.2,F10.2,
    I,F11.1,F11.1,2X,6HINFIN./)
    GO TO 120
C   CALCULATION OF BENDING STRESS, SHEAR STRESS AND STRESS RATIO FOR
C   ALL FINITE RATIOS
51  SOUTHF=(ENVISB*E*RGAGEB)/(ENCALB*ENA*GB*RCALB)
    TAUTHF=(ENVIST*E*RGAGET)/(ENCALT*ENA*GT*RCALT)
    SOUTH=SOUTHF*CTB*TAUTHF
    TAUTH=TAUTHF*CBT*SOUTH
    STRGR(I) = SOUTH / (CGRTH * CBGR)
    TAUGR(I)=CT*TAUTH/.0157)
    R(I) = STRGR(I) / (TAUGR(I) * 1.732)
    PRINT 70,NOTEST,NOSPEC,MACHNO,NPANWT,RCALB,ENCALB,ENVISB,RCALT,
    I,ENCALT,ENVIST,STRGR(I),TAUGR(I),R(I)
70  FORMAT(4X,I3,6X,I3,8X,I1,8X,I2,F14.1,F10.2,F11.2,F12.1,F9.2,F10.2,
    I,F11.1,F11.1,F8.3/)
120 CONTINUE
C   CALCULATION OF MEAN AND STANDARD DEVIATION OF BENDING STRESS, SHEAR
C   STRESS, AND STRESS RATIO
    CALL MEAN (STRGR, CARDS, NCARDS, XMEAN, DEV)
    PRINT 3
3   FORMAT (1H0)
    PRINT 130, XMEAN, DEV
130 FORMAT (19X,31HMEAN BENDING STRESS IN GROOVE =,F10.1,5H PSI.//11X,
    139HSTD. DEV. OF BENDING STRESS IN GROOVE =,F10.2,5H PSI./)
    IF (ENVIST.EQ.0.0) GO TO 200
    CALL MEAN (TAUGR, CARDS, NCARDS, XMEAN, DEV)
    PRINT 3
    PRINT 140, XMEAN, DEV
140 FORMAT (20X,30HMEAN TORQUE STRESS IN GROOVE =,F10.1,5H PSI.//12X,
    138HSTD. DEV. OF TORQUE STRESS IN GROOVE =,F10.2,5H PSI./)
    CALL MEAN ( R, CARDS, NCARDS, XMEAN, DEV)

```

FIGURE 30. DATA REDUCTION PROGRAM (continued).

```
PRINT 3
PRINT 150, XMEAN, DEV
150  FORMAT (31X,19HMEAN STRESS RATIO =,F10.5//18X,32HSTD. DEV. OF MEAN
1    STRESS RATIO =,F10.5)
200  IF(NCOUNT,LT.NOSTLV) GO TO 170
STOP
END
```

FIGURE 30. DATA REDUCTION PROGRAM (continued).

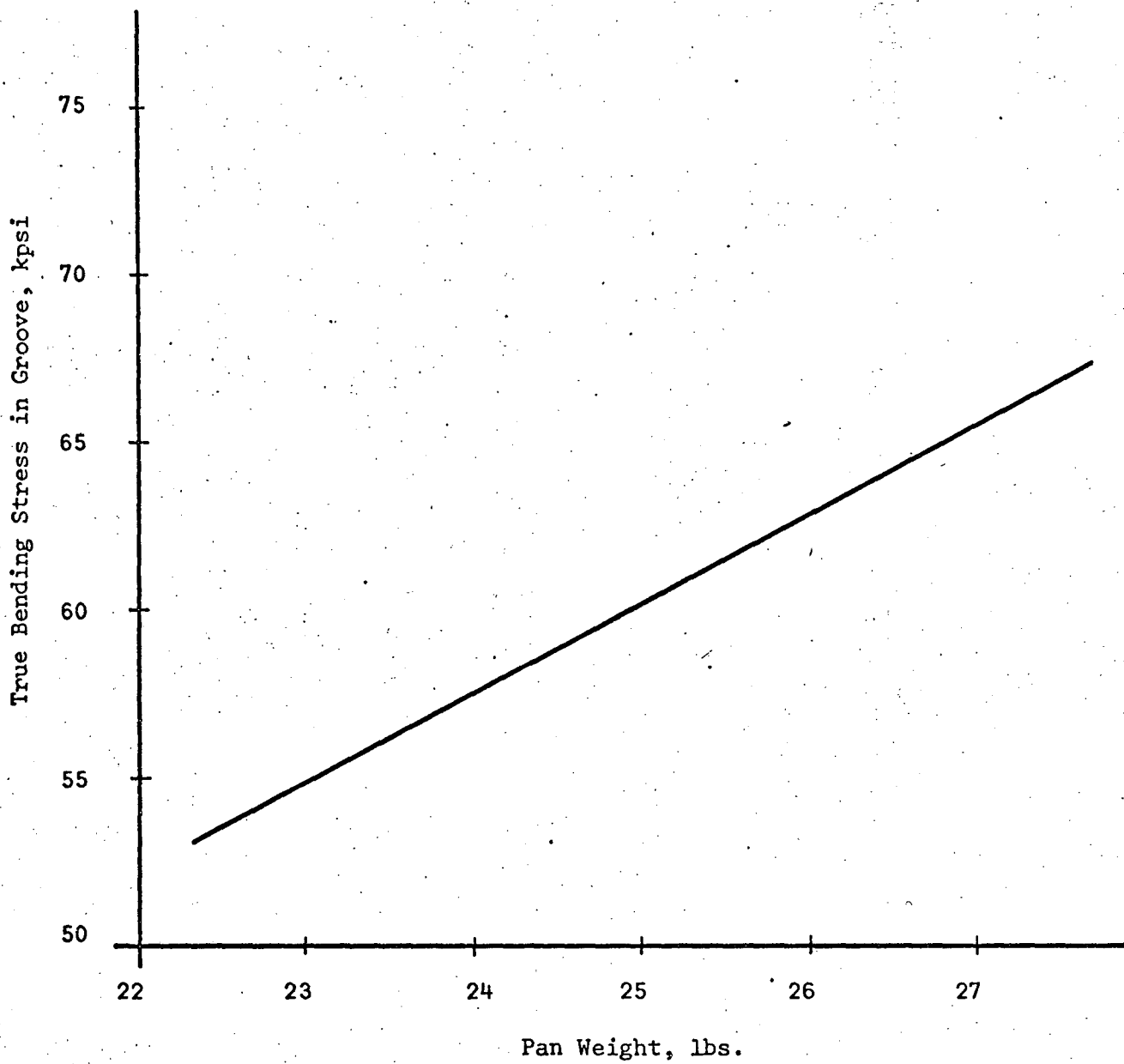


FIGURE 31. PAN WEIGHT VERSUS TRUE BENDING STRESS FOR ENDURANCE STRENGTH FOR $r_s = \infty$.

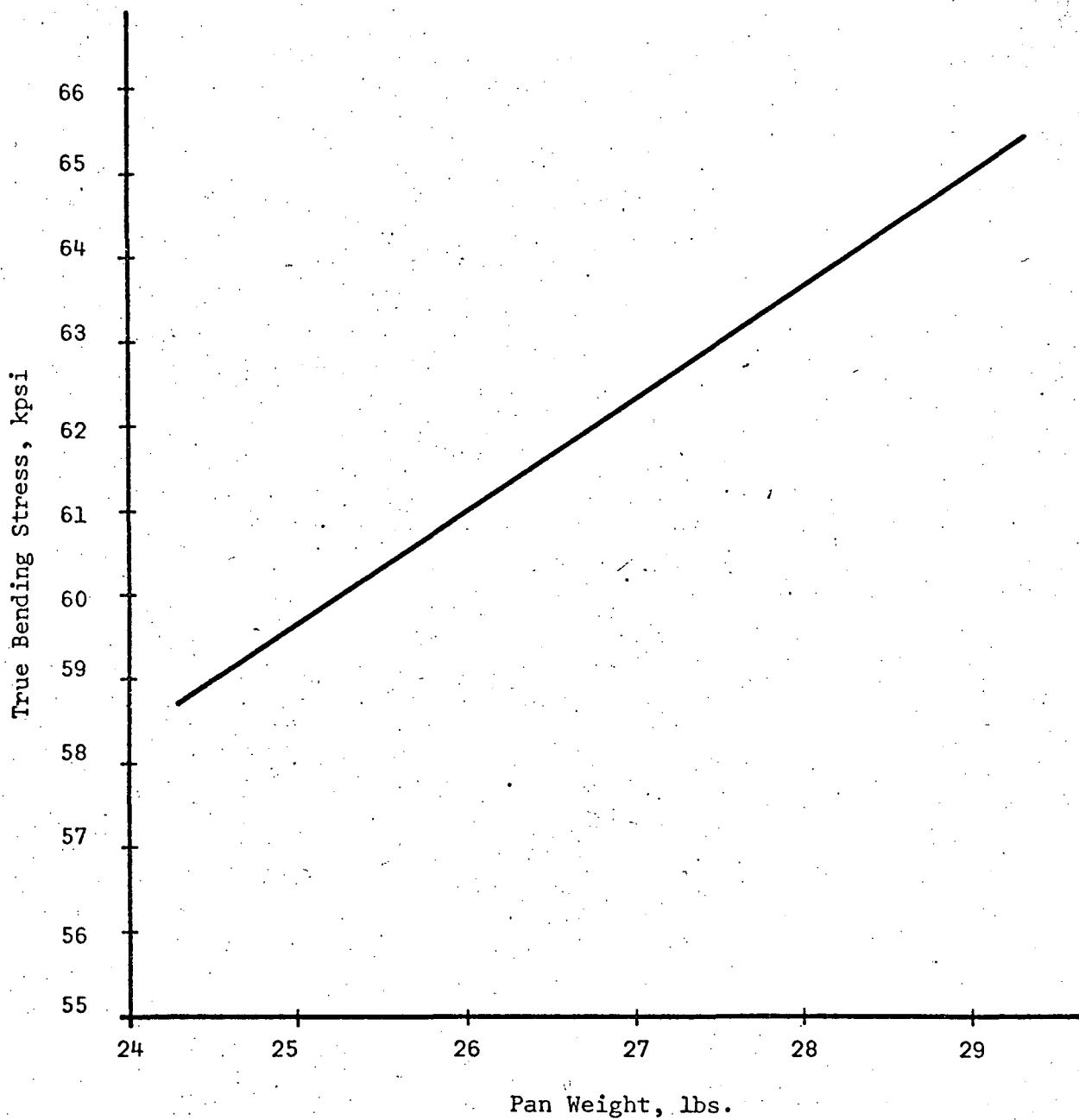
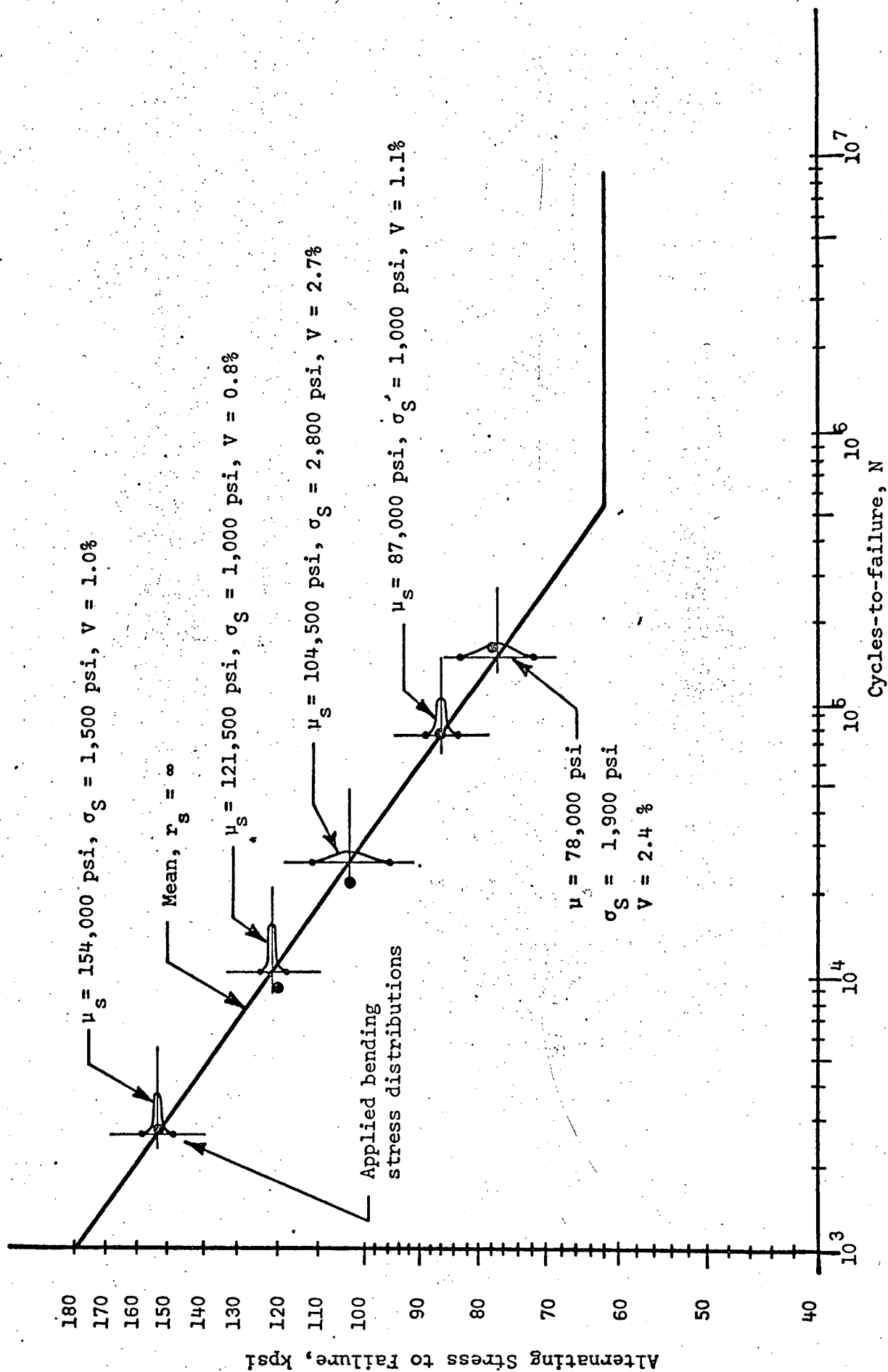


FIGURE 32. PAN WEIGHT VERSUS TRUE BENDING STRESS FOR ENDURANCE STRENGTH FOR $r_s = 0.90$.

FIG. 32

FIGURE 33. APPLIED BENDING STRESS DISTRIBUTIONS FOR STRESS RATIO OF ∞ .

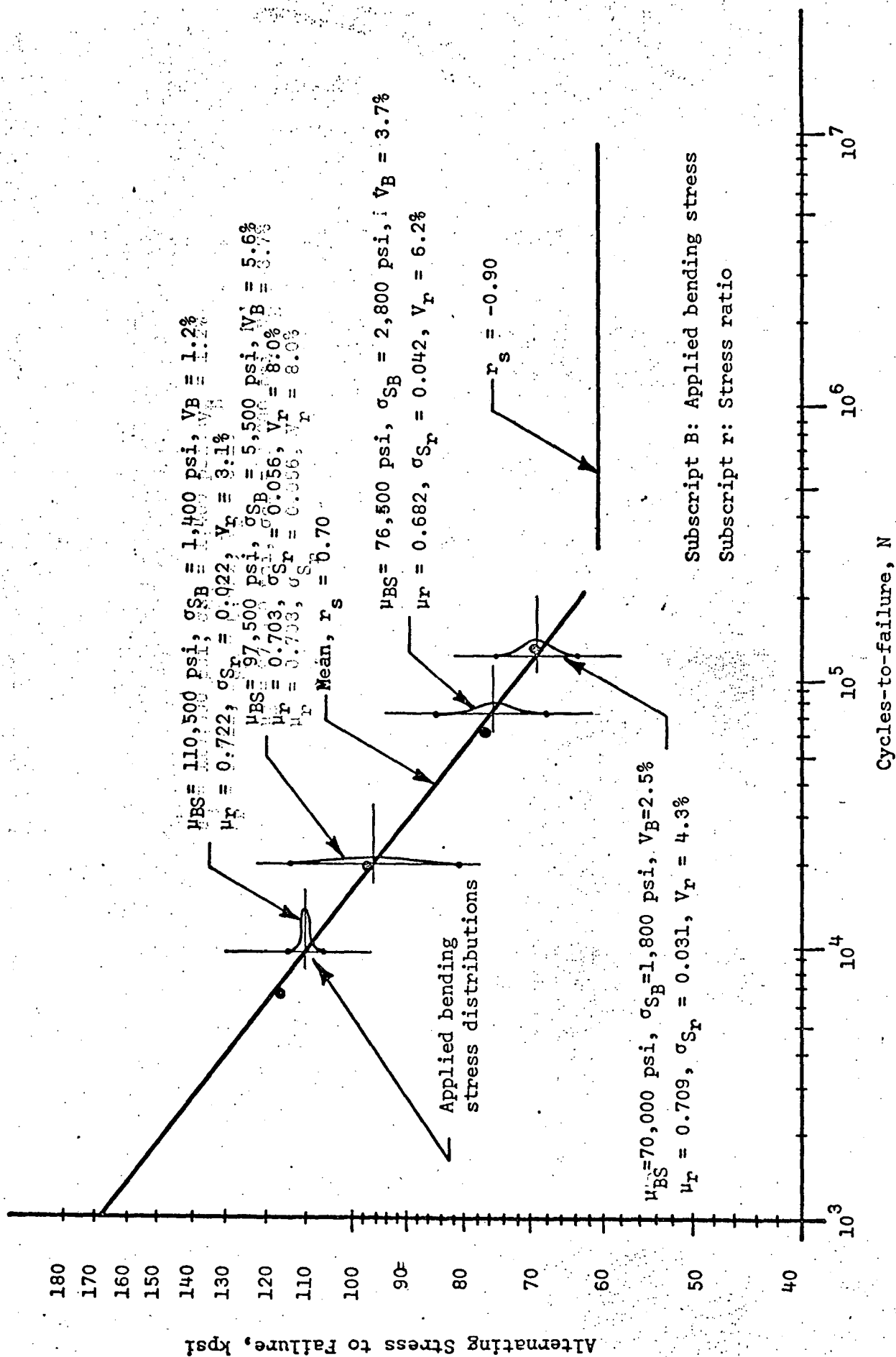


FIGURE 34. APPLIED BENDING STRESS DISTRIBUTIONS FOR A STRESS RATIO OF 0.70 AND ENDURANCE STRENGTH FOR A STRESS RATIO OF 0.90.

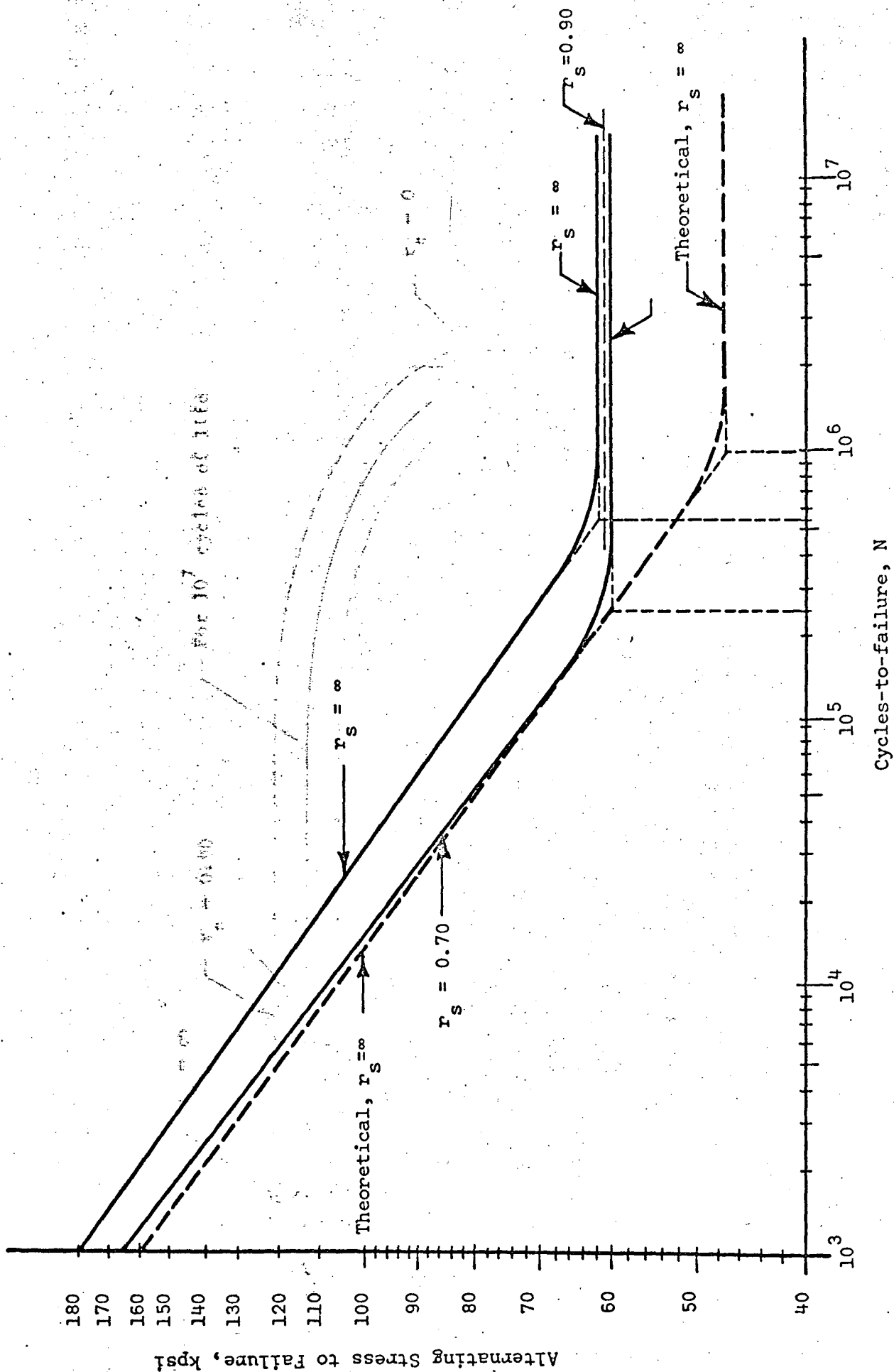


FIGURE 35. FATIGUE STRENGTH VERSUS MEAN CYCLES-TO-FAILURE AND ENDURANCE STRENGTH FOR r_s OF ∞ , 0.70, AND 0.90, AND THE THEORETICAL S-N DIAGRAM FOR $r_s = \infty$.

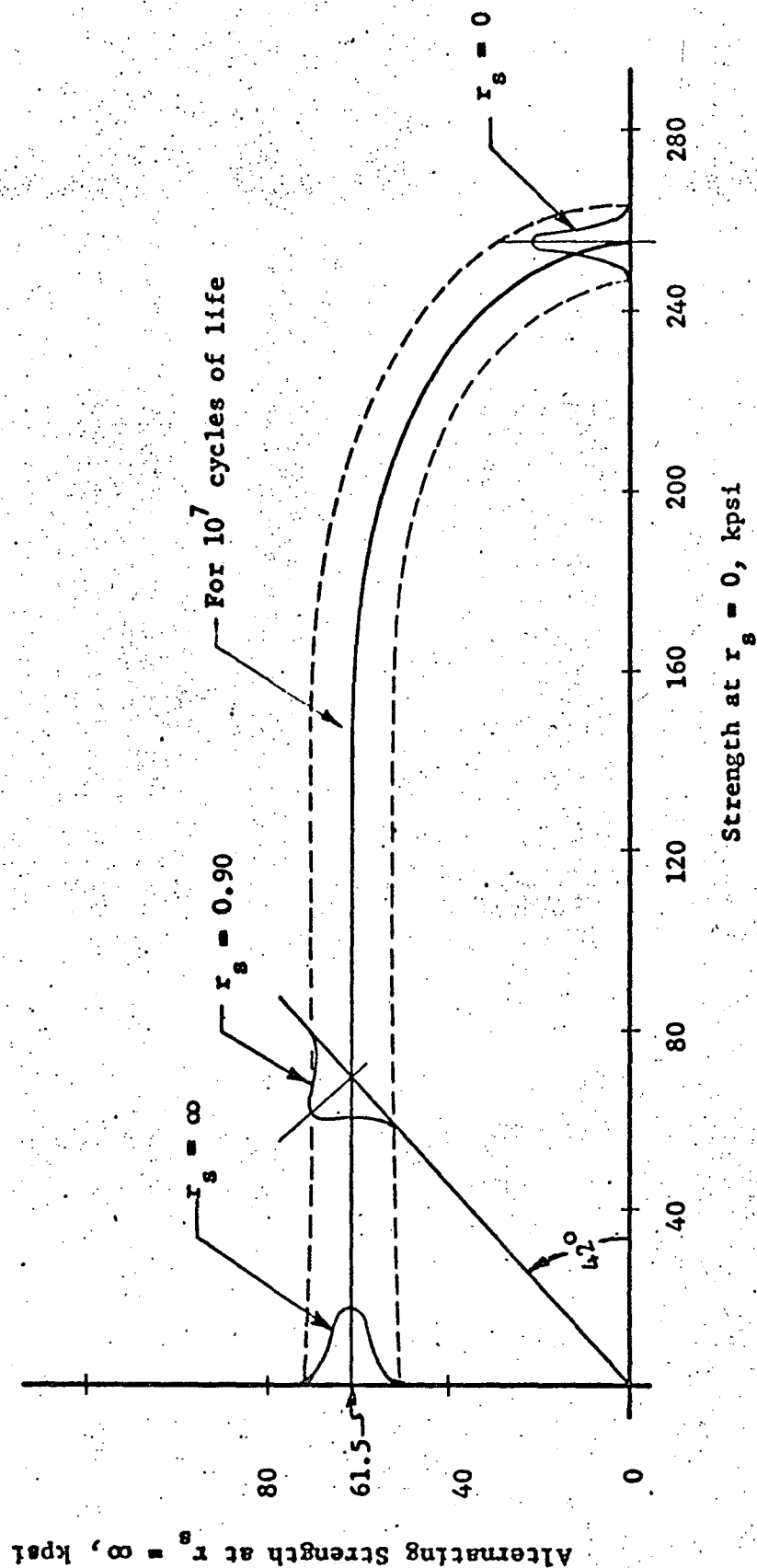


FIGURE 36. THREE-DIMENSIONAL DISTRIBUTIONAL GOODMAN FATIGUE STRENGTH SURFACE BASED ON RESEARCH RESULTS REPORTED HERE FOR 10^7 CYCLES OF LIFE.

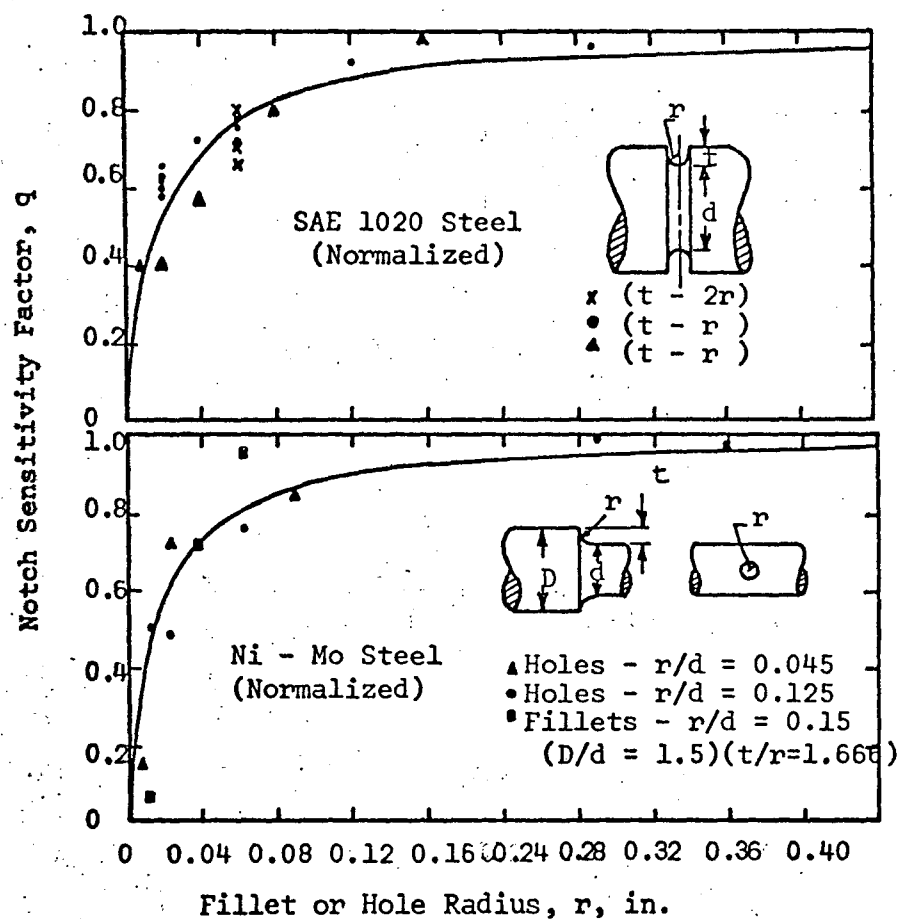


FIGURE 37. NOTCH SENSITIVITY OF NORMALIZED STEEL SPECIMENS.

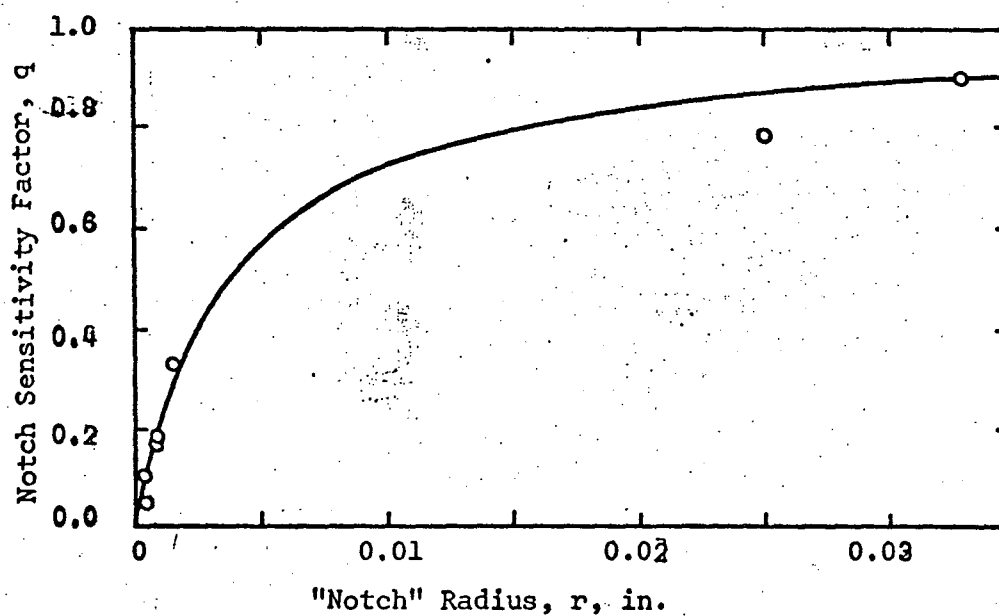


FIGURE 38. NOTCH SENSITIVITY OF QUENCHED AND TEMPERED ALLOY STEEL SPECIMENS.

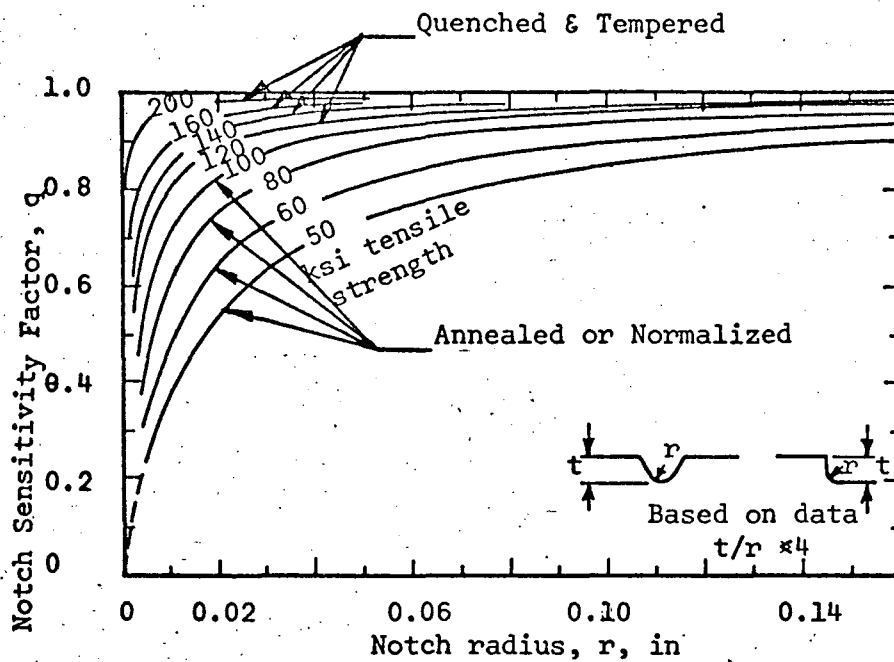


FIGURE 39. CURVES OF NOTCH SENSITIVITY VERSUS RADIUS FOR STEELS, BENDING OR AXIAL LOADING.

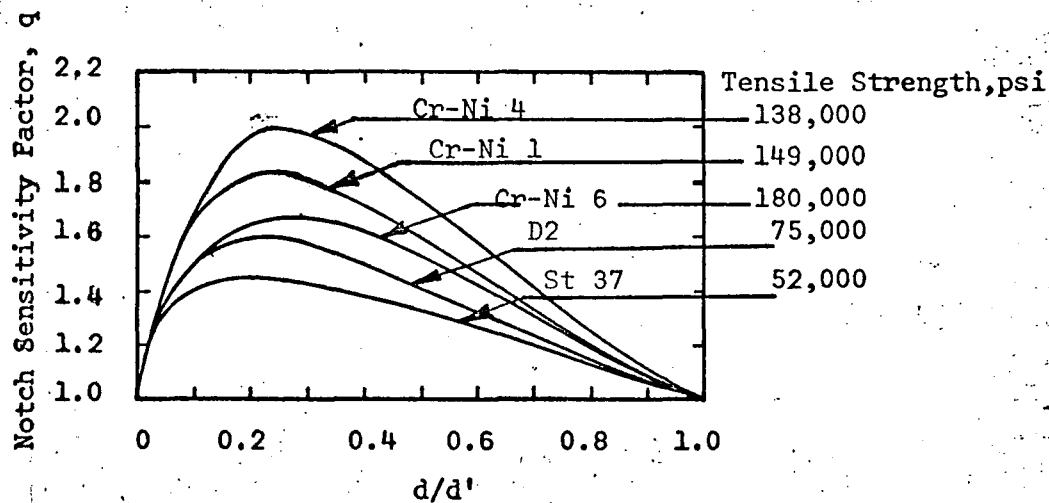


FIGURE 40. THE FATIGUE NOTCH FACTOR.

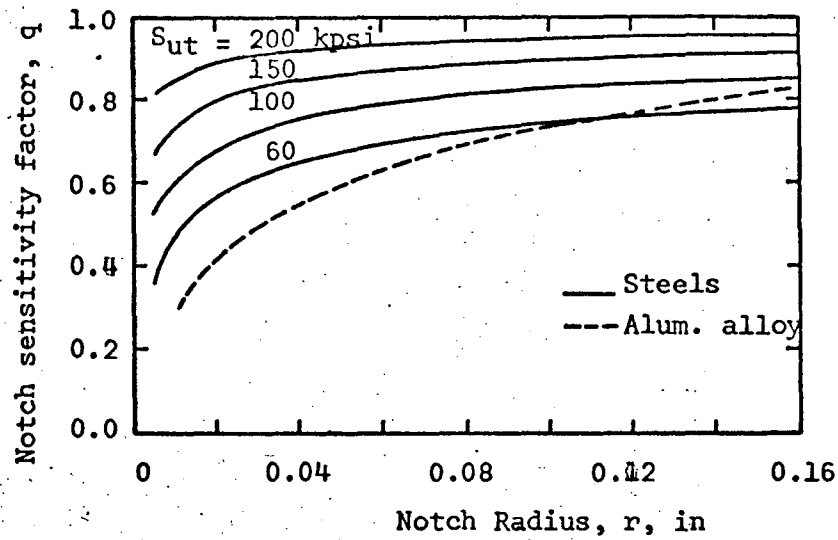


FIGURE 41. NOTCH SENSITIVITY CHARTS FOR STEELS AND 245-T WROUGHT ALUMINUM ALLOYS SUBJECTED TO REVERSED BENDING OR REVERSED AXIAL LOADS.

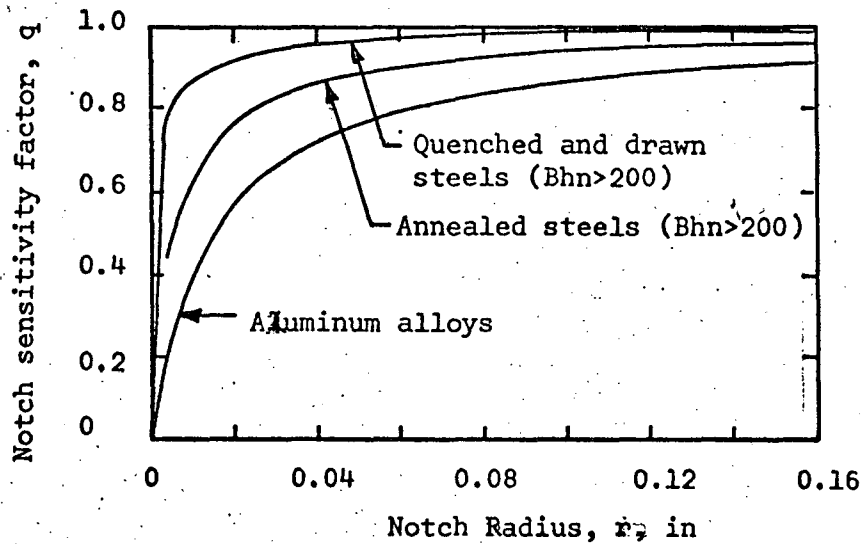


FIGURE 42. NOTCH SENSITIVITY CURVES FOR MATERIALS IN REVERSED TORSION.

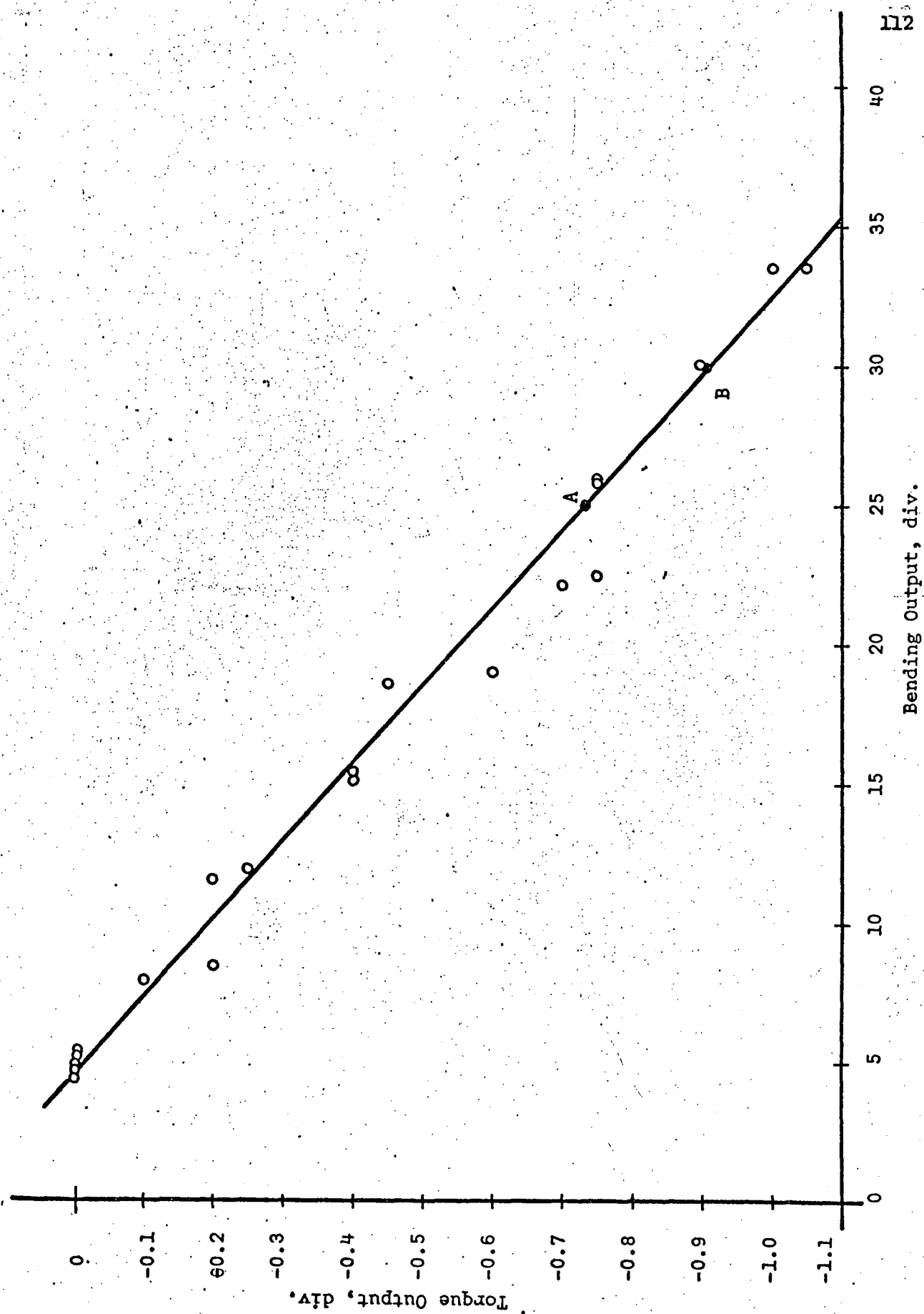


FIGURE 43. BENDING INTERACTION INTO TORQUE - MACHINE #3, JUNE 1969.

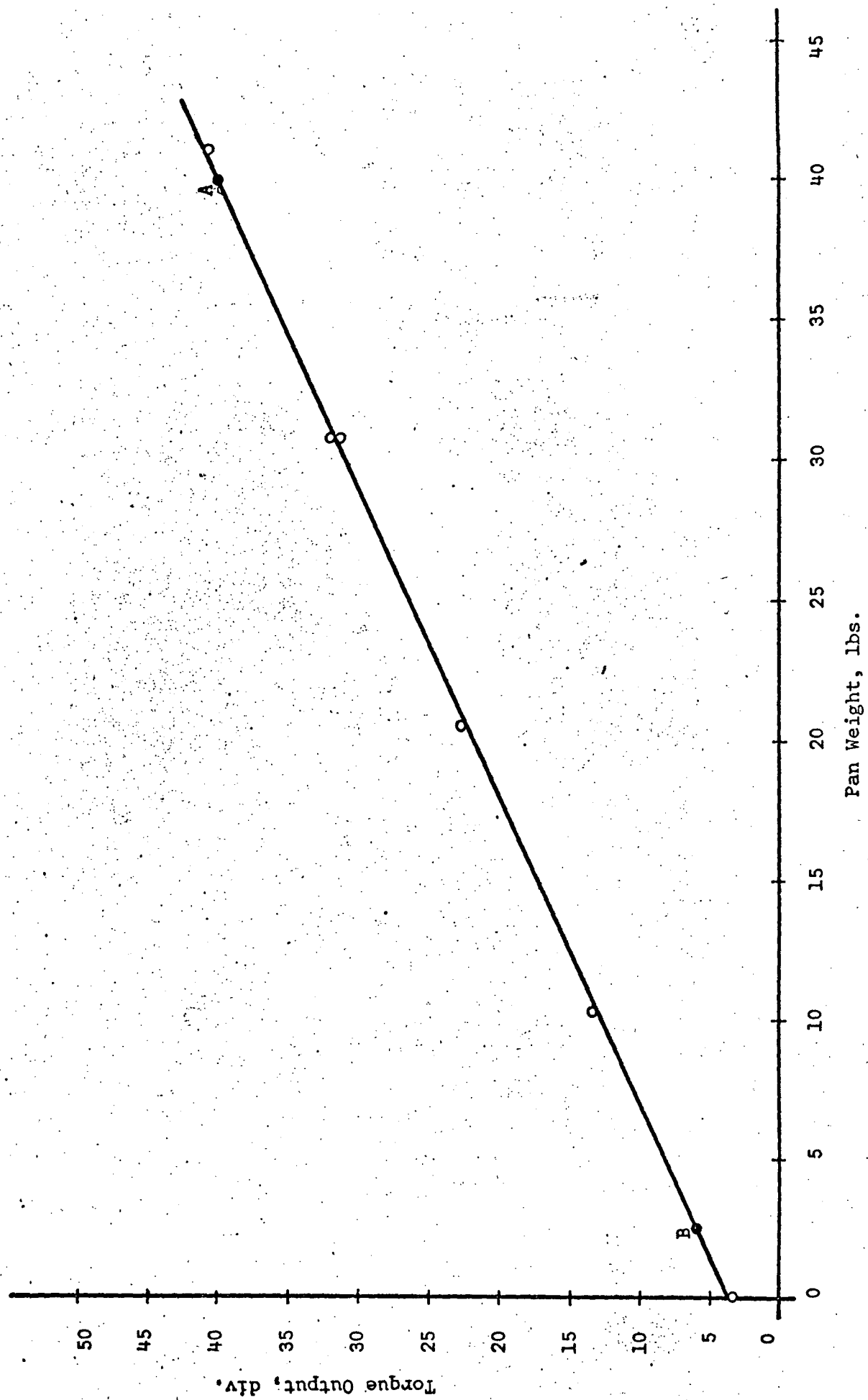


FIGURE #44. TORQUE OUTPUT VERSUS PAN WEIGHT - MACHINE #3, JUNE 1969.

TABLE 1

INSTRUMENTATION

<u>Part Name</u>	<u>Part Number</u>	<u>Manufacturer</u>	<u>Catalog Number</u>	<u>Qty.</u>	<u>Remarks</u>
Metalfilm strain gages with leads	324B-190	The Budd Co. Instruments Division	BG 2400	4	Bending moment-shank of tool holder
Metalfilm strain gages with leads	3 x 4 - M15E-240	"	"	2	Bending moment groove of specimen
Metalfilm strain gages with leads	C6-121-R2VC	"	"	2	Torque-shank of tool holder
Slip rings and brushes	AJ-8005-A8	Breeze Corporation, Inc.	66SR	1	Transfer of data
Visicorder	906 C-1	Honeywell	D-2009	1	With grid line system, 14 magnetic assembly channels
Galvanometer	M1650	"	D-2007	6	0-5000 cps
Amplifier	119	"	D-2005	6	Carrier and linear/integrating system with carrier channels 0-5000 cps

TABLE 2

TOOLHOLDER OUTPUT VERSUS PAN WEIGHT DATA
FOR BENDING BRIDGE CALIBRATION

MACHINE #1			MACHINE #2		MACHINE #3	
Data Point Number	Toolholder Output div.	Pan Weight lbs.	Toolholder Output div.	Pan Weight lbs.	Toolholder Output div.	Pan Weight lbs.
1	2.2	0	3.5	0	2.4	0
2	13.9	30.81	6.8	10.27	14.4	30.81
3	25.6	61.62	10.3	20.54	23.6	61.62
4	17.8	41.08	13.5	30.81	18.6	41.08
5	9.9	20.54	17.2	41.08	22.4	51.35
6	21.3	51.35	21.0	51.35	7.0	10.27
7	5.8	10.27	24.9	61.62	10.8	20.54
8	2.1	0	20.8	51.35	3.0	0
9	9.7	20.54	17.1	41.08	10.7	20.54
10	17.3	41.08	13.4	30.81	22.1	51.35
11	25.1	61.62	10.0	20.54	18.5	41.08
12	21.2	51.35	6.0	10.27	26.1	61.62
13	13.3	30.81	2.1	0	14.4	30.81
14	5.8	10.27			6.7	10.27
15	2.0	0			2.7	0
16	5.6	10.27			18.1	41.08
17	17.1	41.08			25.8	61.62
18	24.8	61.62			6.5	10.27
19	13.2	30.81			14.3	30.81
20	21.0	51.35			10.4	20.54
21	9.5	20.54			21.8	51.35
22	1.7	0			2.5	0

Visicorder Calibration Resistances :

Machine #1 - 500 k Ω at 24.9 divisions

Machine #2 - 500 k Ω at 25.2 divisions

Machine #3 - 500 k Ω at 25.0 divisions

TABLE 3

TOOLHOLDER OUTPUT VERSUS PAN WEIGHT DATA IN INCREMENTAL FORM
 FOR BENDING BRIDGE CALIBRATION IN TERMS OF CHANGE
 IN TOOLHOLDER OUTPUT DIVISIONS
 FOR 10.27 LBS. OF PAN
 WEIGHT

Data Point Increment	Machine #1	Machine #2	Machine #3
1-2	3.90	3.3	4.00
2-3	3.90	3.5	3.96
3-4	3.90	3.2	3.85
4-5	3.95	3.7	3.80
5-6	3.80	3.8	3.85
6-7	3.87	3.9	3.80
7-8	3.70	4.1	3.90
8-9	3.60	3.7	3.85
9-10	3.80	3.7	3.60
10-11	3.90	3.4	3.60
11-12	3.90	4.0	3.80
12-13	3.95	3.9	3.90
13-14	3.75		3.85
14-15	3.80		4.00
15-16	3.60		3.85
16-17	3.83		3.85
17-18	3.85		3.86
18-19	3.86		3.90
19-20	3.90		3.90
20-21	3.83		3.80
21-22	3.90		3.86
Average	3.838	3.683	3.850

TABLE 4
 CALIBRATION SPECIMEN GROOVE STRAIN GAGE
 OUTPUT VERSUS PAN WEIGHT DATA

Data Point Number	MACHINE #1		MACHINE #2		MACHINE #3	
	Groove Output μin/in	Pan Weight lbs.	Groove Output div.	Pan Weight lbs.	Groove Output μin/in	Pan Weight lbs.
1	39670	0	0.1	0	39655	0
2	40190	30.81	2.3	10.27	40174	30.81
3	40703	61.62	4.6	20.54	40695	61.62
4	40357	41.08	6.9	30.81	40346	41.08
5	40015	20.54	9.4	41.08	40518	51.35
6	40539	51.35	11.6	51.35	39825	10.27
7	39838	10.27	14.2	61.62	39998	20.54
8	39668	0	11.4	51.35	39655	0
9	40013	20.54	9.1	41.08	39998	20.54
10	40357	41.08	7.0	30.81	40516	51.35
11	40697	61.62	4.8	20.54	40345	41.08
12	40527	51.35	2.5	10.27	40785	61.62
13	40182	30.81	0	0	40172	30.81
14	39834	10.27			39825	10.27
15	39661	0			39655	0
16	39834	10.27			40345	41.08
17	40351	41.08			40687	61.62
18	40691	61.62			39824	10.27
19	40181	30.81			40171	30.81
20	40522	51.35			39995	20.54
21	39005	20.54			40514	51.35
22	39661	0			39654	0

Visicorder Calibration Resistance :

Machine #2 - 30 kΩ at 25.0 divisions

TABLE 5
REDUCTION OF MACHINE #2 DATA GIVEN IN TABLE 4

Data Point Increment			Change in Toolholder Output in Divisions per 10.27 lbs. of Pan Weight
Point	Average	Standard	
Weight	Weight	Weight	
100.	100.00	100.00	
1	1-2	100.00	2.2
10.27	2-3	100.00	2.3
20.54	3-4	100.00	2.3
30.81	4-5	100.00	2.5
41.08	5-6	100.00	2.2
51.35	6-7	100.00	2.6
61.62	7-8	100.00	2.8
	8-9	100.00	2.3
Average	9-10	100.00	2.1
	10-11	100.00	2.2
	11-12	100.00	2.3
	12-13	100.00	2.5
Average			2.358 divisions

TABLE 6
REDUCTION OF MACHINES #1 AND #3
DATA GIVEN IN TABLE 4

Pan Weight lbs.	MACHINE #1		MACHINE #3	
	Average Strain $\mu\text{in/in}$	ΔStrain $\mu\text{in/in}$	Average Strain $\mu\text{in/in}$	ΔStrain $\mu\text{in/in}$
0	39666.3	169.0	39654.7	170.0
10.27	39835.3	175.7	39824.7	172.0
20.54	40011.0	173.3	39996.7	175.6
30.81	40184.3	170.7	40172.3	173.0
41.08	40355.0	174.3	40345.3	171.7
51.35	40529.3	170.7	40516.0	173.0
61.62	40697.0		40689.0	
Average		170.7		172.7

TABLE 7

TORQUE OUTPUT VERSUS BENDING OUTPUT DATA
FROM TORQUE INTO BENDING INTERACTION CALIBRATION

	MACHINE #1		MACHINE #2		MACHINE #3	
Data Point Number	Torque Output div.	Bending Output div.	Torque Output div.	Bending Output div.	Torque Output div.	Bending Output div.
1	8.8	11.6	5.6	17.6		
2	41.9	10.0	14.9	18.3		
3	8.8	11.8	23.8	18.5		
4	41.7	10.2	32.4	18.9		
5	33.9	10.6	40.4	19.0		
6	25.7	11.1	32.5	18.6		
7	17.4	11.6	23.9	18.3		
8	8.8	12.0	14.9	18.0		
9	17.3	11.5	5.7	17.6		
10	25.3	11.3	14.9	17.9	SEE DATA REDUCTION IN SECTION IV - B - 3	
11	34.0	10.8	23.7	18.1		
12	41.9	10.4	32.3	18.3		
13	8.8	10.9	40.3	18.8		
14			32.4	18.5		
15			23.8	18.2		
16			14.9	17.9		
17			5.6	17.6		
18			5.3	12.9		
19			14.5	13.1		
20			23.4	13.3		
21			32.2	13.6		
22			40.2	13.8		
23			32.2	13.6		
24			23.5	13.5		
25			14.6	13.2		
26			5.3	12.8		

Visicorder Calibration Resistances:

- Machine #1 - Bending 500 k Ω at 25.0 divisions
Torque 304 k Ω at 45.0 divisions
- Machine #2 - Bending 500 k Ω at 25.0 divisions
Torque 30 k Ω at 44.7 divisions
- Machine #3 - Bending 500 k Ω at 25.0 divisions
Torque 304 k Ω at 45.0 divisions

TABLE 8

TOOLHOLDER VERSUS GROOVE BRIDGE OUTPUT DATA
FOR QUASI-STATIC CALIBRATION OF GROOVE STRESS

Data Point Number	MACHINE #1		MACHINE #2		MACHINE #3	
	Toolholder Output div.	Groove Output div.	Toolholder Output div.	Groove Output div.	Toolholder Output div.	Groove Output div.
1	21.6	16.2	20.0	31.1	25.0	26.8
2	25.1	18.6	23.9	36.2	28.6	41.8
3	29.1	21.7	27.2	41.3	32.0	47.3
4	33.1	24.2	30.3	45.3	39.1	57.0
5	36.1	26.1	37.6	56.0	21.6	31.9
6	40.3	29.3	36.6	52.8	25.1	36.3
7	43.9	31.7	34.7	50.7	28.2	40.9
8	39.9	29.3	30.0	44.6	32.4	46.2
9	35.9	26.4	27.7	40.6	40.0	56.0
10	32.7	23.9	23.7	34.3	21.7	31.3
11	29.2	21.5	20.1	30.5	25.2	36.3
12	25.7	18.9	23.1	34.8	28.8	41.3
13	22.0	16.4	27.0	39.9	32.0	46.6
14	25.8	19.2	30.0	43.6	35.3	50.3
15	28.8	21.3	33.9	49.3		
16	33.3	24.3	36.2	52.2		
17	36.1	26.7				
18	40.2	29.3				
19	44.0	31.7				

Visicorder Calibration Resistances:

Machine #1 - Toolholder 200 k Ω at 24.9 divisions
Groove 22.22 k Ω at 24.9 divisions

Machine #2 - Toolholder 190 k Ω at 24.8 divisions
Groove 11 k Ω at 24.6 divisions

Machine #3 - Toolholder 190 k Ω at 25.0 divisions
Groove 11 k Ω at 25.0 divisions

TABLE 9

TABLE 8 VISICORDER DIVISIONS CONVERTED TO STRAIN
IN TOOLHOLDER AND SPECIMEN GROOVE

	$\Delta N_{\text{vis Toolholder}}$ div.	$\Delta \epsilon_{\text{Toolholder}}$ $\mu\text{in/in}$	$\Delta N_{\text{vis groove}}$ div.	$\Delta \epsilon_{\text{groove}}$ $\mu\text{in/in}$
Machine #1	22.2	32.85	15.75	1620
Machine #2	40.0	62.40	59.0	3145
Machine #3	10.7	16.55	15.0	786

TABLE 10

TORQUE OUTPUT VERSUS PAN WEIGHT DATA
FOR TORQUE BRIDGE CALIBRATION

Data Point Number	MACHINE #1		MACHINE #2		MACHINE #3	
	Torque Output div.	Pan Weight lbs.	Torque Output div.	Pan Weight lbs.	Torque Output div.	Pan Weight lbs.
1	8.8	0	5.6	0	5.4	0
2	41.9	41.08	14.9	10.27	13.2	10.27
3	8.8	0	23.8	20.54	21.1	20.54
4	41.7	41.08	32.4	30.81	28.6	30.81
5	33.9	30.8	40.4	41.08	35.9	41.08
6	25.7	20.54	32.5	30.81	28.5	30.81
7	17.4	10.27	23.9	20.54	20.8	20.54
8	8.8	0	14.9	10.27	12.9	10.27
9	17.3	10.27	5.7	0	5.1	0
10	25.8	20.54	14.9	10.27	5.2	0
11	34.0	30.81	23.7	20.54	13.1	10.27
12	41.9	41.08	32.3	30.81	20.9	20.54
13	8.8	0	40.3	41.08	28.6	30.81
14			32.4	30.81	35.6	41.08
15			23.8	20.54	28.3	30.81
16			14.9	10.27	20.8	20.54
17			5.6	0	12.9	10.27
18			5.3	0	5.4	0
19			14.5	10.27		
20			23.4	20.54		
21			32.2	30.81		
22			40.2	41.08		
23			32.2	30.81		
24			23.5	20.54		
25			14.6	10.27		
26			5.3	0		

Visicorder Calibration Resistances:

Machine #1 - 304 k Ω at 45.0 divisionsMachine #2 - 304 k Ω at 44.7 divisionsMachine #3 - 304 k Ω at 44.5 divisions

TABLE 11

TORQUE REDUCTION TABLE
FROM THE RESULTS OF TABLE 10

Machine No.	Point A	Point B	ΔW lbs.	ΔN_{vis} div.	$\Delta \tau_{out}$ psi	$\Delta \tau_{True}$ psi	Slope K_T
1	(30.0,33.0)	(10.0,17.0)	20.0	16.0	513	452	0.882
2	(40.0,40.0)	(5.0, 10.5)	35.0	29.5	943	792	0.840
3	(35.0,31.5)	(15.0,16.5)	20.0	15.0	480	452	0.944

TABLE 12
BENDING OUTPUT VERSUS TORQUE OUTPUT DATA FOR BENDING
INTO TORQUE INTERACTION CALIBRATION

Data Point Number	MACHINE #1		MACHINE #2		MACHINE #3	
	Torque Output div.	Bending Output div.	Torque Output div.	Bending Output div.	Torque Output div.	Bending * Output div.
1	-0.1	0.2	0	2.7	-0.3	2.4
2	+0.5	17.3	0.8	21.0	-0.5	9.0
3	-0.1	0.8	0	3.2	-0.8	20.1
4	+0.4	17.1	0.1	6.9	-0.3	9.1
5	+0.2	8.2	0.3	10.5	0	1.1
6	-0.1	0.5	0.6	14.1	-0.1	8.9
7	+0.1	8.0	0.7	17.1	-0.7	20.2
8	+0.4	16.9	0.9	22.6	-0.3	9.0
9	+0.2	7.8	1.0	25.2	+0.1	1.1
10	-0.1	0.3	0.8	21.6	-0.5	8.9
11	+0.1	7.7	0.6	18.0	-1.0	20.2
12	+0.4	16.5	0.5	14.4	-0.4	8.8
13	-0.1	0.1	0.3	10.7	+0.2	0.9
14			0.1	7.1	-0.4	8.8
15			0	3.3	-0.9	20.0
16			1.0	21.5	-0.3	8.9
17			1.2	25.2	+0.1	1.1
18			1.3	29.0	-0.4	8.8
19			1.5	32.8	-0.9	20.1
20			1.7	36.0	-0.3	9.0
21			1.8	40.0		
22			2.0	44.0		
23			2.0	44.2		
24			1.8	40.5		
25			1.6	36.0		
26			1.4	33.2		
27			1.2	29.5		
28			1.0	25.8		
29			0.8	22.0		
30						

*All bending data appears at 0.2 amplifier attenuation, therefore a 5/2 correction factor is required.

Visicorder Calibration Resistances:

Machine #1 - Bending 500 k Ω at 25.1 div.; Torque 304 k Ω at 44.9 div.

Machine #2 - Bending 500 k Ω at 24.0 div.; Torque 350 k Ω at 44.8 div.

Machine #3 - Bending 500 k Ω at 25.0 div.; Torque 350 k Ω at 44.8 div.

TABLE 13
 BENDING OUTPUT VERSUS TORQUE OUTPUT DATA AT HIGH TORQUE LEVEL
 FOR BENDING INTO TORQUE INTERACTION CALIBRATION

MACHINE #2		
Data Point Number	Torque Output div.	Bending Output div.
1	25.2	9.4
2	25.3	11.8
3	25.5	14.1
4	25.6	16.3
5	25.7	18.7
6	25.9	21.1
7	26.0	23.4
8	25.8	21.1
9	25.9	18.8
10	25.6	16.6
11	25.5	14.2
12	25.4	11.8
13	25.3	9.5
14	25.5	13.5
15	25.8	21.0
16	26.0	23.5
17	26.1	25.8
18	26.3	28.0
19	26.4	30.2
20	26.5	32.8
21	26.7	34.8
22	26.5	32.8
23	26.4	30.5
24	26.3	28.0
25	26.2	25.8
26	26.3	28.0
27	26.2	25.8
28	26.1	23.5
29	25.9	21.0
30	25.4	13.7

Visicorder Calibration Resistances:

Machine #2 - Bending 500 k Ω at 25.0 divisions
 Torque 350 k Ω at 44.8 divisions

TABLE 14
 AXIAL OUTPUT VERSUS BENDING OUTPUT FOR AXIAL TO
 BENDING INTERACTION CALIBRATION

MACHINE #1		
Data Point Number	Bending Level div.	Groove Bending Mean div.
1	20.8	-0.2
2	24.2	-0.5
3	27.9	-0.5
4	31.5	-0.6
5	35.0	-0.9
6	38.7	-1.1
7	41.9	-0.8
8	19.6	0
9	42.2	-1.4
10	19.7	+0.2
11	41.9	-1.0
12	19.4	+0.3
13	41.8	-1.0

Visicorder Calibration Resistances:

Machine # 1 - Bending (toolholder) 190 k Ω at 50.0 divisions
 Bending (groove) 290 k Ω at 50.0 divisions

TABLE 15
 AXIAL OUTPUT VERSUS TORQUE OUTPUT FOR AXIAL LOAD
 INTO TORQUE INTERACTION CALIBRATION

MACHINE #1		
Data Point Number	Torque Level div.	Groove Axial Mean div.
1	0	-0.6
2	11.8	+0.3
3	36.7	+1.8
4	27.1	+0.8
5	1.5	-1.2
6	40.0	+1.5
7	21.5	+0.5
8	7.8	-1.5
9	1.1	-1.9
10	31.3	+2.0
11	41.5	+0.8
12	27.6	+1.0
13	15.6	0
14	0.5	-1.8

Visicorder Calibration Resistances:

Bending (groove) 290 k Ω at 49.8 divisions

Torque 304 k Ω at 45.0 divisions

TABLE 16
THE CALIBRATION COEFFICIENTS FOR EACH
RESEARCH MACHINE

Machine	K_{BGR}	K_{GR-TH}	K_T	$K_{T/B}$	$K_{B/T}$
1	0.967	0.0203	0.882	0.0548	0.0298
2	0.902	0.0198	0.840	0.0343	0.0410
3	0.972	0.0215	0.944*	0.0000	-0.0170**

*After June 1, 1969 $K_T = 0.842$ because of gage replacement

**After June 1, 1969 $K_{B/T} = -0.0238$ because of gage replacement

TABLE 17
 TORQUE ON STRESS LEVELS AND VISICORDER DIVISIONS
 FOR $r_s = 3$ AND MACHINE #1

Alternating Bending Stress psi	Bending Divisions div.	Calibration Div/Resistance div/k Ω	Mean Shear Stress psi	Shear Divisions div.	Calibration Div/Resistance div/k Ω
154,800	43.5	50/125	29,800	19.4	45/304
121,800	34.2	50/125	23,400	15.3	45/304
104,350	44.5	50/190	20,080	13.1	45/304
86,800	37.0	50/190	16,700	10.9	45/304
77,700	33.2	50/190	14,950	9.8	45/304

TABLE 16
 TORQUE OUTPUT VERSUS PAN WEIGHT DATA FOR NEW TORQUE GAGES,
 MACHINE #3, JUNE 1969

Data Point Number	Torque Output div.	Pan Weight div.
1	3.3	0
2	13.1	10.27
3	22.6	20.54
4	31.3	30.81
5	40.6	41.08
6	31.9	30.81
7	22.6	20.54
8	13.2	10.27
9	3.4	0
10	13.2	10.27
11	22.7	20.54
12	31.9	30.81
13	40.7	41.09
14	31.9	20.54
15	22.7	20.54
16	13.3	10.27
17	3.4	0

Visicorder Calibration Resistance:

Machine #3 - 304 k Ω at 44.8 divisions

TABLE 19
BENDING OUTPUT VERSUS TORQUE OUTPUT DATA FOR NEW TORQUE GAGES,
MACHINE #3, JUNE 1969

Data Point Number	Bending Output div.	Torque Output div.
1	4.4	0
2	7.9	-0.10
3	11.5	-0.20
4	15.1	-0.40
5	18.6	-0.45
6	22.2	-0.70
7	25.8	-0.75
8	30.0	-0.90
9	33.5	-1.00
10	30.0	-0.90
11	26.0	-0.75
12	22.5	-0.75
13	19.0	-0.60
14	15.4	-0.40
15	11.9	-0.25
16	8.4	-0.20
17	4.8	0
18	4.9	0
19	33.5	-1.00
20	5.5	0
21	33.5	-1.00
22	5.3	0
23	33.5	-1.05
24	5.5	0

Visicorder Calibration Resistances:

Machine #3 - Bending 490 k Ω at 25.0 divisions
Torque 304 k Ω at 45.3 divisions

APPENDIX A. DATA REDUCTION RESULTS FOR $r_s = \infty$.

TEST NO.	SPECIMEN NO.	MACHINE NO.	PAN WEIGHT	RCAL BENDING	NCAL BENDING	NVIS BENDING	MCAL TORQUE	NCAL TORQUE	NVIS TORQUE	BENDING STRESS	SHEAR STRESS	STRESS RATIO
125	166	2	29	140000.0	50.20	59.30	-0.0	-0.00	-0.00	153581.2	0.0	INFIN.
126	204	2	29	90000.0	50.10	28.20	-0.0	-0.00	-0.00	154403.2	0.0	INFIN.
127	225	2	29	90000.0	49.70	27.40	-0.0	-0.00	-0.00	151318.6	0.0	INFIN.
128	133	2	29	90000.0	50.00	27.90	-0.0	-0.00	-0.00	153155.4	0.0	INFIN.
129	196	2	29	90000.0	49.40	28.00	-0.0	-0.00	-0.00	155571.2	0.0	INFIN.
130	220	2	29	90000.0	49.90	28.20	-0.0	-0.00	-0.00	155112.5	0.0	INFIN.
131	193	2	29	90000.0	49.60	28.00	-0.0	-0.00	-0.00	154943.9	0.0	INFIN.
132	191	2	29	90000.0	50.40	28.40	-0.0	-0.00	-0.00	154662.8	0.0	INFIN.
133	143	2	29	90000.0	50.20	28.40	-0.0	-0.00	-0.00	155279.0	0.0	INFIN.
134	342	1	30	150000.0	50.20	51.60	-0.0	-0.00	-0.00	153216.2	0.0	INFIN.
135	341	1	30	150000.0	50.10	50.70	-0.0	-0.00	-0.00	150844.3	0.0	INFIN.
136	365	1	30	150000.0	50.30	51.55	-0.0	-0.00	-0.00	152763.5	0.0	INFIN.

MEAN BENDING STRESS IN GROOVE = 153745.1 PSI.

STD. DEV. OF BENDING STRESS IN GROOVE = 1544.74 PSI.

APPENDIX A: DATA REDUCTION RESULTS FOR $\tau_s = \infty$.

TEST NO.	SPECIMEN NO.	MACHINE NO.	PAN DEFLECTION	RCAL BENDING	RCAL HEMING	NVIS BENDING	RCAL TORQUE	NCAL TORQUE	NVIS TORQUE	BENDING STRESS	SHEAR STRESS	STRESS RATIO
29	63	1	20	290000.0	32.40	51.00	-0.00	-0.00	-0.00	121360.5	0.0	INFIN.
30	22	1	20	290000.0	33.20	52.10	-0.00	-0.00	-0.00	120990.6	0.0	INFIN.
31	100	1	20	290000.0	32.90	51.40	-0.00	-0.00	-0.00	120453.5	0.0	INFIN.
32	82	1	20	190000.0	50.20	51.40	-0.00	-0.00	-0.00	120491.3	0.0	INFIN.
33	42	1	20	190000.0	50.50	52.40	-0.00	-0.00	-0.00	122105.8	0.0	INFIN.
34	59	1	20	190000.0	50.50	52.70	-0.00	-0.00	-0.00	122804.9	0.0	INFIN.
35	52	1	20	190000.0	49.30	50.80	-0.00	-0.00	-0.00	121258.8	0.0	INFIN.
36	76	1	20	190000.0	50.70	51.50	-0.00	-0.00	-0.00	119535.2	0.0	INFIN.
37	66	1	20	190000.0	50.30	51.60	-0.00	-0.00	-0.00	120719.7	0.0	INFIN.
38	111	1	20	190000.0	50.40	52.00	-0.00	-0.00	-0.00	121414.1	0.0	INFIN.
39	20	1	20	190000.0	50.40	52.00	-0.00	-0.00	-0.00	121414.1	0.0	INFIN.
40	73	1	20	190000.0	49.90	51.30	-0.00	-0.00	-0.00	120979.9	0.0	INFIN.
41	69	1	20	190000.0	49.30	50.90	-0.00	-0.00	-0.00	121497.5	0.0	INFIN.
42	86	1	20	190000.0	49.30	51.40	-0.00	-0.00	-0.00	122891.0	0.0	INFIN.
43	96	1	20	190000.0	48.90	50.60	-0.00	-0.00	-0.00	121769.4	0.0	INFIN.
44	80	1	20	190000.0	49.20	51.50	-0.00	-0.00	-0.00	123179.5	0.0	INFIN.
45	101	1	20	190000.0	49.40	51.20	-0.00	-0.00	-0.00	121946.2	0.0	INFIN.
46	89	1	20	190000.0	49.00	51.10	-0.00	-0.00	-0.00	122721.7	0.0	INFIN.

MEAN BENDING STRESS IN GROOVE = 121519.6 PSI.


STD. DEV. OF BENDING STRESS IN GROOVE = 948.34 PSI.

APPENDIX A. DATA REDUCTION RESULTS FOR $F_B = 0$.

TEST NO.	SPECIMEN NO.	MACHINE NO.	MAN WEIGHT	HCAL BENDING	HCAL TENDING	NVIS BENDING	HCAL TORQUE	NCAL TORQUE	NVIS TORQUE	BENDING STRESS	SHEAR STRESS	STRESS RATIO
10	24	1	15	290000.0	39.40	51.00	-0.0	-0.00	-0.00	99799.0	0.0	INFIN.
11	62	2	16	290000.0	41.10	49.80	-0.0	-0.00	-0.00	103212.0	0.0	INFIN.
12	88	1	15	290000.0	38.20	51.00	-0.0	-0.00	-0.00	102934.0	0.0	INFIN.
13	46	2	16	290000.0	40.00	51.00	-0.0	-0.00	-0.00	108605.7	0.0	INFIN.
14	58	1	15	290000.0	38.20	51.00	-0.0	-0.00	-0.00	102934.0	0.0	INFIN.
15	99	2	16	290000.0	40.00	50.50	-0.0	-0.00	-0.00	107541.0	0.0	INFIN.
16	33	1	15	290000.0	38.40	50.50	-0.0	-0.00	-0.00	101394.0	0.0	INFIN.
17	85	2	16	290000.0	40.00	50.00	-0.0	-0.00	-0.00	106476.2	0.0	INFIN.
18	55	1	15	290000.0	38.40	50.50	-0.0	-0.00	-0.00	101394.0	0.0	INFIN.
19	44	2	16	290000.0	39.40	49.10	-0.0	-0.00	-0.00	106151.9	0.0	INFIN.
20	110	1	15	290000.0	39.70	52.00	-0.0	-0.00	-0.00	106994.9	0.0	INFIN.
21	104	2	16	290000.0	40.40	50.40	-0.0	-0.00	-0.00	105741.9	0.0	INFIN.
22	113	1	16	290000.0	37.30	49.70	-0.0	-0.00	-0.00	102730.5	0.0	INFIN.
23	69	2	16	290000.0	40.00	50.30	-0.0	-0.00	-0.00	107114.1	0.0	INFIN.
24	30	1	16	290000.0	38.00	51.70	-0.0	-0.00	-0.00	104896.0	0.0	INFIN.
25	13	2	16	290000.0	39.40	49.50	-0.0	-0.00	-0.00	107014.7	0.0	INFIN.
26	71	1	15	290000.0	38.90	51.10	-0.0	-0.00	-0.00	101279.9	0.0	INFIN.
27	48	2	14	290000.0	39.20	50.60	-0.0	-0.00	-0.00	108026.0	0.0	INFIN.

MEAN BENDING STRESS IN GROOVE = 104340.3 PSI.

STD. DEV. OF BENDING STRESS IN GROOVE = 2001.30 PSI.


 Reproduced from
best available copy.

APPENDIX A. DATA REDUCTION RESULTS FOR $T_3 = \infty$.

TEST NO.	SPECIMEN NO.	MACHINE NO.	PAN WEIGHT	HCAL HENDING	NCAL HENDING	NVIS HENDING	HCAL TORQUE	NCAL TORQUE	NVIS TORQUE	BENDING STRESS	SHEAR STRESS	STRESS RATIO
40	102	1	10	290000.0	45.30	51.30	-0.0	-0.00	-0.00	87311.5	0.0	INFIN.
50	112	1	10	290000.0	45.60	51.30	-0.0	-0.00	-0.00	86737.0	0.0	INFIN.
51	75	1	10	290000.0	46.20	52.00	-0.0	-0.00	-0.00	86778.8	0.0	INFIN.
52	34	1	10	290000.0	45.10	50.20	-0.0	-0.00	-0.00	85818.2	0.0	INFIN.
53	45	1	10	290000.0	45.20	51.70	-0.0	-0.00	-0.00	88186.9	0.0	INFIN.
54	94	1	10	290000.0	46.10	51.70	-0.0	-0.00	-0.00	86466.3	0.0	INFIN.
55	35	1	10	290000.0	45.50	50.80	-0.0	-0.00	-0.00	86080.4	0.0	INFIN.
56	66	1	10	290000.0	44.70	49.00	-0.0	-0.00	-0.00	84516.3	0.0	INFIN.
57	70	1	10	290000.0	46.00	52.10	-0.0	-0.00	-0.00	87323.7	0.0	INFIN.
58	25	1	10	290000.0	45.50	50.40	-0.0	-0.00	-0.00	85402.6	0.0	INFIN.
60	31	1	10	290000.0	46.10	51.60	-0.0	-0.00	-0.00	86298.0	0.0	INFIN.
61	114	1	10	290000.0	45.90	52.80	-0.0	-0.00	-0.00	88689.7	0.0	INFIN.
62	29	1	10	290000.0	45.20	51.30	-0.0	-0.00	-0.00	87504.6	0.0	INFIN.
63	18	1	10	290000.0	46.70	52.50	-0.0	-0.00	-0.00	86675.1	0.0	INFIN.
65	48	1	10	290000.0	44.90	50.60	-0.0	-0.00	-0.00	86887.3	0.0	INFIN.
67	81	1	10	290000.0	44.40	50.00	-0.0	-0.00	-0.00	86827.9	0.0	INFIN.
68	19	1	10	290000.0	44.40	50.00	-0.0	-0.00	-0.00	86823.9	0.0	INFIN.
69	30	1	10	290000.0	43.20	48.90	-0.0	-0.00	-0.00	87272.4	0.0	INFIN.

MEAN BENDING STRESS IN GROOVE = 86755.3 PSI.

STD. DEV. OF BENDING STRESS IN GROOVE = 962.73 PSI.

APPENDIX A. DATA REDUCTION RESULTS FOR $\sigma_s = \infty$.

TEST NO.	SPECIMEN NO.	MACHINE NO.	PAN WEIGHT	HCAL BENDING	NCAL BENDING	NVIS BENDING	HCAL TORQUE	NCAL TORQUE	NVIS TORQUE	BENDING STRESS	SHEAR STRESS	STRESS RATIO
130	135	2	6	190000.0	49.60	30.00	-0.0	-0.00	-0.00	78634.9	0.0	INFIN.
140	147	2	6	190000.0	50.20	30.40	-0.0	-0.00	-0.00	78733.0	0.0	INFIN.
152	198	2	6	190000.0	50.20	29.20	-0.0	-0.00	-0.00	75625.1	0.0	INFIN.
143	214	2	6	190000.0	49.80	29.40	-0.0	-0.00	-0.00	76754.7	0.0	INFIN.
145	215	2	6	190000.0	49.50	29.20	-0.0	-0.00	-0.00	76694.6	0.0	INFIN.
144	134	2	6	190000.0	49.40	30.10	-0.0	-0.00	-0.00	79218.5	0.0	INFIN.
147	125	2	6	190000.0	49.20	29.60	-0.0	-0.00	-0.00	78219.2	0.0	INFIN.
148	144	2	6	190000.0	50.10	29.80	-0.0	-0.00	-0.00	77333.1	0.0	INFIN.
150	149	2	6	190000.0	49.50	30.40	-0.0	-0.00	-0.00	79844.4	0.0	INFIN.
151	148	2	6	190000.0	49.90	29.60	-0.0	-0.00	-0.00	77122.0	0.0	INFIN.
152	128	2	6	190000.0	52.20	31.20	-0.0	-0.00	-0.00	77709.0	0.0	INFIN.
154	219	2	6	190000.0	49.90	30.40	-0.0	-0.00	-0.00	79727.5	0.0	INFIN.
154	123	2	6	190000.0	50.10	31.20	-0.0	-0.00	-0.00	80964.2	0.0	INFIN.
155	121	2	6	190000.0	49.70	30.00	-0.0	-0.00	-0.00	78478.7	0.0	INFIN.
156	145	2	6	190000.0	50.00	29.90	-0.0	-0.00	-0.00	77747.8	0.0	INFIN.
157	171	2	6	190000.0	49.70	30.40	-0.0	-0.00	-0.00	79525.1	0.0	INFIN.
160	156	2	6	190000.0	49.50	27.60	-0.0	-0.00	-0.00	72492.1	0.0	INFIN.
163	143	2	6	190000.0	49.20	29.10	-0.0	-0.00	-0.00	76898.0	0.0	INFIN.

MEAN BENDING STRESS IN GROOVE = 77873.8 PSI.

STD. DEV. OF BENDING STRESS IN GROOVE = 1905.81 PSI.

APPENDIX B. DATA REDUCTION RESULTS FOR $r_8 = 0.7$ AND $r_9 = 0.9$.

TEST NO.	SPECIMEN NO.	MACHINE NO.	PAN FLOUT	MCAL PENDING	MCAL HENDING	NVIS HENDING	MCAL TORSION	MCAL TORSION	NVIS TORSION	RENDING STRESS	SHEAR STRESS	STRESS RATIO
411	354	1	19	140000.0	50.10	47.75	200000.0	45.20	32.50	108353.6	84677.9	.739
412	345	1	21	140000.0	50.35	49.65	200000.0	45.20	34.30	112014.6	89444.6	.723
413	345	1	21	140000.0	50.45	49.90	200000.0	45.10	33.55	112460.8	87595.7	.741
415	335	1	22	140000.0	50.10	49.30	200000.0	45.15	33.30	111900.3	86833.5	.744
416	358	1	21	140000.0	49.95	48.45	200000.0	45.10	32.90	110284.0	85998.5	.741
417	406	1	20	140000.0	50.50	48.60	200000.0	45.10	34.30	109194.5	89743.7	.703
418	347	1	21	140000.0	50.10	49.25	200000.0	45.10	33.60	111734.7	87755.5	.735
419	356	1	21	140000.0	50.45	48.75	200000.0	45.30	35.50	109521.9	92571.8	.683
420	397	1	22	140000.0	50.75	49.00	200000.0	45.30	33.90	112193.1	88149.6	.735
421	437	1	21	140000.0	50.35	49.15	200000.0	45.15	34.55	110601.1	90267.2	.709
422	402	1	21	140000.0	50.30	48.65	200000.0	45.10	35.50	109604.4	92995.5	.680
423	348	1	21	140000.0	49.40	48.75	200000.0	45.15	33.75	11236.3	88074.5	.729

W. A. BEING 1125 IN WARD • 110774.6 PSI.

MIN. REV. OR RESIGN FILING IN GERMANY = 125M.98 PSI.

REF ID: A66077

THE NEW YORK PUBLIC LIBRARY
ASTOR LENOX TILDEN FOUNDATION
500 5TH AVENUE
NEW YORK 17, N.Y.

WYATT INVESTS RATIO • 0.72107

IN. REF. OF REAN 31453 MATLO = 02275.

APPENDIX B. DATA REDUCTION RESULTS FOR $r_s = 0.7$ AND $r_s = 0.9$.

TEST NO.	SPECIMEN NO.	MACHINE NO.	PAY WEIGHT	RCAL BENDING	NCAL BENDING	RVIS BENDING	RCAL TORQUE	NCAL TORQUE	RVIS TORQUE	BENDING STRESS	SHEAR STRESS	STRESS RATIO
207	172	1	10	190000.0	49.80	32.20	304000.0	44.30	32.59	73539.3	56814.4	.747
209	200	1	10	190000.0	50.10	34.60	304000.0	45.10	36.90	78408.5	63480.5	.713
210	185	1	10	190000.0	50.20	33.90	304000.0	44.80	35.10	76735.6	60733.9	.729
211	176	1	10	190000.0	49.80	33.00	304000.0	45.00	36.00	75173.2	62118.9	.699
212	141	1	10	190000.0	49.80	29.70	304000.0	44.60	37.00	67216.2	64769.9	.599
213	154	1	10	190000.0	50.00	34.00	304000.0	44.80	35.30	77273.8	61076.7	.730
215	218	1	10	190000.0	49.90	33.70	304000.0	44.90	36.00	76668.3	62213.6	.712
217	277	3	10	190000.0	49.90	34.70	304000.0	44.00	36.60	77265.0	73527.6	.607
218	320	3	10	190000.0	50.00	35.30	304000.0	44.50	37.50	78443.8	74492.8	.608
222	285	3	10	190000.0	49.90	36.50	304000.0	45.00	35.60	81273.0	70095.5	.669
304	363	1	10	190000.0	50.30	34.30	304000.0	45.10	37.50	77324.9	64590.2	.691
306	427	1	10	190000.0	50.10	33.75	304000.0	45.20	37.65	76342.4	64741.9	.681
387	404	1	10	190000.0	50.20	34.90	304000.0	45.25	37.80	78883.8	64851.7	.702
390	441	1	10	190000.0	50.10	34.10	304000.0	44.95	37.80	77136.7	65359.3	.681
391	416	1	10	190000.0	49.70	33.45	304000.0	45.00	37.80	76241.5	65313.2	.674
392	405	1	10	190000.0	50.15	34.20	304000.0	44.90	37.40	77324.3	64709.4	.690
393	382	1	10	190000.0	50.15	33.60	304000.0	45.00	37.60	75898.7	64965.7	.675
433	471	1	10	190000.0	49.80	33.95	304000.0	45.00	38.50	77206.8	66537.4	.670

MEAN BENDING STRESS IN GROOVE = 76575.3 PSI.

STD. DEV. OF BENDING STRESS IN GROOVE = 2833.40 PSI.

MEAN TORQUE STRESS IN GROOVE = 65021.6 PSI.

STD. DEV. OF TORQUE STRESS IN GROOVE = 4279.40 PSI.

MEAN STRESS RATIO = .68211

STD. DEV. OF MEAN STRESS RATIO = .04200

APPENDIX B. DATA REDUCTION RESULTS FOR $r_s = 0.7$ AND $r_s = 0.9$.

TEST NO.	SPECIMEN NO.	MACHINE NO.	PAN WEIGHT	RCAL BENDING	NCAL BENDING	NCAL BENDING	RCAL TORQUE	NCAL TORQUE	NCAL TORQUE	NCAL TORQUE	BENDING STRESS	SHEAR STRESS	STRESS RATIO
245	287	2	7	190000.0	49.86	29.10	304000.0	44.60	32.30	73972.6	52788.3		.809
252	228	3	7	190000.0	49.60	30.70	304000.0	44.80	27.00	68771.9	55089.1		.721
253	230	3	7	190000.0	49.80	30.50	304000.0	44.60	28.70	68049.4	57037.8		.689
254	327	3	7	190000.0	49.50	30.20	304000.0	44.80	28.00	67789.5	55453.8		.706
256	304	3	7	190000.0	49.60	31.00	304000.0	44.50	29.20	69443.9	58183.5		.689
257	321	3	7	190000.0	49.40	30.70	304000.0	44.80	28.20	69050.3	55866.5		.714
258	232	3	7	190000.0	49.20	30.20	304000.0	44.80	30.10	60201.0	59513.2		.662
259	255	3	7	190000.0	49.80	30.30	304000.0	44.60	28.60	67603.2	56854.6		.687
260	272	3	7	190000.0	49.50	31.60	304000.0	44.70	29.20	70931.0	57961.5		.707
261	247	3	7	190000.0	49.70	30.80	304000.0	45.00	28.70	68857.0	56580.8		.703
262	231	3	7	190000.0	49.60	30.90	304000.0	44.80	29.10	69219.9	57606.1		.694
263	229	3	7	190000.0	49.30	31.70	304000.0	44.60	29.10	71444.1	57905.3		.712
264	288	3	7	190000.0	49.50	32.00	304000.0	44.80	28.90	71028.8	57276.0		.724
394	385	1	7	190000.0	49.90	30.55	304000.0	44.80	32.70	69489.7	56646.9		.708
396	337	1	7	190000.0	50.10	30.00	304000.0	44.85	33.10	67869.5	57354.5		.683
398	442	1	7	190000.0	50.15	31.05	304000.0	44.80	33.35	70249.8	57793.3		.702
400	413	1	7	190000.0	50.15	31.15	304000.0	45.00	33.00	70530.1	56889.0		.716
402	360	1	7	190000.0	49.95	31.70	304000.0	45.00	32.80	72144.6	56477.1		.738

MEAN BENDING STRESS IN GROOVE = 69747.0 PSI.

STD. DEV. OF BENDING STRESS IN GROOVE = 1765.29 PSI.

MEAN TORQUE STRESS IN GROOVE = 56849.9 PSI.

STD. DEV. OF TORQUE STRESS IN GROOVE = 1453.79 PSI.

MEAN STRESS RATIO = .70895

STD. DEV. OF MEAN STRESS RATIO = .03092

APPENDIX B. DATA REDUCTION RESULTS FOR $r_b = 0.7$ AND $r_s = 0.9$

TEST NO.	SPECIMEN NO.	MACHINE NO.	PAN WEIGHT	RCAL BENDING	NCAL BENDING	NVIS BENDING	RCAL TORQUE	NCAL TORQUE	NVIS TORQUE	BENDING STRESS	SHEAR STRESS	STRESS RATIO
280	248	3	27	390000.0	50.15	50.15	304000.0	45.15	24.30	54130.6	47662.4	.656
317	288	2	27	190000.0	50.10	25.95	304000.0	44.55	25.15	65783.9	40830.9	.930
318	267	2	26	190000.0	49.70	24.35	304000.0	44.45	24.30	62189.7	39599.0	.907
321	300	2	27	190000.0	49.60	23.15	304000.0	44.65	24.10	59191.7	39183.8	.872
323	275	2	26	190000.0	49.60	24.85	304000.0	44.10	22.25	63745.0	36297.4	1.014
330	409	2	25	190000.0	49.90	23.90	304000.0	44.95	23.60	60821.7	37987.6	.924
339	364	2	24	190000.0	53.05	23.55	304000.0	45.00	22.40	56341.6	36067.8	.902
348	372	2	26	190000.0	49.65	24.55	304000.0	45.20	25.00	62759.8	40070.0	.904
377	362	2	28	190000.0	49.80	25.75	304000.0	45.00	26.30	65612.5	42368.6	.894
378	429	2	27	190000.0	50.00	24.75	304000.0	45.00	25.45	62795.5	41026.6	.884
381	359	2	27	190000.0	50.00	24.65	304000.0	45.10	24.60	62590.9	39489.0	.915
383	417	2	26	190000.0	49.55	23.15	304000.0	44.60	24.30	59238.9	39573.3	.864
388	336	2	26	190000.0	50.30	22.95	304000.0	45.15	26.15	57721.5	42273.0	.788
395	435	2	26	190000.0	50.10	23.65	304000.0	47.10	23.40	60002.2	35650.4	.966
397	401	2	25	190000.0	49.95	24.00	304000.0	45.00	23.40	61033.9	37592.7	.937
430	400	2	29	190000.0	50.10	25.30	304000.0	44.65	24.75	64125.4	40109.9	.923
431	386	2	28	190000.0	50.10	24.65	304000.0	47.15	25.50	62475.8	39137.7	.922
432	402	2	27	190000.0	50.00	24.45	304000.0	47.10	24.80	62123.1	38052.9	.943

MEAN STRESS RATIO = .89701

ENDURANCE

STD. DEV. OF MEAN STRESS RATIO = .07582

APPENDIX C

OPERATING CHECKLIST FOR NASA
COMPLEX FATIGUE RESEARCH MACHINESTO INSTALL SPECIMEN

1. Turn power off at the wall - block up loading arm.
2. Choose correct specimen for test using data book.
3. Prepare specimen for test.
 - a) Inspect specimen for defect or damage
 - b) Clean any oil or foreign matter off specimen
4. Clean inside of toolholders.
5. Clean collets.
6. Use WD-40 on collets - insure there is no binding.
7. Block up one side of loading arm with support bolt.
8. Insert specimen and install collets.
9. Block up other side of loading arm with support bolt.
10. Level the toolholder arms using the support bolts.
11. Place coupling gauges over the flex couplings. Be sure the coupling gauges fit snug.
12. Check the toolholder arms to see if they are still level. If not, adjust the support bolts to make the arms level.
13. Install keys in specimen.
14. Center specimen in toolholder.
15. Tighten outboard side (with strain gages) of specimen by hand.
16. Tighten outboard side of specimen using the wrench. Make sure it is very tight as it cannot be tightened again after this step.

17. With the inboard side (without strain gages) still loose, place brushes on the slip rings. They should be firm against the rings, but not bent tight.
18. Zero the instrumentation.
 - a) Turn milliammeter to "in"
 - b) Check B⁺ (5 volts) - Bridge Balance Switch to "B⁺"
 - c) Check GV (5 volts) - Bridge Balance Switch to "GV"
 - d) Turn Bridge Balance Switch to "BB"
 - e) Turn Channel Selector to desired channel
 - f) Set Atten Switch to desired level
 - g) Use C. Bal. to "dip" voltmeter
 - h) Use R. Bal. to "zero" milliammeter
 - i) Repeat (g) and (h) until minimum voltmeter reading and zero milliammeter readings are obtained simultaneously
 - j) Lock C. Bal. and R. Bal. controls
 - k) Take a short visicorder run
 - l) Repeat (e) through (k) for each channel to be used in the test
 - m) Turn milliammeter switch to "out"
19. Calibrate the instrumentation.
 - a) Connect to Ext. Cal. the appropriate value of calibration resistance
 - b) Using the gain control, obtain the appropriate deflection on the visicorder (some adjustment of the R. Bal. may be necessary) - do not change C. Bal.
 - c) Take a short visicorder run for each deflection - be sure instrumentation is calibrated for both bending and torque.
20. Tighten the inboard side of the test specimen.
21. Remove flex coupling gauges.
22. Clean the specimen and specimen groove.
23. Lower support bolts. Make sure horizontal link is not resting on a support bolt (check both sides).
24. Lower the loading arm - no pan load.
25. Check to see if pins are loose and all nuts are tight.
26. Check to see if bearings are vertical.

27. Check to see if vertical link is vertical.
28. Check to see if brushes are still correctly on the slip rings.
29. Rotate machine by hand.
30. Turn the power on at the wall.
31. Clean the slip rings (with machine running).
32. Turn the machine off.
33. Apply the appropriate load to the pan.
34. Set microswitch.
35. Record static bending.
36. If torque is to be applied, see Procedure for Operating NASA Complex Fatigue Research Machines with Bending and Torque Loads.
37. Set the clock to zero.
38. Put on the bridges.
39. Record dynamic conditions.
40. Check lub. and oil level.

TO REMOVE SPECIMEN

1. Turn power off at the wall.
2. Block up loading arm.
3. Remove the brushes from the slip rings - this step is very important.
4. Loosen both collets so the specimen is free to slide.
5. Remove the bridges.
6. Remove the keys.
7. Raise one side of the toolholder using a support bolt.
8. Remove collets and specimen.

APPENDIX D
PROCEDURE FOR OPERATING NASA COMPLEX
FATIGUE RESEARCH MACHINES WITH
COMBINED BENDING AND TORQUE LOADS

1. Install specimen and balance visicorder as per "Checklist."
2. Apply the torque to the required number of divisions, including the bending interaction divisions, using the Infnit-Indexer.
3. Stabilize the torque divisions as follows:
 - 3.1 Turn the machine by hand for at least five cycles. You will probably observe a decrease in the torque divisions.
 - 3.2 Re-torque machine to desired divisions and repeat the process until the mean torque level remains constant.
4. Start the run and observe the mean torque divisions insuring that it doesn't decrease. If no more than 2 divisions of downward shift in the mean torque divisions is observed, continue the run.
5. If more than 2 divisions of shift in the mean torque level in the downward direction is observed or if excessive upwards drift in the mean torque divisions is observed, particularly 10 or more divisions, stop machine, remove pan weight, block up bending load train, block up loading arm until level, and remove torque by loosening in-board collet only (the side without the strain gages). Check to see where the new torque zero is. If the shift in the zero is within one division of the drift in the mean of the torque divisions, re-zero the torque channel, re-tighten the specimen and repeat Steps 3, 4, 5, and 6 until torque is stabilized.
6. If the zero shift is in excess of the drift in the mean torque divisions initiate an investigation as to its cause.

Probable causes may be the following:

1. True change in torque beyond the intended level.
2. Change in strain gage characteristics, perhaps indicating a strain gage deterioration.
3. Deterioration of amplifier components.

7. If the drift in the mean torque divisions is not in excess of 10 divisions, and a few specimens at the same stress level check out favorably in Steps 1 through 4, do not re-check the zero; finish run.

APPENDIX E

CALIBRATION OF NEW TORQUE GAGES FOR MACHINE #3, JUNE 1969

In May 1969, one of the strain gages in the torque bridge of the toolholder of Machine #3 failed. The gage was replaced and it was necessary to recalibrate. Since the bending bridge was left untouched, the only tests which had to be conducted were the torque load versus visicorder output calibration and the bending interaction into torque calibration.

The results of these tests are presented below.

Torque Load Versus Visicorder Output

The procedure used is identical to the one presented in Section IV-C-1. The data appears in Table 18.

Data Reduction

The same data reduction technique that was used in Section IV-C-1 is used. Figure 43 gives the plot of the data of Table 18.

Machine	Point	Point	W lbs	N _{vis} div	τ_{out} psi	τ_{true} psi	slope K_T
3	(40.0,40.0)	(2.5,6.0)	37.5	34.0	1008	848	0.842

Therefore

$$K_T = 0.842$$

Bending Interaction Into Torque

For the bending interaction into torque procedure, consult Section IV-C-2. The method given there was followed exactly for this test. The data appears in Table 19.

Data Reduction

Using the graphical reduction technique from Figure 44,

$$\text{Point A} = (25.0, 0.73)$$

$$\text{Point B} = (35.0, 1.00)$$

$$N_{\text{vis}_B} = -10.0$$

$$N_{\text{vis}_T} = +0.27$$

$$\epsilon_B = \frac{N_{\text{vis}_B}}{N_{\text{cal}_B}} \frac{R_{\text{gage}}}{N_a G R_{\text{cal}}} = \frac{(-10.0)(190)}{(25.0)(4)(2.23)(490)(10^3)} = 12.00 \mu\text{in/in}$$

$$\epsilon_T = \frac{N_{\text{vis}_T}}{N_{\text{cal}_T}} \frac{R_{\text{gage}}}{N_a G R_{\text{cal}}} = \frac{(0.27)(120)}{(45.3)(4)(2.06)(304)(10^3)} = -.2855 \mu\text{in/in}$$

Therefore

$$K_{B/T} = \frac{-0.2855}{12.00} = -0.0238$$

APPENDIX F
MAINTENANCE CHECKLIST

EACH RUN

The level of the grease in the front shaft couplings and the level of oil in the gear box shall be checked and lubrication added if needed. The oil to be used in the gear box is Mobil D. T. E. Oil - BB.

Log the hours each machine has been run.

EVERY MONTH

Check front Shaft Couplings for proper amount of Marfak #1 grease.

EVERY FOUR MONTHS

Front and back shaft couplings shall be cleaned, inspected and regreased with Texaco Marfak #1.